

ORNL
SUB
AA-SG828/1

ORNL
SUB
90-
SG828/1
c.1

ORNL/Sub/90-SG8

ornl

OAK RIDGE
NATIONAL
LABORATORY

MARTIN MARIETTA

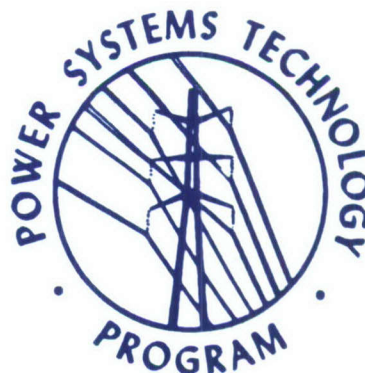
**Magnetohydrodynamic
Electromagnetic Pulse (MHD-EMP)
Interaction with Power Transmission
And Distribution Systems**

F. M. Tesche
Consultant

P. R. Barnes
Oak Ridge National Laboratory

A. P. Sakis Meliopoulos
Georgia Institute of Technology

LOAN COPY: RETURN TO
PL TECHNICAL LIBRARY
KIRTLAND AFB, NM 87117-6008



20080303034

MANAGED BY
MARTIN MARIETTA ENERGY SYSTEMS, INC.
FOR THE UNITED STATES
DEPARTMENT OF ENERGY

DISTRIBUTION STATEMENT A
Approved for Public Release
Distribution Unlimited



This report has been reproduced directly from the best available copy.

Available to DOE and DOE contractors from the Office of Scientific and Technical Information, P.O. Box 62, Oak Ridge, TN 37831; prices available from (615) 576-8401, FTS 626-8401.

Available to the public from the National Technical Information Service, U.S. Department of Commerce, 5285 Port Royal Rd., Springfield, VA 22161.

This report was prepared as an account of work sponsored by an agency of the United States Government. Neither the United States Government nor any agency thereof, nor any of their employees, makes any warranty, express or implied, or assumes any legal liability or responsibility for the accuracy, completeness, or usefulness of any information, apparatus, product, or process disclosed, or represents that its use would not infringe privately owned rights. Reference herein to any specific commercial product, process, or service by trade name, trademark, manufacturer, or otherwise, does not necessarily constitute or imply its endorsement, recommendation, or favoring by the United States Government or any agency thereof. The views and opinions of authors expressed herein do not necessarily state or reflect those of the United States Government or any agency thereof.



MAGNETOHYDRODYNAMIC ELECTROMAGNETIC PULSE (MHD-EMP)
INTERACTION WITH POWER TRANSMISSION
AND DISTRIBUTION SYSTEMS

F.M. Tesche
Consultant
6921 Spanky Branch Dr.
Dallas, Texas

P.R. Barnes
Energy Division
Oak Ridge National Laboratory
Oak Ridge, Tennessee

A.P. Sakis Meliopoulos
Department of Electrical Engineering
Georgia Institute of Technology
Atlanta, Georgia

February 1992

Research Jointly Sponsored by

Defense Nuclear Agency
Washington, DC 20585
DNA IACRO 90-822

Department of Energy
Office of Energy Management
Washington, DC 20585

Under Interagency Agreement No. 0046-C156-A1

Prepared by the
OAK RIDGE NATIONAL LABORATORY
Oak Ridge, Tennessee 37831-6285

Managed by
MARTIN MARIETTA ENERGY SYSTEMS, INC.
for the
U.S. DEPARTMENT OF ENERGY
Under Contract DE-AC05-84OR21400

ABSTRACT

This report discusses the effects of the late-time high-altitude electromagnetic pulse (HEMP) on electrical transmission and distribution (T&D) systems. This environment, known as the magnetohydrodynamic electromagnetic pulse (MHD-EMP), is a very slowly varying electric field induced in the earth's surface, similar to the field induced by a geomagnetic storm. It can result in the flow of a quasi-dc current in grounded power lines and in the subsequent magnetic saturation of transformers. This saturation, in turn, causes 60-Hz harmonic distortion and an increase in the reactive power required by generation facilities. This report analyzes and discusses these phenomena. The MHD-EMP environment is briefly discussed, and a simplified form of the earth-induced electric field is developed for use in a parametric study of transmission line responses. Various field coupling models are described, and calculated results for the responses of both transmission- and distribution-class power lines are presented. These calculated responses are compared with measurements of transformer operation under dc excitation to infer the MHD-EMP response of these power system components. It is found that the MHD-EMP environment would have a marked effect on a power system by inducing up to several hundreds of amperes of quasi-dc current on power lines. These currents will cause transformers to saturate which could result in excessive harmonic generation, voltage swings, and voltage suppression. The design of critical facilities which are required to operate during and after MHD-EMP events will have to be modified in order to mitigate the effects of these abnormal power system conditions.

FOREWORD

This work was sponsored by the Defense Nuclear Agency (DNA) under Interagency Agreement No. 0046-C156-A1 with the Department of Energy and conducted under DOE Contract DE-AC05-84OR-21400 with Martin Marietta Energy Systems, operator of the Oak Ridge National Laboratory. The authors would like to acknowledge useful discussions with John Kappenman of the Minnesota Power and Light Company and Ed Vance of SRI International during the course of this work.

TABLE OF CONTENTS

	<u>Page</u>
TABLE OF CONTENTS	iii
LIST OF FIGURES	v
LIST OF TABLES	ix
1.0 INTRODUCTION	1
2.0 THE MHD-EMP ENVIRONMENT	3
2.1 Overview	3
2.2 Simplified MHD-EMP Electric Fields	5
2.3 Curve-Fit Representation of the E-Field Environments	9
3.0 ANALYSIS MODELS FOR MHD-EMP RESPONSES	14
3.1 Isolated Line Section	14
3.2 Considerations for Shielded Lines	22
3.2.1 Solution for a Small Number of Towers	27
3.2.2 Solution for a Large Number of Towers	29
3.2.2.1 Determination of V_{oc}	33
3.2.2.2 Determination of R_{in}	35
3.2.3 Sample Line Responses	37
3.3 Induced Current on Grounded Neutral Conductors	45
3.4 Cumulative Probability Distribution for Line Responses	50
4.0 PARAMETRIC STUDY OF MHD-EMP EFFECTS ON A POWER TRANSMISSION SYSTEM	52
4.1 Introduction	52
4.2 Description of the 500-kV Transmission System	52
4.3 Description of the Parametric Analysis	56

TABLE OF CONTENTS (Con't)

	<u>Page</u>
4.4 Parametric Study Results	57
5.0 MHD-EMP EFFECTS ON THE POWER SYSTEM	66
5.1 Harmonic Generation	66
5.2 Reactive Power Demand Caused by MHD-EMP	70
5.3 Changes in System Time Constant	70
5.4 Observed Geomagnetic Storm Effects	79
6.0 SUMMARY AND CONCLUSIONS	86
REFERENCES	88

LIST OF FIGURES

<u>Figure</u>	<u>Page</u>
Figure 1. Normalized Early-Time MHD-EMP E-Field Outside the X-Ray Patch.	6
Figure 2. Normalized Early-Time MHD-EMP E-Field Under the X-Ray Patch.	6
Figure 3. Normalized Late-Time MHD-EMP E-Field.	7
Figure 4. Normalized Composite MHD-EMP E-Field.	8
Figure 5. Plot of the Normalized Curve-Fit (Solid) and Waveform (Data Points) for the MHD-EMP E-Field Outside the X-Ray Patch.	10
Figure 6. Plot of the Normalized Curve-Fit (Solid) and Waveform (Data Points) for the Blast-Wave Component of the MHD-EMP E-Field Under the X-Ray Patch.	11
Figure 7. Plot of the Normalized Curve-Fit (Solid) and Waveform (Data Points) for the Late-Time Component of the MHD-EMP E-Field.	13
Figure 8. Three-Phase Line and Equivalent Circuit for Computing MHD-EMP-Induced Current.	15
Figure 9. MHD-EMP-Induced Current for Transmission Lines (Case 1).	19
Figure 10. MHD-EMP-Induced Current for Subtransmission and Distribution Lines (Case 2 - Substation Grounding).	20
Figure 11. MHD-EMP-Induced Current for Subtransmission and Distribution Lines (Case 3 - Stake Grounding at One End and Substation Grounding at the Other).	21
Figure 12. Three-Phase Line with N Towers and Overhead Shield Wires Not Electrically Connected.	23
Figure 13. Three-Phase Line with N Towers and Overhead Shield Wires with Interconnected Grounds.	25
Figure 14. Analysis Procedure for the Current I_c .	26

LIST OF FIGURES (Con't)

<u>Figure</u>		<u>Page</u>
Figure 15.	Behavior of the Equivalent Circuit at A and A' for Different Numbers of Tower Sections, Using Circuit Analysis.	28
Figure 16.	Contours of Normalized MHD-EMP-Induced Current I_c/E_o (A · km/V) for the Shielded 138-kV Line, Using the Circuit Model.	30
Figure 17.	Continuous Model of the Overhead Shield Wire and Tower Supports.	32
Figure 18.	Two-Port Representation of the Shield Line Between Points A and A'.	35
Figure 19.	Behavior of the Equivalent Circuit at A and A' for Different Numbers of Tower Sections, Using the Continuous Model.	38
Figure 20.	Contours of Normalized MHD-EMP-Induced Current I_c/E_o (A · km/V) for the Shielded 138 kV Line, Using the Continuous Model.	39
Figure 21.	Contours of Normalized MHD-EMP-Induced Current I_c/E_o (A · km/V) for Shielded Lines.	41
Figure 22.	Three-phase Line With Un-grounded Δ Transformer and Periodically Grounded Neutral Conductor.	46
Figure 23.	Contours of Normalized MHD-EMP-Induced Current I_n/E_o (A · km/V) at the End of the Periodically Grounded Neutral Conductor.	48
Figure 24.	Normalized MHD-EMP-Induced Current vs. Number of Tower Sections for Different Line Lengths.	49
Figure 25.	Normalized MHD-EMP-Induced Current vs. Line Length for Different Numbers of Tower Sections.	49
Figure 26.	Normalized MHD-EMP-Induced Current vs. Line Length for Different Section Spacings.	50
Figure 27.	Universal Cumulative Probability Curve for Induced MHD-EMP Current Responses.	51
Figure 28.	500-kV Transmission Line Configuration for Parametric Study.	54
Figure 29.	Transformer Core Magnetization Characteristics.	55

LIST OF FIGURES (Con't)

<u>Figure</u>	<u>Page</u>
Figure 30. Transmission Line Response for the Early-Time E_3 Waveform, (E_3 Amplitude = 10 V/km, $\rho = 100 \Omega \cdot \text{m}$, Shield Is Grounded, Line Length = 30 km, and Span Length = 0.16 km).	58
Figure 31. Test System Response for the Late-Time E_3 Waveform, (E_3 Amplitude = 10 V/km, $\rho = 100 \Omega \cdot \text{m}$, Shield Is Grounded, Line Length = 1000 km, Span Length = 0.16 km).	59
Figure 32. The Maximum Magnetization Current for the Early-Time MHD-EMP Waveform when $\rho = 100 \Omega \cdot \text{m}$.	60
Figure 33. The Maximum Magnetization Current for the Late-Time MHD-EMP Waveform when $\rho = 100 \Omega \cdot \text{m}$.	62
Figure 34. Time Delay to Transformer Saturation for the Late-Time MHD-EMP Waveform when $\rho = 100 \Omega \cdot \text{m}$.	64
Figure 35. Measured Harmonic Content for Dc Injection in the Primary of an Unloaded 500/230-kV Autotransformer, from Ref.[13].	68
Figure 36. Measured Harmonic Content for Dc Injection in the Primary of a Loaded 230/115-kV Autotransformer, from Ref.[13].	68
Figure 37. Measured Harmonic Content for DC Injection in the Neutral of a Three-Phase 480-V/12.47-kV/208-V Power Distribution System, from Ref.[14].	69
Figure 38. Reactive Power Demand for the 500/230-kV Transformer, from Ref.[13].	71
Figure 39. Reactive Power Demand for the 480-V/12.47-kV/208-V Power Distribution System, from Ref.[14].	71
Figure 40. System Relaxation Time vs. DC Current Injection for the Three-Phase 480-V/12.47-kV/208-V Power Distribution System, from Ref. [14].	72
Figure 41. System Response to MHD-EMP with Transformer Unloaded.	74
Figure 42. System Response to MHD-EMP with 20% Transformer Load.	75
Figure 43. System Response to MHD-EMP with 40 % Transformer Load.	76
Figure 44. System Response to MHD-EMP with 100% Transformer Load.	77

LIST OF FIGURES (Con't)

<u>Figure</u>		<u>Page</u>
Figure 45.	Measured Geomagnetic Field at Ottawa, Canada, from Ref.[16].	80
Figure 46.	Computed Earth-Induced Electric Field for $\sigma_g = 0.0001$ Mhos/m.	82
Figure 47.	Computed E-Field Components for October 28, 1991.	83
Figure 48.	Comparison of MHD-EMP with Geomagnetic Storm E-field Waveforms.	85

LIST OF TABLES

<u>Table</u>		<u>Page</u>
Table 1	Parameters for Transmission Line Analysis	17
Table 2	Parameters for Subtransmission and Distribution Line Analysis	17
Table 3	Maximum Normalized MHD—EMP—Induced Current	18
Table 4	Parameters for Shielded Line Analysis	40
Table 5	Data for 500 kV Transmission Line	53
Table 6	Peak MHD—EMP E—Fields Used in Parametric Study	56
Table 7	Line and Ground Constants Used in Parametric Study	57
Table 8	Saturation Time Constant for Loaded Transformer	73

MAGNETOHYDRODYNAMIC ELECTROMAGNETIC PULSE (MHD-EMP) INTERACTION WITH POWER TRANSMISSION AND DISTRIBUTION SYSTEMS

1.0 INTRODUCTION

A large-yield nuclear detonation at altitudes of several hundred kilometers above the earth will distort the earth's magnetic field and result in a time-varying geomagnetic field on the earth's surface. This varying geomagnetic field interacts with the finitely conducting earth to produce a time-varying electric field (E-field), also on the earth's surface. Known as the magnetohydrodynamic electromagnetic pulse (MHD-EMP), this E-field can induce a net voltage in long electrical conductors such as power transmission lines. If these conductors are electrically connected to the earth at both ends, a current can be induced in the conductors, causing damage or upset to certain electrical systems.

This MHD-EMP environment, also referred to as the E_3 environment, is only one component of the total electromagnetic pulse, called the high-altitude electromagnetic pulse (HEMP), produced by a high-altitude nuclear detonation. The other components, denoted as E_1 and E_2 , have much larger amplitudes and a shorter duration. Consequently, they interact differently with the electrical power system. The MHD-EMP environment is characterized by a rather low E-field strength, on the order of several tens of V/km, and by a typical waveform pulse of several hundreds of seconds in duration. This part of the HEMP environment is similar to, but more intense than, that occurring for a solar geomagnetic storm.

Very intense solar geomagnetic storms have previously upset long-line communications and power systems. It is predicted that the E_3 environment, which is much stronger than that of solar storms, will have significant effects. Most of the previous solar storm effects have been noted for systems near the polar region, and some measures have been taken to mitigate these effects. The E_3 environment, however, could be experienced by power systems which are normally not affected by geomagnetic storms, and could therefore have an adverse effect on systems nationwide. Furthermore, this E_3 environment would be applied to the power system after the system has been excited by E_1 and E_2 environments that have possibly been caused by other nuclear detonations. It is presently viewed that the synergistic effects of these environments will increase the likelihood of electrical power interruption in the event of a HEMP occurrence.

This report documents the results of a study on the interaction of MHD-EMP with power transmission and distribution (T&D) systems. Section 2.0 presents a brief overview of the MHD-EMP environments used in the study. Normalized MHD-EMP electric field waveforms are assumed to be simple excitation functions, which permits an analytical curve-fit representation for the time history of these fields. A more accurate description of this environment would involve a detailed transient waveform, its polarization, and its spatial dependence.

Section 3.0 describes the analytical models useful for coupling this MHD-EMP environment to T&D lines. Because of the quasi-static nature of the excitation, the models are essentially simple direct current (dc) circuit models. However, complications arise in attempting to model realistic line configurations having a large number of support towers and an overhead shield or neutral wires. These models are discussed in detail.

Using the analysis models described in Section 3.0, a parametric study of a 500-kV power transmission line was conducted, and the results are documented in Section 4.0. In this study, the line length, the MHD-EMP waveform and amplitude, and the tower connections to the neutral conductor of the transmission line are varied.

The possible effects of this HEMP environment on electric power systems are discussed in Section 5.0. Unlike the solar geomagnetic storm, which can last for many hours (or sometimes days), the E_3 environment for a single burst lasts for only several minutes. Consequently, direct damage to large power system components is not thought to be a problem. More serious, however, is the effect of power transformer saturation and the subsequent generation of 60-Hz harmonics. These phenomena can upset instrumentation in the system as well as lead to an increase in the reactive power required from the power generators. Both of these effects can lead to power system instability.

Finally, Section 6.0 presents a summary of the findings of this report. The references are listed after Section 6.

2.0 THE MHD-EMP ENVIRONMENT

2.1 Overview

As discussed in ref.[1], the MHD-EMP or E_3 environment arises from a variation of the earth's magnetic field caused by a high-altitude nuclear detonation. The interaction of this time-varying magnetic flux field (B-field) with the imperfectly conducting ground causes a transient electric field to be induced on the surface of the earth, in a manner analogous to that occurring in a geomagnetic storm [2]. For a tangential B-field on the earth's surface, denoted by $B(t)$, the corresponding electric field tangential to the earth is computed as

$$E(t) = \frac{1}{\sqrt{\sigma\mu\pi}} \int_0^t \frac{1}{\sqrt{t-t'}} \frac{\partial B}{\partial t'} dt' \quad (1)$$

where σ is the earth electrical conductivity and $\mu = 4\pi \times 10^{-7}$ h/m is the permeability of the soil [1]. This resulting E-field is orthogonal to the B-field on the earth's surface and is much slower than the early-time E_1 HEMP environment. Typical waveform times for the MHD-EMP environment are on the order of several hundreds of seconds.

The E_3 environment may be divided into two parts, based on the postulated mechanisms of production. The first part, for times between $0 \leq t < 10$ sec, arises from the initial nuclear burst and its interaction with the earth's magnetic field. This part is referred to as the blast-wave component. At later times for $10 \leq t < 500$ sec, a second contribution to the geomagnetic field variation arises due to the late-time atmospheric heave. These production mechanisms are illustrated and discussed in ref.[1].

The environment used in refs.[1] and [3] for an EMP assessment of commercial power networks was based on early work reported in ref.[4]. This work involved performing a numerical simulation of the time development of the disturbed atmosphere using a code named MICE.

Recent refinements in the theory of MHD-EMP production by Austin Research Associates [5] have led to an alternate computer model for predicting the blast-wave environment. In addition, there are some preliminary results for the late-time heave component of the E_3 environment. This work has been used to develop an updated composite MHD-EMP environment, which can be used to estimate the behavior of induced currents in long transmission and distribution lines.

According to ref.[5], a simplified way of viewing the early-time, blast-wave E_3 environment is to consider a quasi-static problem in which a magnetic dipole moment at the burst point is used to represent a perturbation source for the geomagnetic field. This dipole is oriented in a direction opposing the earth's magnetic field. Below this dipole, at an altitude of about 110 km, is a conducting region, or patch, which is created by downward-streaming x-rays from the detonation. For our model, this x-ray patch is assumed to be perfectly conducting, with no penetration by the early-time magnetic field. However, the B-field from the dipole moment does reach under the patch by flowing out around the ends of the patch and then reconnecting in the region between the patch and the ground. In some of the MHD-EMP literature, this process is variously described as "propagation" or "diffraction," but since these are nominally high-frequency concepts and the MHD-EMP is quasi-static in nature, the use of these terms is avoided here.

Under the x-ray patch, the blast-wave E-field is observed to be smaller than outside this shielded region. The field is oriented primarily in the west-east direction and does not appear to vary drastically with position. Outside the shielded region, the E-field appears to fall off with distance away from the burst, with the largest field occurring just outside the x-ray shield.

For a burst near the magnetic north pole, these electric fields are also predominantly in the west-east direction. Although the field variation with position may be computed using the elementary dipole model representing the center of the magnetic bubble, our view of the E_3 environment assumes that the E-fields outside the x-ray shield are also in the west-east direction.

2.2 Simplified MHD-EMP Electric Fields

For the purpose of illustrating the coupling of MHD-EMP environments to power systems, several different E-field waveforms may be used. Figures 1 and 2 present two different waveforms for the early-time blast component of the E-field on the earth's surface. The MHD-EMP E-field, denoted by $E_o(t)$, is normalized by a factor E_{\max} . Figure 1 is typical for observation locations outside of the x-ray patch, while Figure 2 is for a location under the patch. The normalization factor, E_{\max} , depends on many factors, including the burst yield and other parameters, the exact observer location, and the earth's electrical conductivity.

Figure 3 presents a typical late-time heave contribution to the E-field. As in the previous figures, this waveform is also normalized to unity. This component of the MHD-EMP environment is believed to be strongest directly under the burst, falling off rapidly as the observer moves away from ground zero.

The total MHD-EMP E-field on the ground consists of some suitable combination of Figures 1-3, depending on the actual location of the observer. For some locations the late-time component of the environment will be very small, but for others it can be substantial. As an example of such a composite MHD-EMP waveform, Figure 4a presents a complete normalized waveform. Its frequency-domain spectral magnitude is shown in Figure 4b; note that most of the spectrum is located well below 1 Hz. For power systems, this implies that the MHD-EMP waveform appears as a quasi-dc signal, and that dc circuit modeling concepts will be appropriate for calculating system responses.

For reasons mentioned previously, the MHD-EMP E-field vector direction depends on the burst location relative to the magnetic north pole. As in the case of solar geomagnetic storms, for burst locations near the north pole, much of the earth's surface experiencing the MHD-EMP environment sees a predominantly east-west E-field. Consequently, for this study, the direction of the E-field is assumed to be east-west.

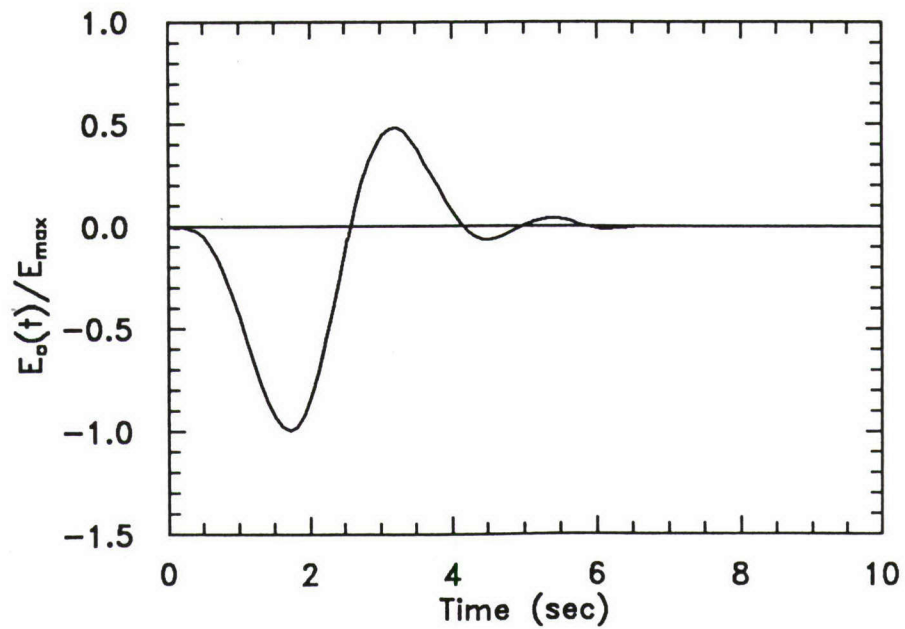


Figure 1. Normalized Early-Time MHD-EMP E-Field Outside the X-Ray Patch.

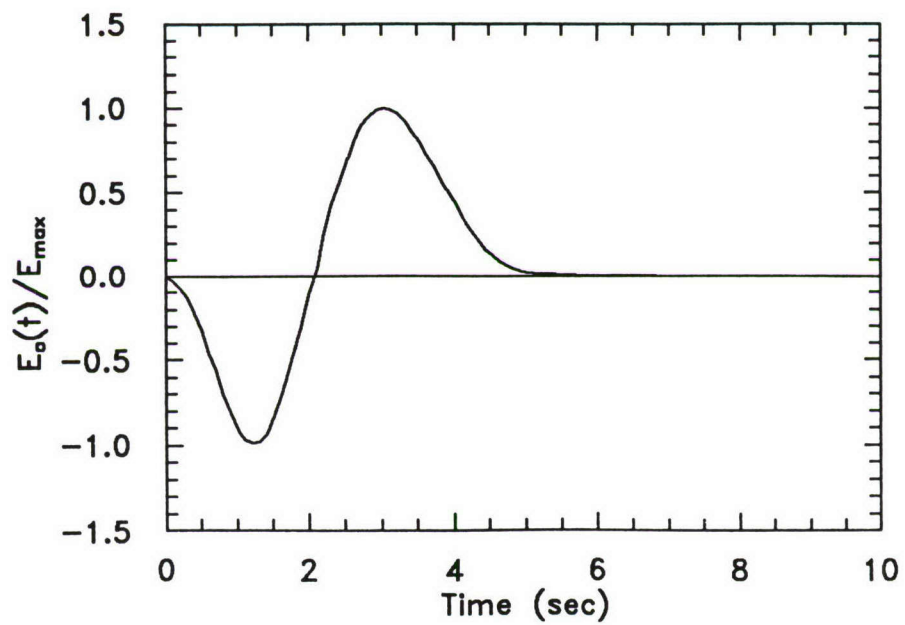


Figure 2. Normalized Early-Time MHD-EMP E-Field Under the X-Ray Patch.

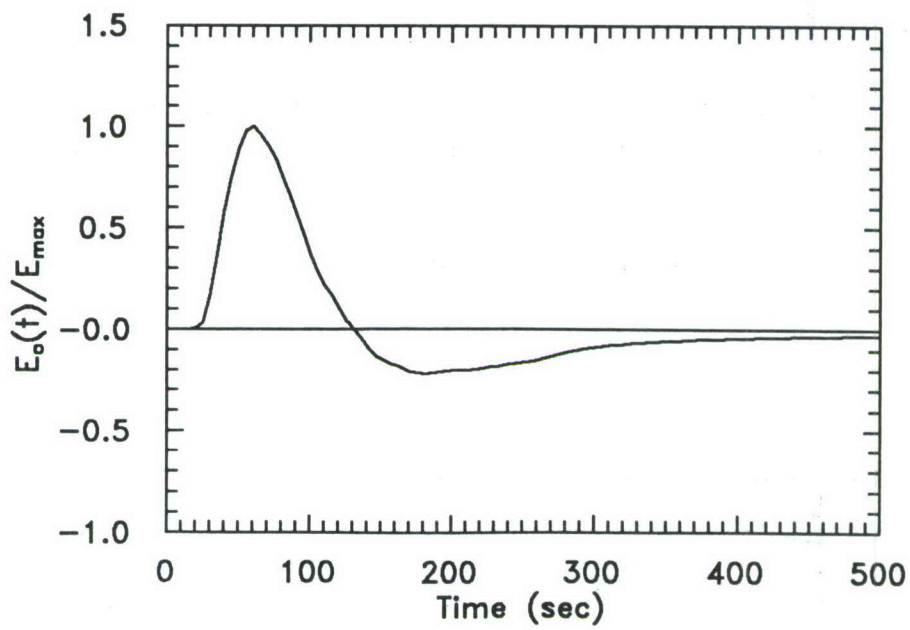
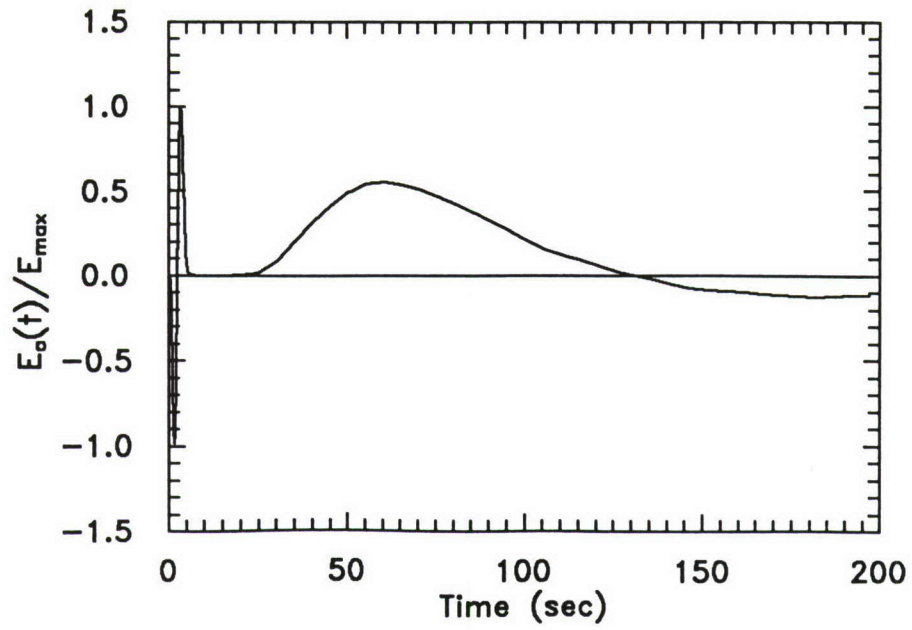
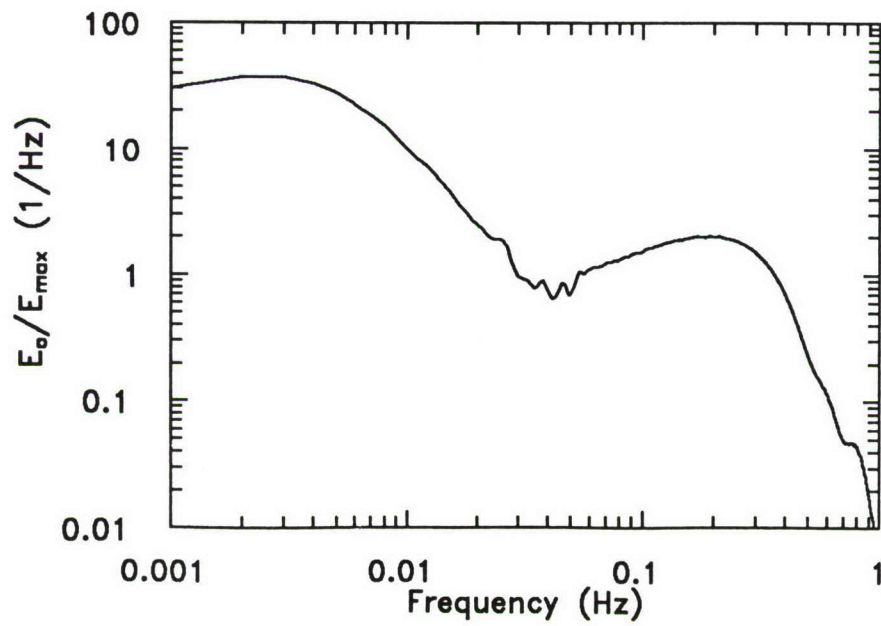


Figure 3. Normalized Late-Time MHD-EMP E-Field.



a. Time-Domain Waveform



b. Frequency-Domain Spectrum Magnitude

Figure 4. Normalized Composite MHD-EMP E-Field.

2.3 Curve-Fit Representation of the E-Field Environments

For some calculational procedures, an explicit expression for the waveforms shown in Figures 1, 2 and 3 is useful. This expression may be obtained by fitting the waveform components to a suitable functional form using commercial curve-fitting software [6].

A suitable fit for the time-dependent E-field environment outside the x-ray shield, illustrated in Figure 1, is given by ref.[6] in the form of a power series expansion:

$$E_o(\tau)/E_{\max} = a + b\tau + c\tau^2 + d\tau^3 + e\tau^4 + f\tau^5 + g\tau^6 + h\tau^7 + i\tau^8 + j\tau^9 + k\tau^{10} \quad (2)$$

for $0 > \tau \geq 3.75$ seconds. Here τ is a shifted time variable given by $\tau = (t - 0.4)$ seconds, and the following terms are computed in the curve-fitting process:

Coefficient	Value
a	-0.00066220
b	-0.16634115
c	-0.89240008
d	0.547750685
e	-2.28495005
f	3.687696276
g	-2.39828948
h	0.788893721
i	-0.13926466
j	0.012495192
k	-0.00044058

Figure 5 illustrates this curve-fit (the solid line), along with the original waveform data for the normalized MHD-EMP waveform. Clearly, for shifted times $\tau > 3.75$, the curve-fit begins to deviate from the actual waveform, indicating that the fit should not be used in this region.

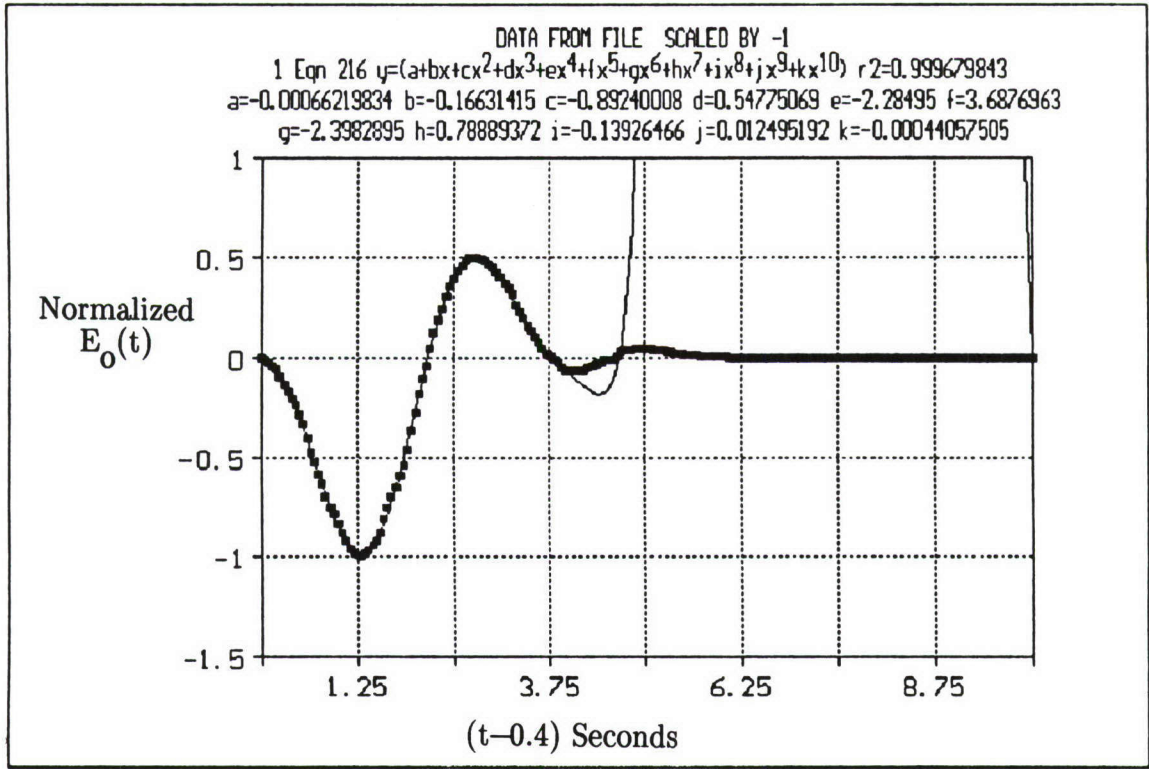


Figure 5. Plot of the Normalized Curve-Fit (Solid) and Waveform (Data Points) for the MHD-EMP E-Field Outside the X-Ray Patch.

For the early-time component of the E_3 waveform for observation locations under the x-ray shield, the following curve-fit representation is possible:

$$E_o(\tau)/E_{\max} = a+b\tau+c\tau^2+d\tau^3+e\tau^4+f\tau^5+g\tau^6+h\tau^7+i\tau^8+j\tau^9+k\tau^{10} \quad (3)$$

for $0 < \tau \leq 10$ seconds, and again τ is a shifted time variable given by $\tau = (t - 0.4)$ seconds. For this expression, the following terms are defined:

Coefficient	Value
a	-0.15830209
b	2.806631745
c	-10.7123990
d	11.35846963
e	-5.53539948
f	1.485628864
g	-0.23541413
h	0.022193314
i	-0.00117987
j	2.99420E-05
k	-1.9980e-07

Figure 6 illustrates this curve-fit (the solid line), along with the original waveform data for the early-time blast-wave component of the environment shown in Figure 2.

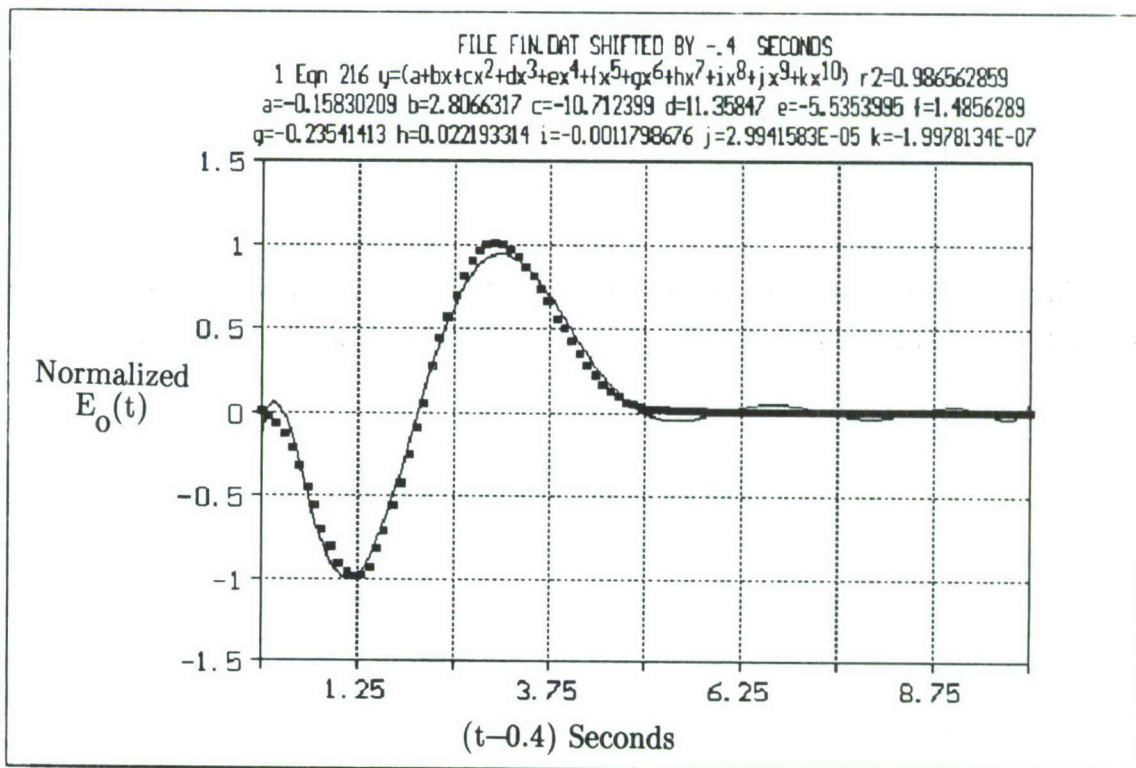


Figure 6. Plot of the Normalized Curve-Fit (Solid) and Waveform (Data Points) for the Blast-Wave Component of the MHD-EMP E-Field Under the X-Ray Patch.

The late-time heave contribution to the E_3 E-field under the x-ray shield can be expressed as a ratio of polynomials as

$$E_o(\tau)/E_{\max} = \frac{(a+b\tau+c\tau^2+d\tau^3+e\tau^4+f\tau^5)}{(g\tau^6+h\tau^7+i\tau^8+j\tau^9+k\tau^{10})} \quad (4)$$

for $0 \leq \tau$ seconds, where the shifted time variable is now given by $\tau = (t - 22)$ seconds. For this expression, the following terms are defined:

Coefficient	Value
a	-0.00541799
b	-0.03056179
c	0.031475266
d	0.000660923
e	-0.00051925
f	-5.0690E-06
g	2.61420E-06
h	2.18120E-08
i	-5.2680E-09
j	-3.4780E-11
k	3.73010E-12

Figure 7 illustrates this curve-fit (the solid line), along with the original waveform data for the normalized late-time blast-wave component of the environment of Figure 3.

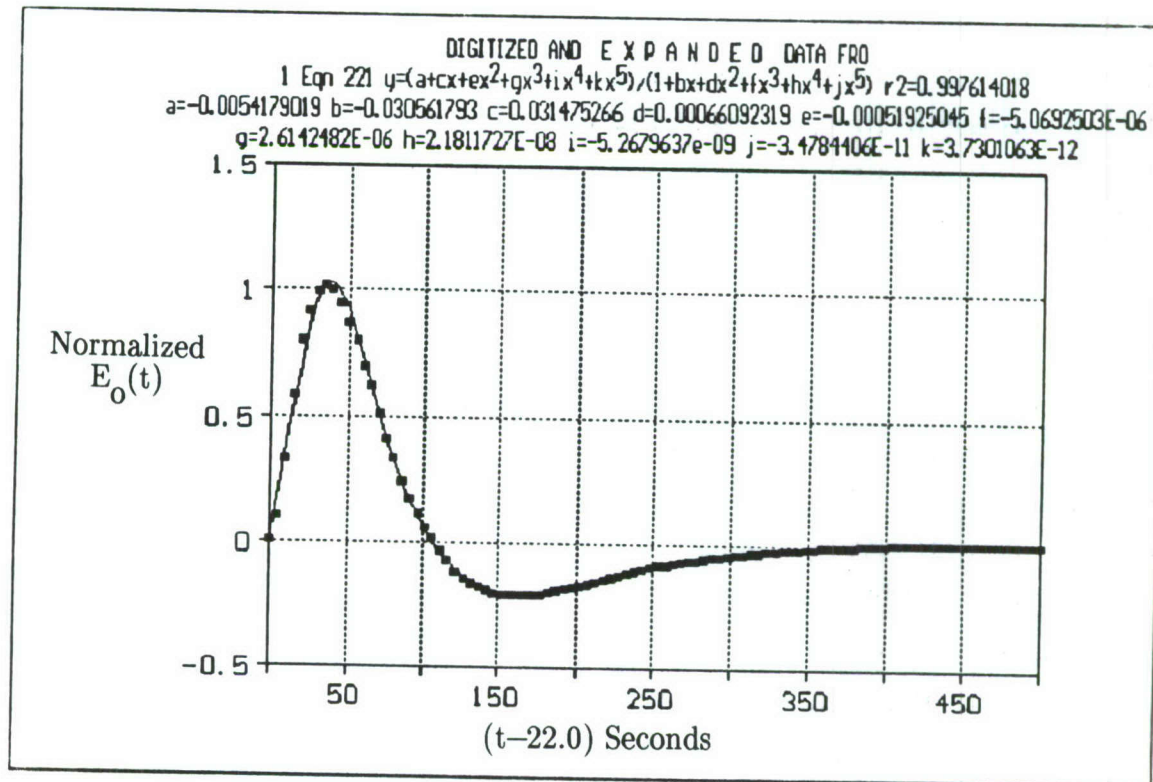


Figure 7. Plot of the Normalized Curve-Fit (Solid) and Waveform (Data Points) for the Late-Time Component of the MHD-EMP E-Field.

3.0 ANALYSIS MODELS FOR MHD-EMP RESPONSES

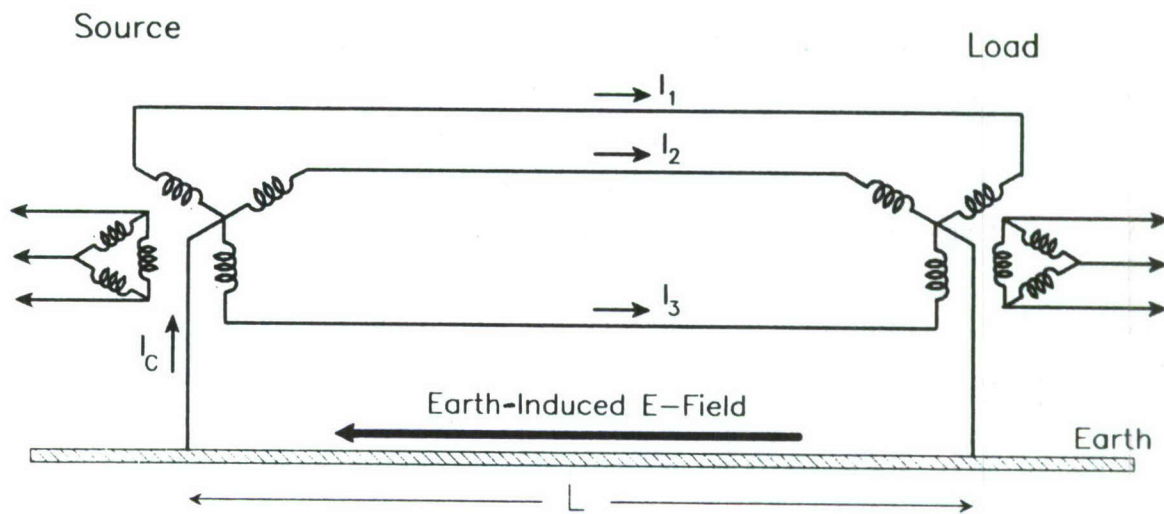
The MHD-EMP electric field environment described in the previous section is capable of inducing currents in long sections of transmission or distribution lines in electrical power systems. Unlike the early-time E_1 HEMP environment, which can induce large currents in conductors that are not connected to the ground, the E_3 environment will induce currents in the lines only if the lines are connected to the earth at two or more points. This is due to the quasi-static nature of the MHD-EMP fields. In this section, models of several different transmission and distribution lines are examined and the MHD-EMP-induced currents computed.

3.1 Isolated Line Section

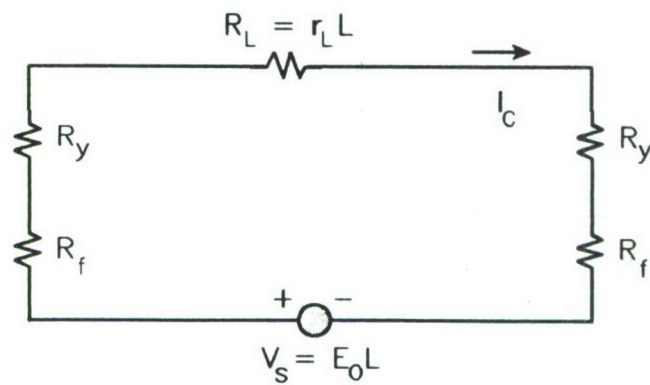
Single-phase electrical transmission or distribution lines are not usually connected to the earth through low impedance loads at each end of a long line, as this will short out the transmitted power. Consequently, the E_3 environment is not generally a problem for these lines. However, three-phase power systems with grounded Y transformers at each end can have this grounding configuration, as shown in Figure 8. Under normal operation, the 60-Hz power currents flowing along the line, I_1 , I_2 and I_3 , are all 120° out of phase so that the total return current through the earth or other neutral is approximately zero. The MHD-EMP earth-induced electric field, E_o , acts over the length L of the line to produce a net quasi-dc excitation voltage of

$$V_s = E_o(t)L \quad . \quad (5)$$

Although the peak value of the MHD-EMP E-field is relatively small compared with the 50-kV/m early-time E_1 field, the line length L can be very long. Consequently, the excitation voltage can be on the order of several kV in certain cases. Of course, this value depends on the line length, the line orientation, and the environmental details.



a. Three-Phase Line and Transformer Configuration



b. Simple Equivalent Circuit

Figure 8. Three-Phase Line and Equivalent Circuit for Computing MHD-EMP-Induced Current.

This MHD-EMP excitation of the line will induce a current to flow in the neutral conductors of the transformer, as indicated in the figure. This current, denoted by I_c , will divide and flow through each of the transformer windings, flow along each of the phase conductors, and return to the earth through the neutral of the second transformer. This current may be calculated by the equivalent circuit shown in Figure 8b, where R_f represents the footing or grounding resistance of the neutral conductors of the transformer to the earth ground, R_y is the parallel combination of the three transformer winding resistances, and R_L is the parallel combination of the three line conductor resistances. This latter quantity depends on the length of the section of line being considered. Using the term r_L to represent the total per-unit-length resistance (in Ω/km) of the three phase conductors in parallel, this resistive component has the value $R_L = r_L L \ \Omega$.

Specific values for R_f , R_y , and R_L depend on the voltage class of the transmission or distribution line being considered, as well as on the location and construction of the transformer site. An efficient power system design attempts to minimize each of these resistances. Unfortunately, this minimization will lead to large MHD-EMP-induced currents. For example, overall circuit resistances can be on the order of several ohms to tens of ohms, with resulting currents of several hundreds of amps.

A simple analysis of the circuit in Figure 8b results in the current response

$$I_c = \frac{E_o L}{2(R_f + R_y) + r_L L} \quad (6)$$

For short lines, the induced current is seen to be proportional to the line length. However, for long lines when the term $r_L L$ dominates, the current is seen to approach a constant value, independent of the line length.

To obtain an indication of possible current responses for different line configurations, several line classes have been examined. The first case involves power transmission lines of the 138-, 345-, and 500-kV class. For these types of lines, an effort is made to keep the transformer neutral grounding resistance low, usually between 0.5 to 1.0 Ω . For this study, therefore, the grounding resistance for these lines is assumed to be $R_f = 0.75 \ \Omega$. Table 1 presents the other appropriate line and transformer resistances for

these line classes. Typical lengths of these transmission lines are indicated as the "Nominal L."

Table 1
Parameters for Transmission Line Analysis

Line Class	Nominal L (km)	Conductor Data	r_L (Ω/km)	R_y (Ω)
500 kV, 200 MVA	100-500	4x583,200 CM* 18.7 ACSR* Bundle	0.0083	0.060
345 kV, 100 MVA	100-200	1,414,000 CM Expanded ACSR	0.0135	0.025
138 kV, 100 MVA	50-150	397,500 CM ACSR	0.0540	0.010

(* CM = circular mil; ACSR = aluminum cable, steel reinforced)

The second case considered is for subtransmission and distribution class lines operating at 12, 25, 34, and 69 kV, assuming that the transformer neutrals are connected to a substation ground mat at both ends of the line. This configuration provides a grounding resistance of $R_f \approx 1 \Omega$. Table 2 provides the length and resistance data for this case. The value for r_L for the 12-kV line assumes that a 2/0 phase conductor wire is used.

Table 2
Parameters for Subtransmission and Distribution Line Analysis

Line Class	Nominal L (km)	Conductor Data	r_L (Ω/km)	R_y (Ω)
69	30-60	4/0 Cu	0.062	0.04
34	15-30	3/0 Cu	0.072	0.40
25	5-20	3/0 Cu	0.072	0.30
12	2-15	2/0 Cu	0.091	0.14

The third case considered is for subtransmission and distribution class lines operating at the same voltage levels as in Case 2, but with the transformer neutrals connected to a grounding rod on one end of the line and to the substation mat on the other end. The grounding rod typically provides a footing resistance of $R_f = 5.0$ to 20.0Ω . For this study, this value has been taken as $R_f \approx 10 \Omega$. The other data for this case are the same as in Table 2.

For Case 1, involving the 138-, 345- and 500-kV transmission lines, Figure 9 illustrates the behavior of the MHD-EMP-induced neutral current, shown as a function of the line length, L , for the three different line classes. These currents are normalized by the MHD-EMP E-field, E_0 . Thus, the time-dependent induced current is given by the sample waveform of Figure 4a, multiplied by the proper factor I_c/E_0 in Figure 9 for the line having a length specified by L .

Figure 10 shows the induced neutral currents for the 12, 25, 34, and 69 kV line classes for Case 2 (i.e., the transformer neutrals grounded to the substation ground.) As in Case 1, the current limiting effect is apparent, especially in the case of the 12-kV line. Figure 11 illustrates the corresponding responses for the same lines, with the alternate grounding scheme (Case 3). Neutral currents in this case are significantly lower than in the previous case due to the higher grounding resistance provided by the grounding rod.

Eq. (6) indicates that for very long lines the induced current is dependent only on the per-unit-length line resistance as $I_c/E_0 = 1/r_L$. This current limiting is apparent in some of the curves in Figures 9-11. For the transmission and distribution lines considered above, Table 3 summarized these peak MHD-EMP-induced currents.

Table 3
Maximum Normalized MHD-EMP-Induced Current

Voltage Class (kV)	I_c/E_0 (A·km/V)
500	120.5
345	74.1
138	18.5
69	16.1
34	13.8
25	13.8
12	11.0

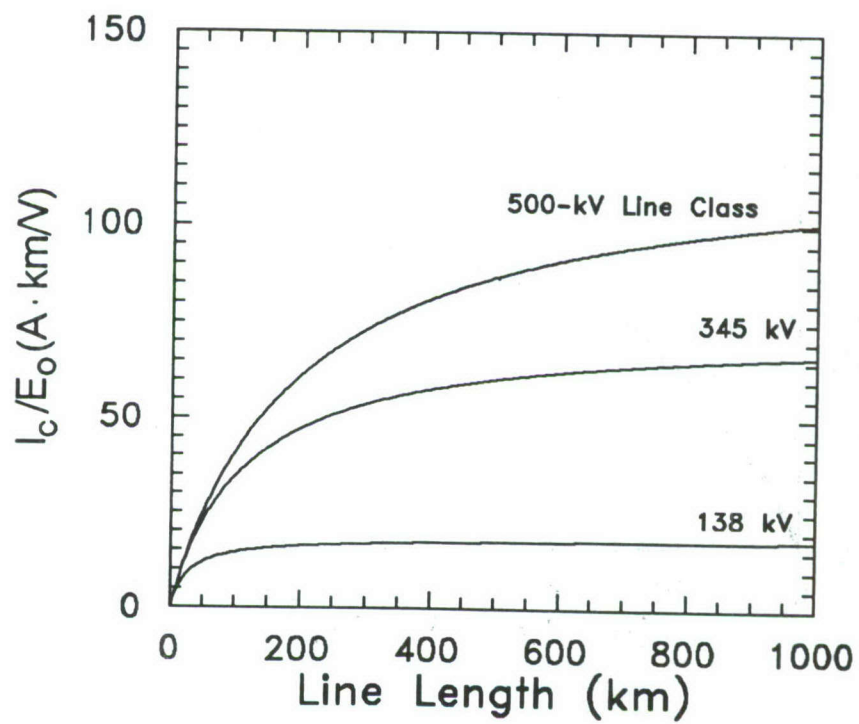


Figure 9. MHD-EMP-Induced Current for Transmission Lines (Case 1).

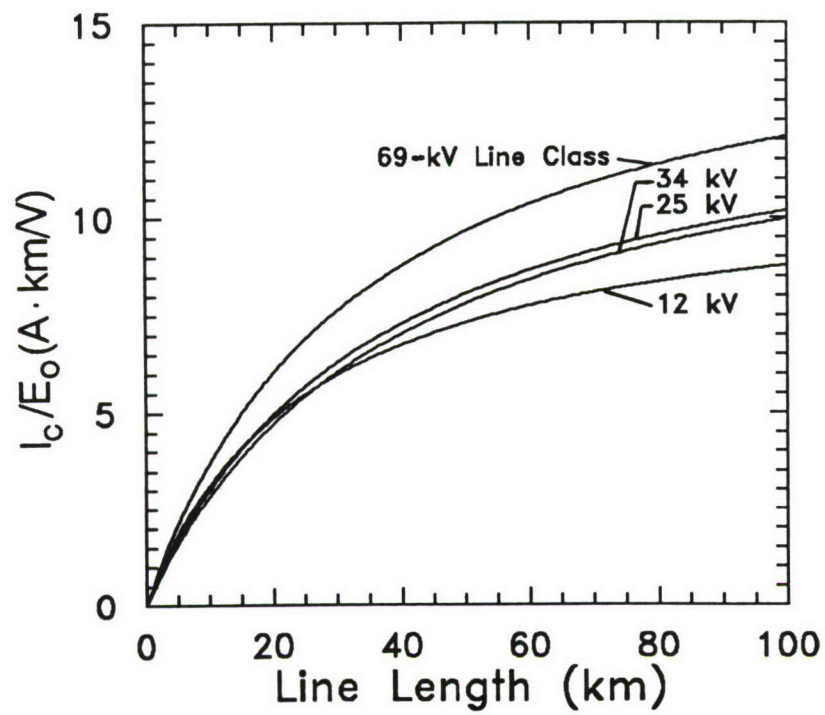


Figure 10. MHD-EMP-Induced Current for Subtransmission and Distribution Lines (Case 2 - Substation Grounding).

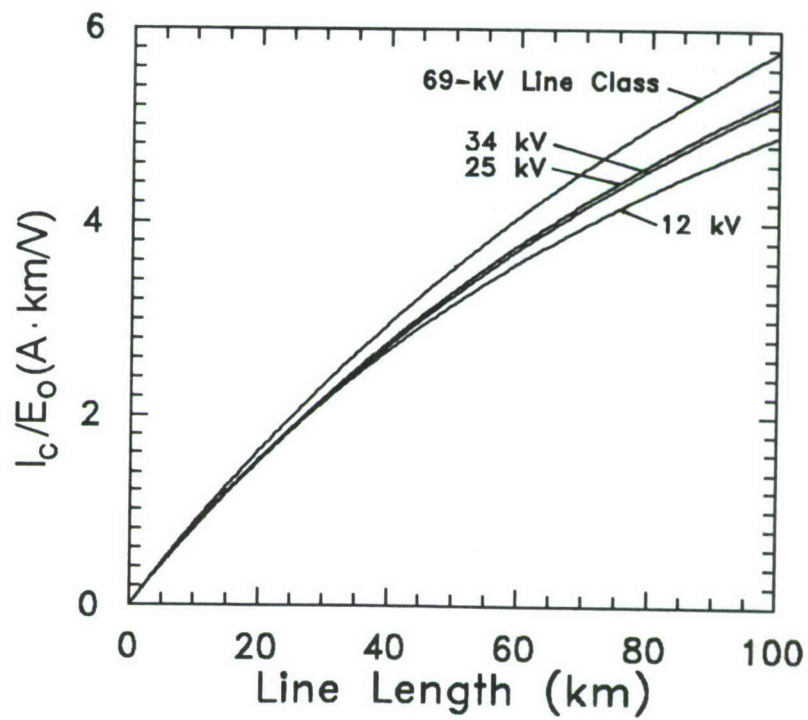


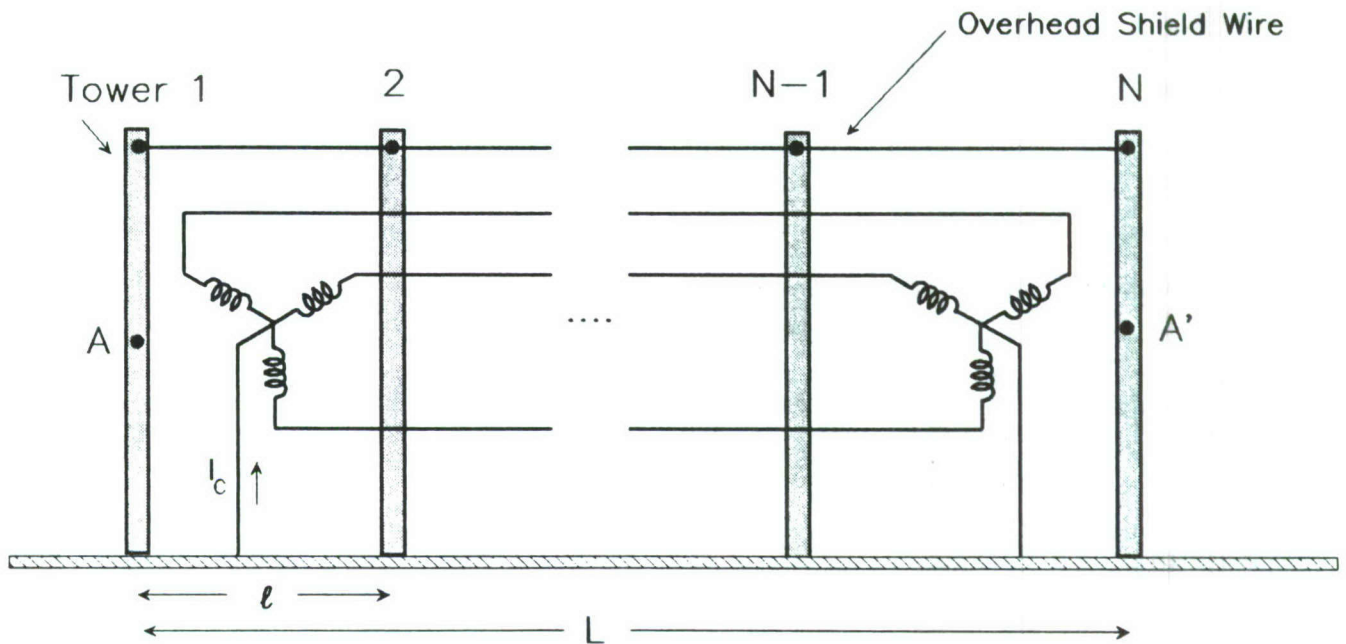
Figure 11. MHD-EMP-Induced Current for Subtransmission and Distribution Lines (Case 3 - Stake Grounding at One End and Substation Grounding at the Other).

3.2 Considerations for Shielded Lines

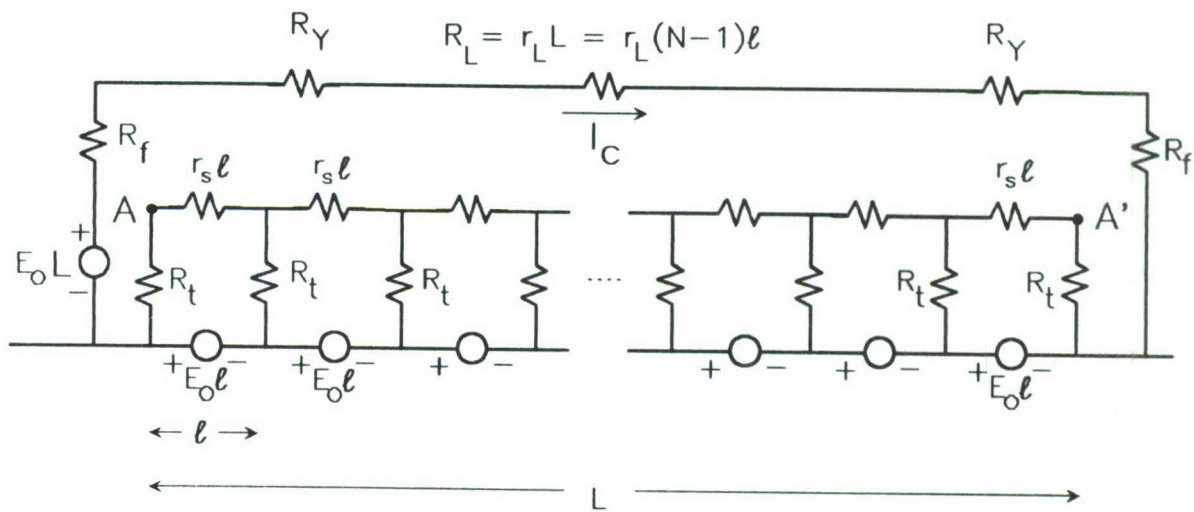
A frequent practice with long transmission lines is to include one or more overhead shield conductors for lightning protection. Typically, these conductors are smaller than the power phase conductors; consequently, they have a larger per-unit-length resistance. These conductors are grounded at each tower, providing a conducting path to local ground. The MHD-EMP earth-induced E-field can also induce currents in these shield wires, and if the 3-phase power system is connected in some manner to the shield system, these currents can influence the level of current flowing in the transformer neutrals.

Consider first the case of support towers and an overhead shield wire added to the 3-phase line previously shown in Figure 8a. The overall line length L has N support towers, with a distance l between them. The phase conductors are supported by the towers, but do not have electrical connections to them. An overhead shield wire having a per-unit-length resistance of $r_s \Omega/\text{km}$ is connected electrically to the towers, and each tower is assumed to have a grounding resistance through the earth of $R_t \Omega$. In this example, the transformer neutrals are assumed to be connected to the earth through a grounding resistance R_f at a point other than the end support tower. This line configuration is illustrated in Figure 12a.

The equivalent circuit for this line configuration is shown in Figure 12b. The $N-1$ loops, or cells, in the part of the circuit representing the shielding line are caused by the sections of line between each of the towers. An induced voltage source of magnitude $E_o l$ volts and a shield wire resistance of $r_s l \Omega$ exist in each cell. The portion of the circuit representing the combined 3-phase conductors is the same as that of Figure 8b. Because the phase conductor line and the shield wire/tower line are assumed to be connected to the earth independently, there is no interaction between the two parts of the line. Consequently, the determination of the induced line current I_c proceeds as discussed earlier, using Eq. (6).



a. Physical Line Configuration



b. Electrical Circuit Model

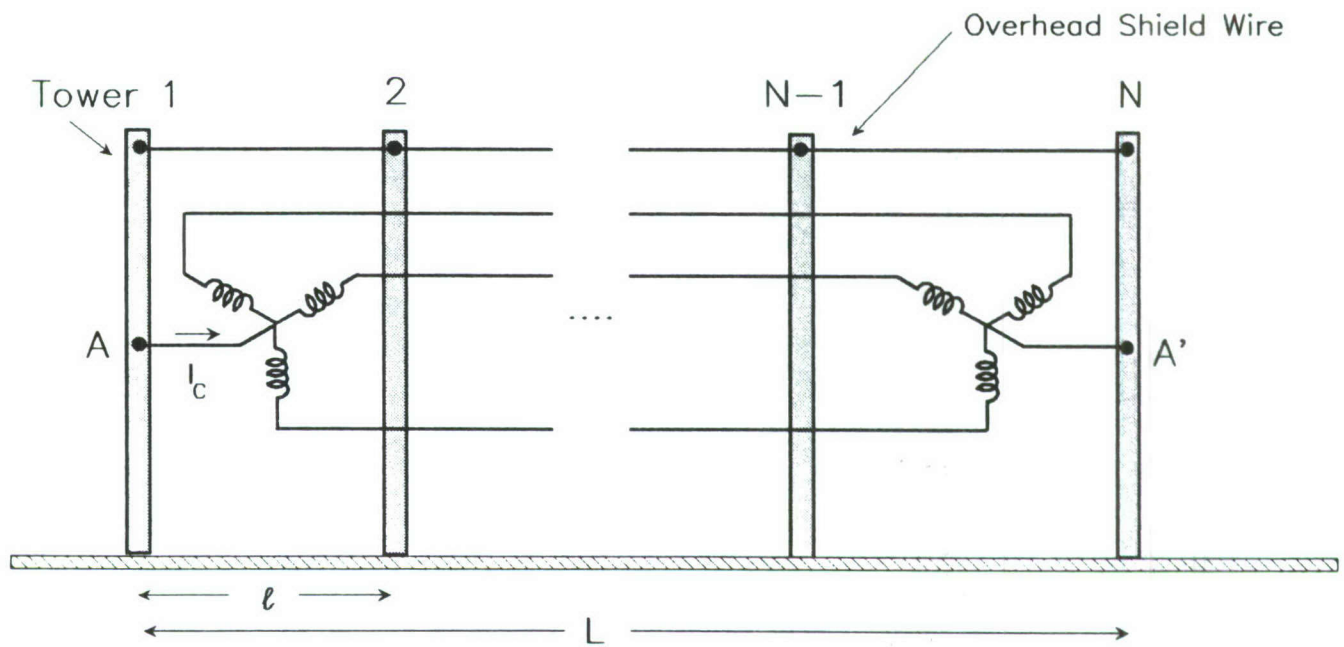
Figure 12. Three-Phase Line with N Towers and Overhead Shield Wires Not Electrically Connected.

The decoupling of the phase conductor and shield line responses is based on the electrical isolation of the grounding resistances at the ends of the lines. In Figure 12a, the grounding resistances are shown as being completely isolated, a condition that is true only if the transformer ground is located far away from the end tower ground. When the transformer neutral ground is in close proximity to the end tower, however, there can be a mutual interaction between the two grounding resistances. This interaction may be modeled using a mutual resistance between the two parts of the circuit, as described by Sunde [7]. The effect on such mutual coupling will be to reduce the levels of the induced current in the transformer. Thus, considering the isolated (or unshielded) line provides a worst-case estimate of the response for these shielded lines.

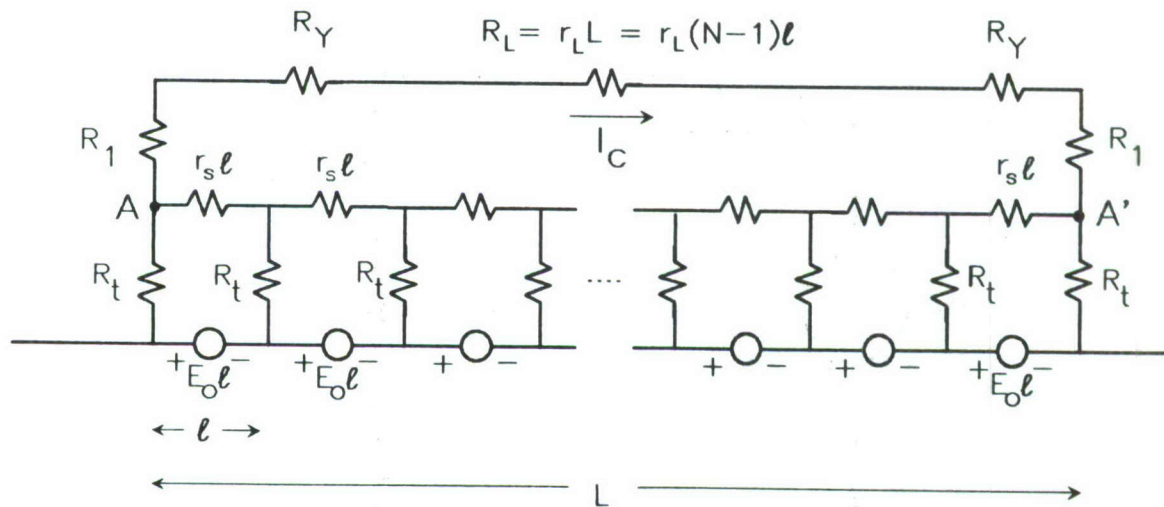
Another possible shielded line configuration is shown in Figure 13a, where the transformer neutral is connected to the tower grounds at locations A and A'. In this configuration, the 3-phase section of the line and the shield wire circuit are tightly coupled, and the transformer current response, I_c , will be greatly influenced by the towers and their grounding impedances. Figure 13b shows the equivalent circuit for this line. The connection between the transformer neutral and the tower ground is represented by the resistance element R_1 in this figure, although this resistance is generally very small and is usually neglected.

In principle, the determination of the current I_c is a straightforward task using circuit analysis. Unfortunately, for more than two of these towers, obtaining an analytic expression for the current is not feasible, due to the complexity of the circuit. As a result, the response must be obtained using numerical methods, and must be displayed parametrically. This may be accomplished by first isolating the effect of the source excitations, the towers, and the shield wire as an equivalent Thevenin circuit seen from the terminals A and A'. This is illustrated in Figure 14a. Once the open circuit voltage, V_{oc} , and the input resistance, R_{in} , are determined, the current I_c can be determined using Figure 14b as

$$I_c = \frac{V_{oc}}{R_{in} + 2(R_1 + R_y) + r_L L} . \quad (7)$$

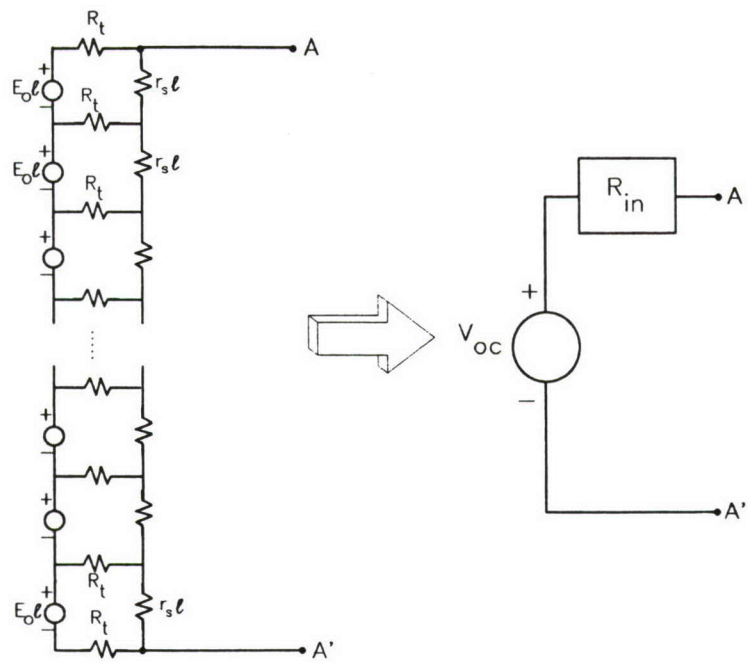


a. Physical Line Configuration

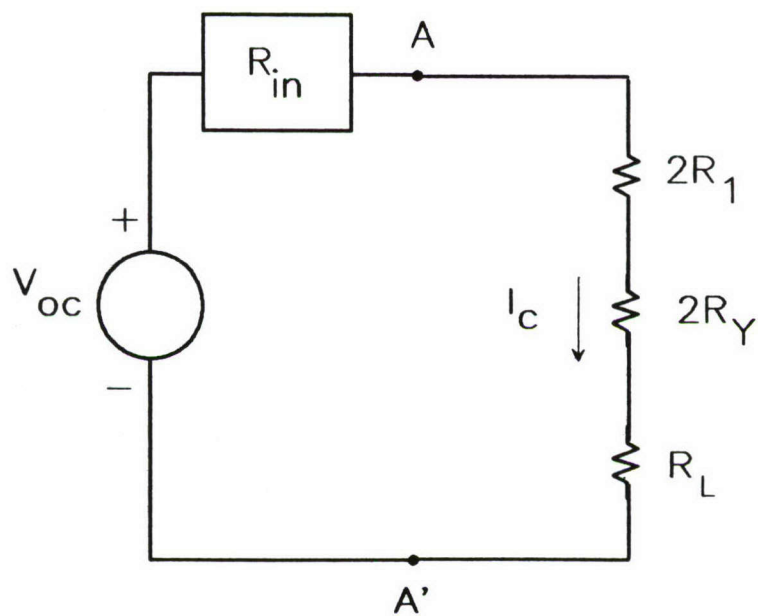


b. Electrical Circuit Model

Figure 13. Three-Phase Line with N Towers and Overhead Shield Wires with Interconnected Grounds.



a. Equivalent Circuit at Terminals A-A'



b. Response Circuit for I_c

Figure 14. Analysis Procedure for the Current I_c .

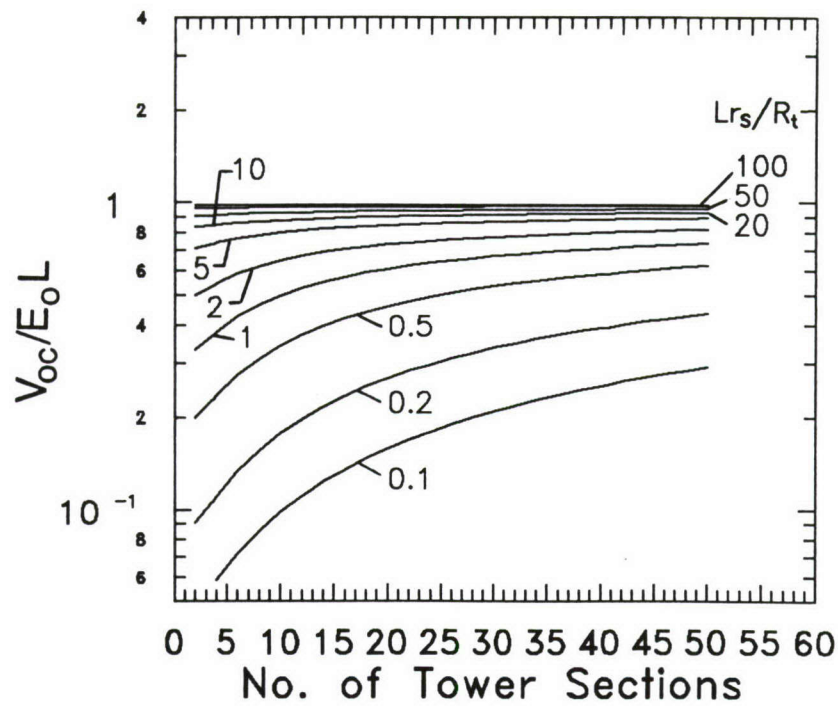
3.2.1 Solution for a Small Number of Towers

The determination of V_{oc} and R_{in} for the equivalent circuit of the tower shown in Figure 14a can be accomplished using mesh circuit analysis [8]. For N towers, this results in an $N \times N$ matrix that must be filled and inverted numerically. Two different forcing vectors are used, one for the determination of V_{oc} and the other for Z_{in} .

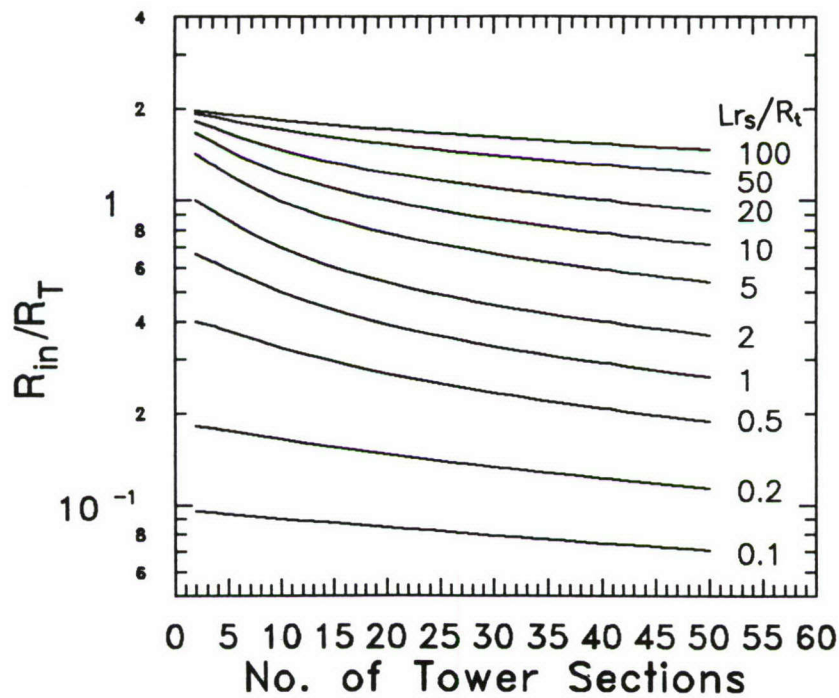
For a moderate number of towers, say on the order of 100 or less, the solution of the circuit equations is possible with minimal computer resources such as a desk-top computer. Figure 15a shows the results of computing the normalized open circuit voltage $V_{oc}/E_0 L$ as a function of the number of tower sections (i.e., the number of towers minus 1). This voltage is shown for a range of different values of the dimensionless parametric ratio $r_s L/R_t$, which covers a wide variety of different circuit element values. As a result of the normalization, the maximum value of the open-circuit voltage response is unity, and the effects of the shield line and towers serve to reduce the effective voltage exciting the 3-phase conductors. Note that in the limiting case of the tower resistance R_t approaching zero, the parameter $r_s L/R_t$ becomes large, and the normalized excitation voltage is unity, with no effect of the overhead shield wires.

The input impedance for the equivalent circuit in Figure 14a is shown in Figure 15b, also in a normalized form as R_{in}/R_t . Input impedance is also plotted as a function of the number of tower sections, with the factor $r_s L/R_t$ as a parameter. Note that for all cases the presence of this R_{in} impedance element in the response circuit of Figure 14b will tend to reduce the induced current response levels from that of the isolated 3-phase line.

The presence of the overhead shield wire system is seen to affect the induced current flowing into the transformer neutrals in two ways: by decreasing the effective voltage source exciting this current, and by increasing the resistance seen at the source. In both cases, the overall effect is to reduce the net flow of MHD-EMP-induced current.



a. Normalized Thevenin Voltage



b. Normalized Input Resistance

Figure 15. Behavior of the Equivalent Circuit at A and A' for Different Numbers of Tower Sections, Using Circuit Analysis.

The values of V_{oc} and Z_{in} in Figure 15 can be used to compute the current induced in the transformer neutrals using Eq. (7). Figure 16 is a contour plot of the normalized current I_c/E_0 for the 138-kV line discussed in the previous section. The transformer and line resistance values used are those in Table 1, and an assumed tower footing resistance of $R_t = 25 \Omega$ was used. This plot shows possible current responses for any combination of line length and number of tower sections for line lengths 1000 km or less, or for 94 line sections or less.

In this plot, several general trends are noted. For a line of fixed length, adding more grounded tower supports is seen to increase the coupled current response. This is due to the fact that as more tower impedance elements are added in parallel to the shielding part of the circuit, the effective input impedance, Z_{in} , is reduced. For the case of a fixed number of towers and an increasing line length, the effective excitation voltage increases due to the longer collection length of the line. Consequently, the induced current also increases. With any combination of length and number of towers, however, the induced current is lower than that which would exist without the shielding structure.

3.2.2 Solution for a Large Number of Towers

Practical transmission or distribution lines have support tower spacings that are relatively small compared with the overall line length. For example, the 138-kV line previously discussed has a typical tower span of 900 ft. (274.3 m); thus, for a 250-km line, approximately 910 towers would be present. Clearly the data presented in Figure 16 will not be adequate for predicting the line responses in this case. Moreover, if the circuit analysis approach were used to compute the V_{oc} and Z_{in} quantities directly, large computer resources would be required. To treat the problem of a 1000-km line with about 3650 towers, the solution of a 3650×3650 matrix equation would be required, which would pose practical problems. What is required is an alternate model for a large number of towers.

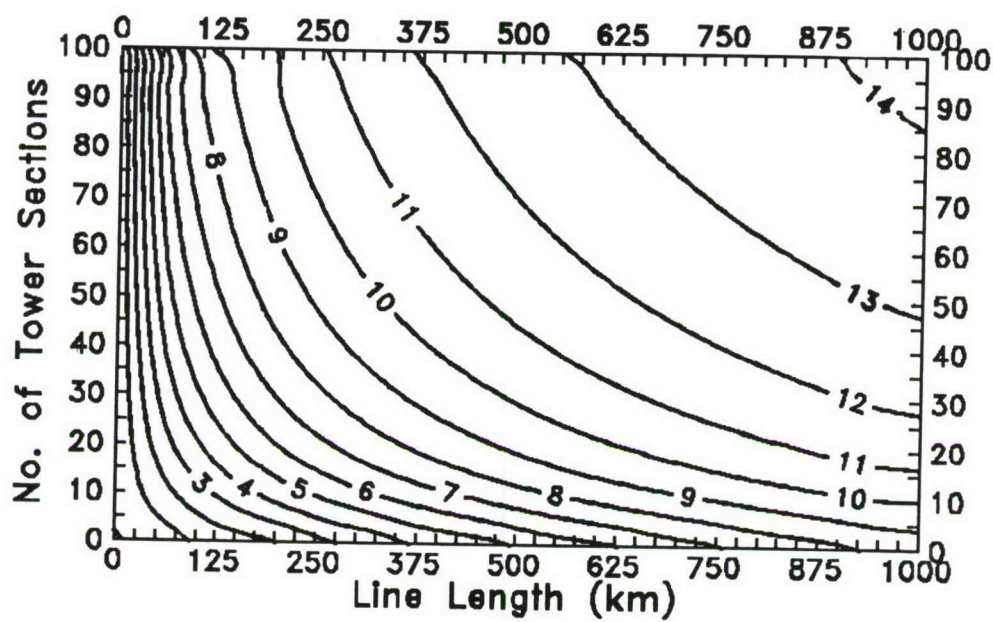


Figure 16. Contours of Normalized MHD-EMP-Induced Current I_c/E_0 (A·km/V) for the Shielded 138-kV Line, Using the Circuit Model.

To conduct an analysis for a large number of towers, it is possible to consider the tower effects as being distributed along the length of the line, not as being individual lumped elements. This is done by defining a per-unit-length tower conductance of

$$g_t = NG_t/L = N/(R_t L) \quad (8)$$

where N is the number of towers. This conductance may be used along with the per-unit-length resistance of the shield conductor r_s to derive a set of coupled differential equations for the current and voltage distributions along the shield conductor. Figure 17 shows this continuously loaded line running from terminal A at $x = 0$ to terminal A' at $x = L$. At an arbitrary point on the line, the line is considered to be made of the differential ladder circuit shown in this figure. By writing the Kirchoff voltage and current equations for this line section and taking the limit of $dx \rightarrow 0$, we derive the following set of differential equations:

$$\frac{dV}{dx} + r_s I(x) = E_o \quad (9a)$$

and

$$\frac{dI}{dx} + g_t V(x) = 0 \quad (9b)$$

To obtain a solution for $V(x)$ at any point along the structure, we must first consider the solution of the homogeneous versions of these equations. These can be manipulated into uncoupled, second-order differential equations of the form

$$\frac{\partial^2 V}{\partial x^2} - \alpha^2 V(x) = 0 \quad (10a)$$

and

$$\frac{\partial^2 I}{\partial x^2} - \alpha^2 I(x) = 0 \quad (10b)$$

where the constant α has the value

$$\alpha = \sqrt{r_s g_t} \quad (11)$$

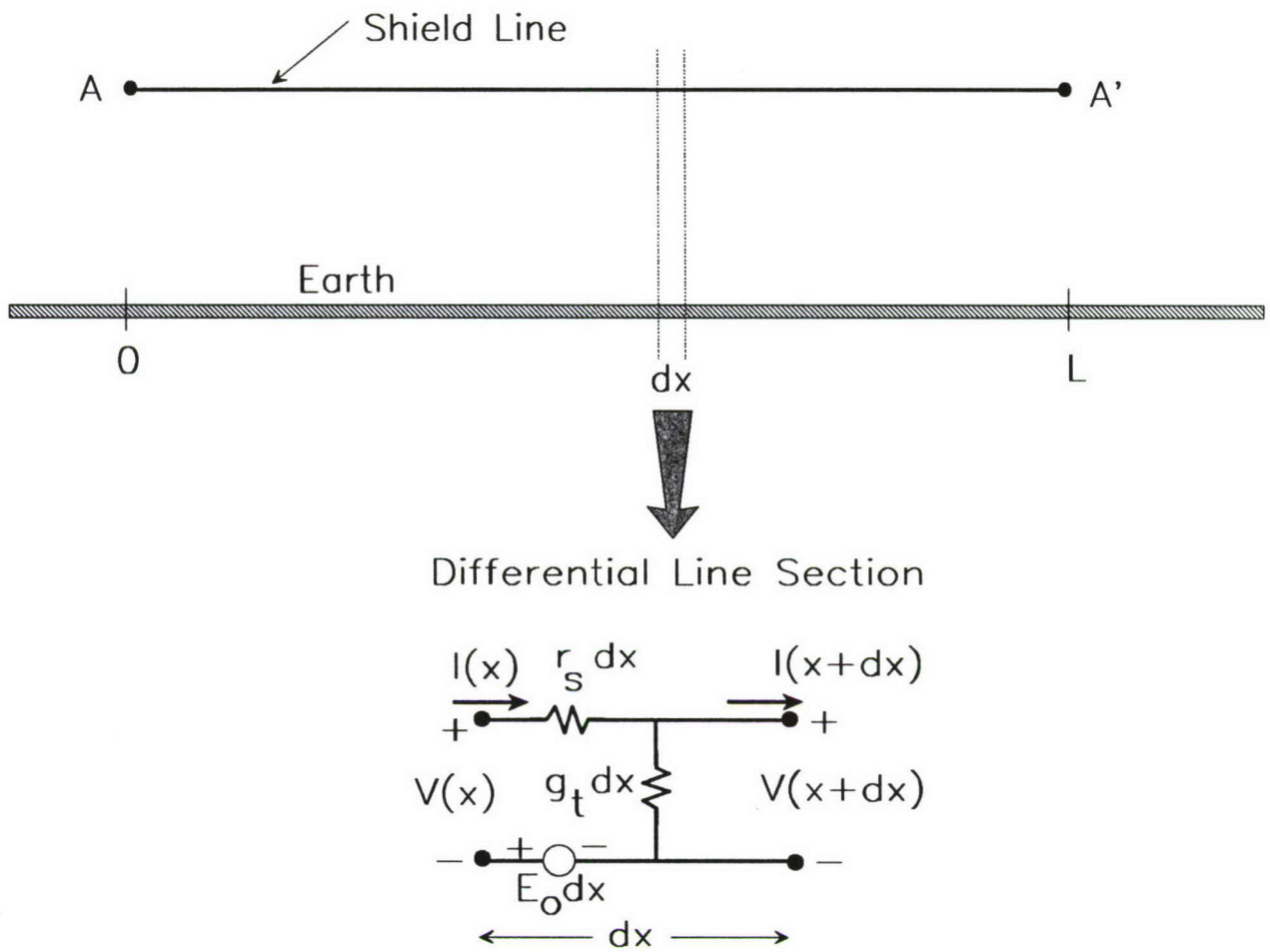


Figure 17. Continuous Model of the Overhead Shield Wire and Tower Supports.

The solutions to Eqs.(9a) and (9b) have the general form

$$V(x) = a e^{-\alpha x} + b e^{+\alpha x} \quad (12a)$$

and

$$I(x) = \frac{a}{R} e^{-\alpha x} - \frac{b}{R} e^{-\alpha x}, \quad (12b)$$

where the constant R has dimensions of resistance and is defined as

$$R = \sqrt{r_s/g_t}. \quad (13)$$

The constants a and b are determined by the boundary conditions at $x = 0$ and L , and by the excitation term E_0 .

As a practical matter, a realistic power line does not always have all towers spaced uniformly. However, this analysis is based on the averaged effects of the tower connections to the earth, and effects such as non-uniform spacing become unimportant as the number of towers becomes large.

3.2.2.1 Determination of V_{oc}

A particularly useful solution to these equations is the Green's function [9], which is the response of the line due to a single excitation of the form $E_0 = V_s \delta(x-x_s)$. This expression corresponds to a single voltage source of strength V_s located at $x = x_s$. Once this generalized solution is obtained, the solution to an arbitrary distribution of excitation sources may be obtained by integration. Because the current on the shield at points A and A' is zero, it is possible to derive the following Green's function for the voltage response:

$$G(x;x_s) = \frac{1}{2} V_s \frac{e^{-\alpha x} + e^{\alpha(x-2L)}}{(1 - e^{-2\alpha L})} (e^{\alpha x_s} - e^{-\alpha x_s}) \quad (14a)$$

for the observation point $x > x_s$, and

$$G(x;x_s) = -\frac{1}{2} V_s \frac{e^{\alpha(x-L)} + e^{-\alpha(x+L)}}{(1 - e^{-2\alpha L})} (e^{\alpha(L-x_s)} - e^{-\alpha(L-x_s)}) \quad (14b)$$

for $x < x_s$.

The excitation of the shield line running from 0 to L is due to the uniformly distributed voltage sources $E_0 dx$. Using our Green's function, the solution for the complete line voltage at any point is expressed as

$$V(x) = \int_0^L G(x;x_s) E_0 dx_s \quad (15)$$

This integral may be integrated analytically for G given in Eq. (14) to yield the following solution for the voltage:

$$V(x) = \frac{E_0}{2\alpha} \frac{1}{(1 - e^{-2\alpha L})} \left[\left[1 + e^{-2\alpha(L-x)} \right] \left[(1 - e^{-\alpha x}) + e^{-2\alpha x} (1 - e^{+\alpha x}) \right] \right. \\ \left. - \left[1 + e^{-2\alpha x} \right] \left[(1 - e^{-\alpha(L-x)}) + e^{-2\alpha(L-x)} (1 - e^{+\alpha(L-x)}) \right] \right] \quad (16)$$

Evaluating this expression at the end points of the line at A' and A gives

$$V(L) = \frac{E_0}{\alpha} \frac{(1 - e^{-\alpha L})^2}{(1 - e^{-2\alpha L})} \quad (17a)$$

and

$$V(0) = -V(L) \quad (17b)$$

These are the line-to-earth voltages. What is needed for the Thevenin circuit voltage is the voltage between these points, which is the V_{oc} quantity shown in Figure 14a. By applying Kirchoff's voltage law to the loop $A-0-L-A'$ in Figure 17, the open circuit voltage may be expressed as

$$V_{oc} = E_o L + V(0) - V(L) \quad (18a)$$

or

$$V_{oc} = E_o L \left(1 - \frac{2}{\alpha L} \frac{(1 - e^{-\alpha L})^2}{(1 - e^{-2\alpha L})} \right) \quad (18b)$$

3.2.2.2 Determination of R_{in}

The input resistance between terminals A and A' is also needed for this analysis. At these terminals, the line of Figure 17 can be represented by the generalized 2-port circuit shown in Figure 18.

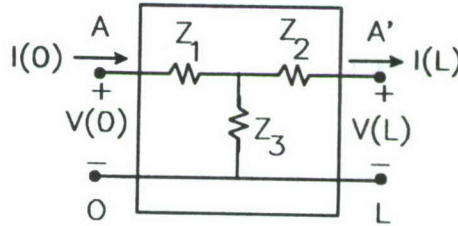


Figure 18. Two-Port Representation of the Shield Line Between Points A and A'.

This circuit can be represented by the open circuit impedance parameter matrix [10] of the form

$$\begin{bmatrix} V_1 \\ V_2 \end{bmatrix} = \begin{bmatrix} z_{11} & z_{12} \\ z_{21} & z_{22} \end{bmatrix} \begin{bmatrix} I_1 \\ I_2 \end{bmatrix} \quad (19)$$

where $z_{12} = z_{21}$ by reciprocity, and $z_{11} = z_{22}$ by structural symmetry. The impedance elements in Figure 18 are related to the impedance parameters in Eq. (19) by

$$Z_1 = Z_2 = z_{11} - z_{12} \quad (20a)$$

and

$$Z_3 = z_{12} \quad (20b)$$

The net resistance between A and A' when both of their terminals are open circuited is immediately seen to be

$$R_{in} = Z_1 + Z_2 = 2 (z_{11} - z_{12}) \quad (21)$$

The impedance parameters z_{11} and z_{12} for the line may be calculated by placing a voltage source V_1 at terminals A-O of Figure 18 and computing the input current I_1 and the transfer voltage V_2 with the open circuit condition $I_2 = 0$ at terminal A'-L. Using Eq. (12) with the end condition that $I(L) = 0$, the following solutions for $V(x)$ and $I(x)$ are obtained for the case of a lumped voltage excitation of V_1 at $x = 0$:

$$V(x) = \frac{V_1}{(1 - e^{-2\alpha L})} (e^{-\alpha x} + e^{-2\alpha L} e^{\alpha x}) \quad (22a)$$

and

$$I(x) = \frac{V_1}{R(1 - e^{-2\alpha L})} (e^{-\alpha x} - e^{-2\alpha L} e^{\alpha x}) \quad (22b)$$

Thus, z_{11} and z_{12} may be evaluated as follows;

$$z_{11} = \left. \frac{V(0)}{I(0)} \right|_{I(L)=0} = R \frac{(1 + e^{-2\alpha L})}{(1 - e^{-2\alpha L})} \quad (23a)$$

and

$$z_{12} = z_{21} = \left. \frac{V(L)}{I(0)} \right|_{I(L)=0} = \frac{2R e^{-\alpha L}}{(1 - e^{-2\alpha L})} \quad (23b)$$

Combining Eqs. (23a) and (23b) with Eq.(21) thus gives the following expression for the input resistance:

$$R_{in} = 2R \frac{(1 - e^{-\alpha L})^2}{(1 - e^{-2\alpha L})} \quad (24)$$

3.2.3 Sample Line Responses

Equations (18b) and (24) are the Thevenin equivalent circuit parameters for the circuit between A and A' for the case of a large number of towers. For small values of N these results should agree with the results of the lumped circuit analysis discussed in the previous section. Both of the parameters αL and R in Eqs. (18b) and (24) may be written in terms of the dimensionless parameter $r_s L/R_t$ used in Figure 15 as

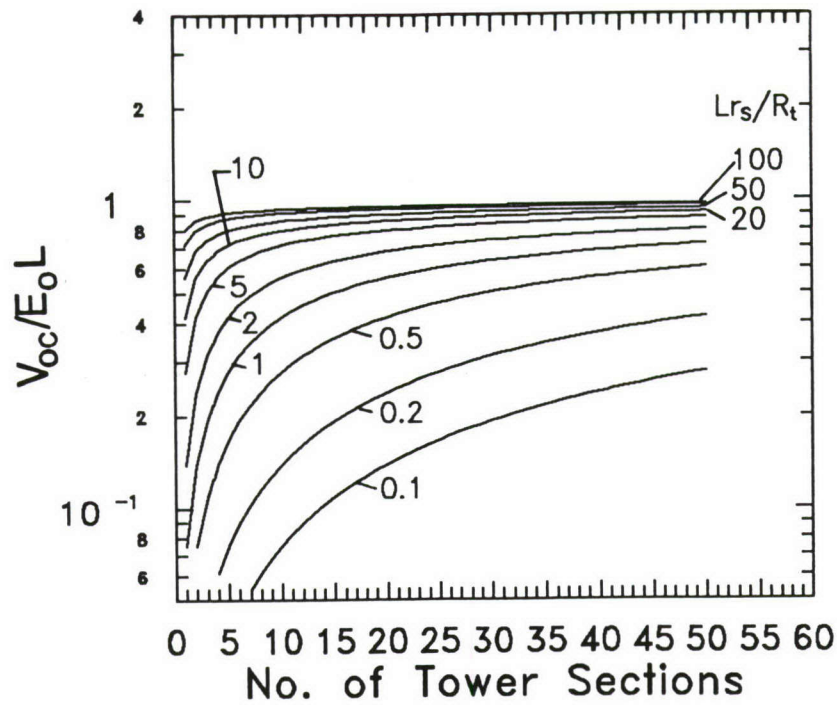
$$\alpha L = \sqrt{N \frac{r_s L}{R_t}} \quad (25)$$

and

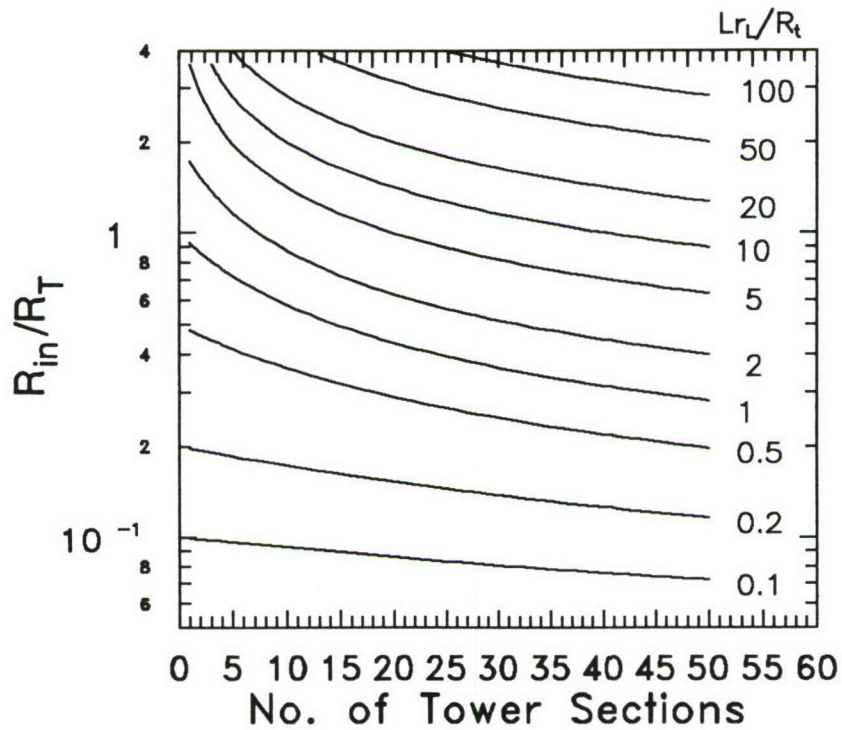
$$R = R_t \sqrt{\frac{1}{N} \frac{r_s L}{R_t}} \quad (26)$$

Figure 19a presents the normalized quantity $V_{oc}/E_o L$ from Eq. (18b) as a function of the number of line sections (N-1) with the factor $r_s L/R_t$ as a parameter. These data compare very well with the discrete-line model results in Figure 15a. Figure 19b presents the input resistance data for the same case using Eq. (24). For low values of the factor $r_s L/R_t$, these plots agree very well with those in Figure 15b. However, as this factor increases, there is a slight difference between the discrete and the continuous models.

As another check of the validity of the formulation for the continuous line model, the calculation of the current in the 138-kV line discussed previously is presented in Figure 20 for up to 94 tower sections. This calculation compares very well with that in Figure 16, showing the same family of responses using the discrete circuit model. Note the differences in the curves occurring for small values (i.e., on the order of 10 to 20) of tower sections where the continuous model is not valid.



a. Normalized Thevenin Voltage



b. Normalized Input Resistance

Figure 19. Behavior of the Equivalent Circuit at A and A' for Different Numbers of Tower Sections, Using the Continuous Model.

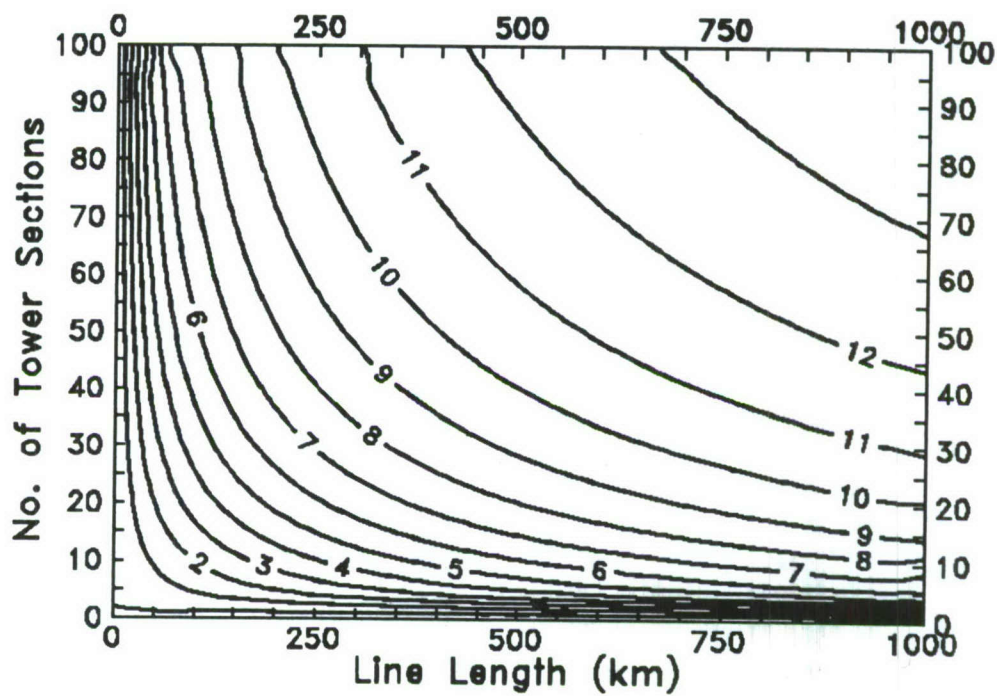


Figure 20. Contours of Normalized MHD-EMP-Induced Current I_c/E_0 (A·km/V) for the Shielded 138-kV Line, Using the Continuous Model.

By way of comparing calculation times for the results in Figures 16 and 20, the lumped circuit model required about 12 hours of CPU time on an 80386/80387 computer running at 33 MHz. The distributed circuit model, however, required only about 30 seconds for the same set of calculations, and this time does not increase as the number of tower sections increases. Therefore, this model is useful for treating the more realistic case of several thousand towers on the line.

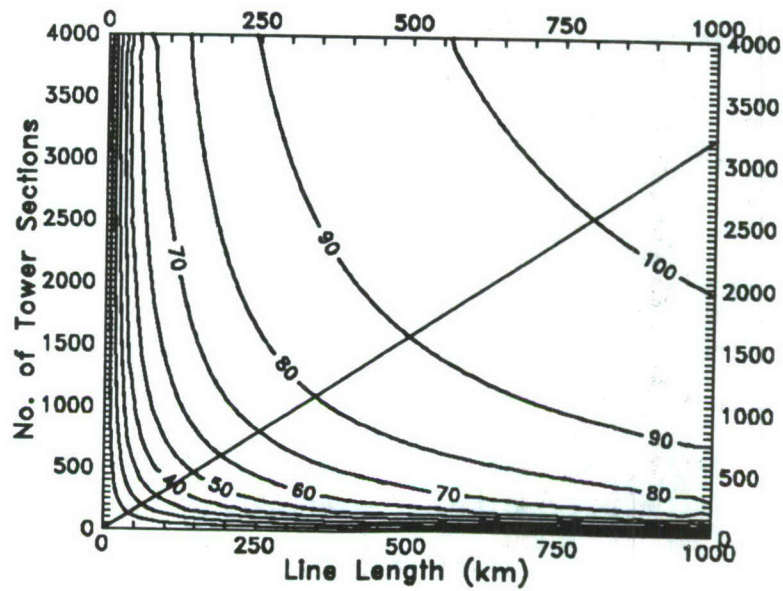
To provide a further indication of the MHD-EMP responses for shielded lines, a set of calculations for the 7 different voltage classes of transmission and distribution lines analyzed previously have been considered. Table 4 presents typical tower span distances for these lines, the assumed tower footing resistance (R_t), the longest length of line and the number of towers in that length (longest L and N), and the resulting per-unit-length tower conductance parameter (g_t).

Table 4

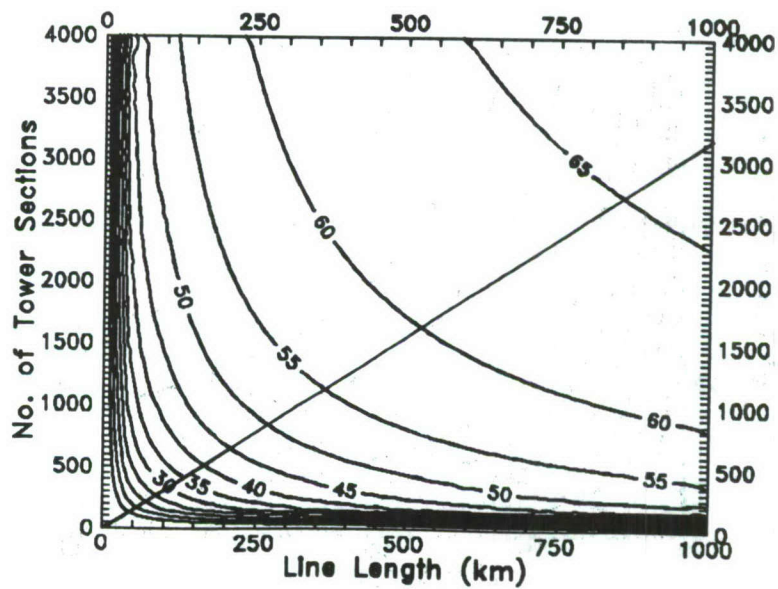
Parameters for Shielded Line Analysis

Voltage Class (kV)	Span (m)	R_t (Ω)	Longest L (km)	N	g_t (mhos/km)
12	60.90	50	100	1642	0.328
25	76.20	50	100	1312	0.262
34	91.40	50	100	1094	0.219
69	152.4	50	100	656	0.131
138	274.3	25	1000	3645	0.146
345	304.8	25	1000	3280	0.131
500	304.8	25	1000	3280	0.131

Using the distributed tower model, we have calculated the MHD-EMP-induced current in the above 7 classes of shielded lines. Tables 1, 2, and 4 summarize the parameters used for each line. Figures 21a-g show the contours of the normalized transformer neutral current I_c/E_o for various combinations of line length and number of tower sections. The straight line in each of these figures represents the locus of points corresponding to the tower span lengths given in Table 4 above. Other span lengths would be represented by similar straight lines having different slopes.

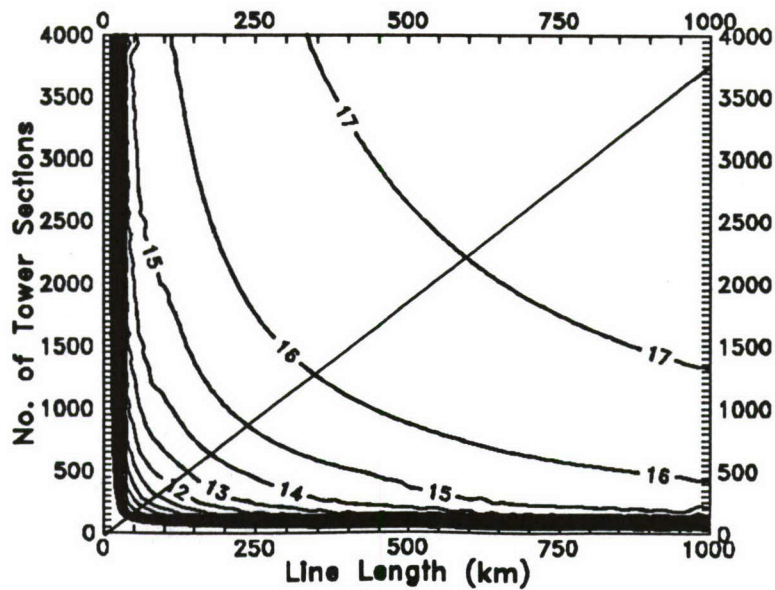


a. 500-kV Class Line

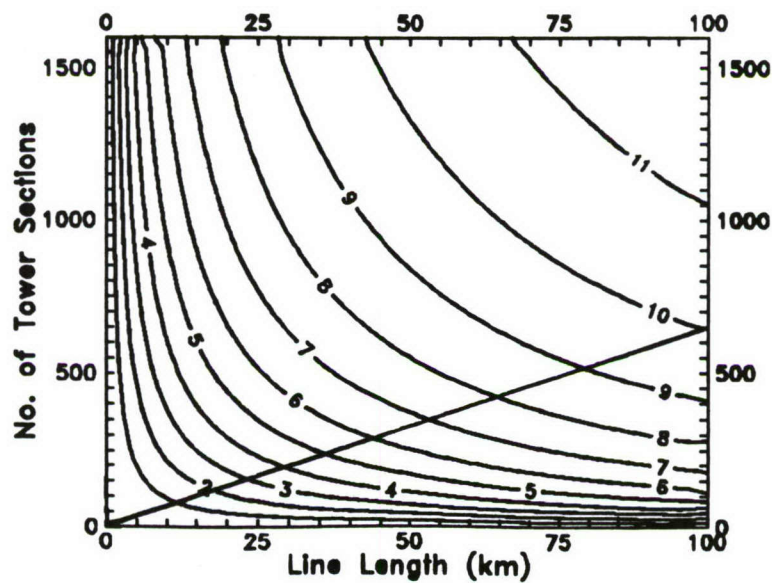


b. 345-kV Class Line

Figure 21. Contours of Normalized MHD-EMP-Induced Current I_c/E_0 ($A \cdot km/V$) for Lines with Grounded Shield Wires.

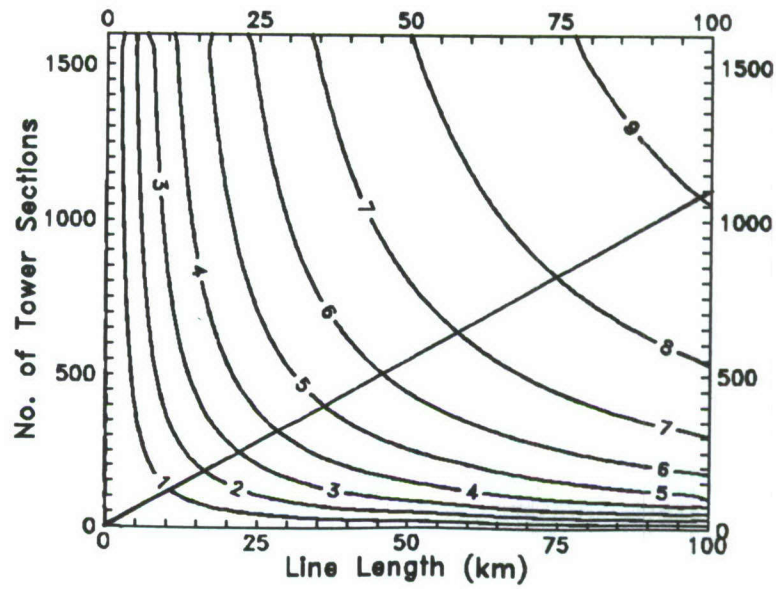


c. 138-kV Class Line

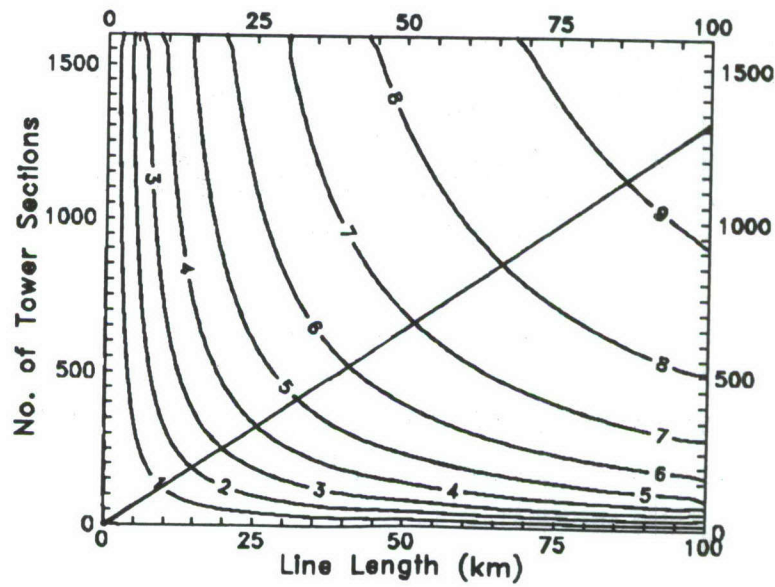


d. 69-kV Class Line

Figure 21. Contours of Normalized MHD-EMP-Induced Current I_c/E_0 ($A \cdot km/V$) for Lines with Grounded Shield Wires (Con't).

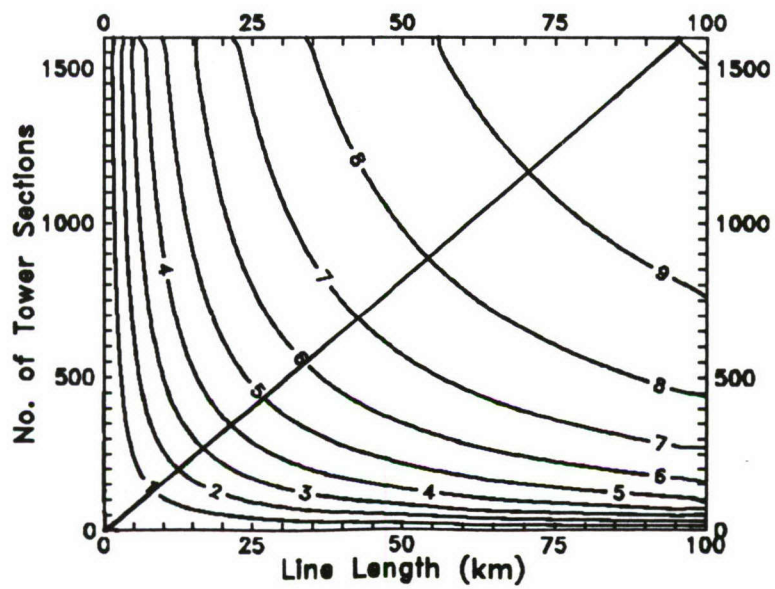


e. 34-kV Class Line



f. 25-kV Class Line

Figure 21. Contours of Normalized MHD-EMP-Induced Current I_c/E_0 ($A \cdot km/V$) for Lines with Periodically Grounded Neutrals (Con't).



g. 12-kV Class Line

Figure 21. Contours of Normalized MHD-EMP-Induced Current I_c/E_0 (A·km/V) for Lines with Periodically Grounded Neutrals (Concluded).

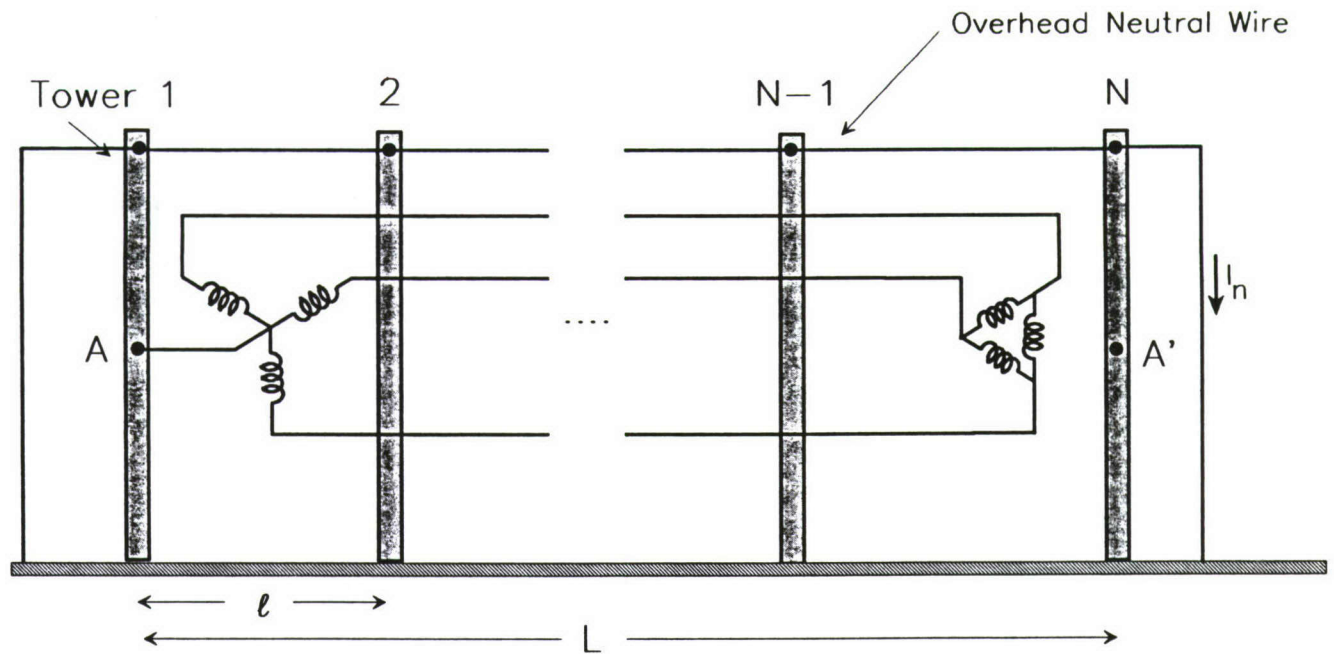
3.3 Induced Current on Grounded Neutral Conductors

Judging from the dc circuit models developed in the previous sections, we can see one way of mitigating the effects of the MHD-EMP environment on the power system is to use an ungrounded Δ transformer at one end of the transmission line, as shown in Figure 22a. Because there is no dc path to ground through this transformer, there will be no dc current flow through the transformer windings. Consequently, no adverse effects on the transformer will be noted.

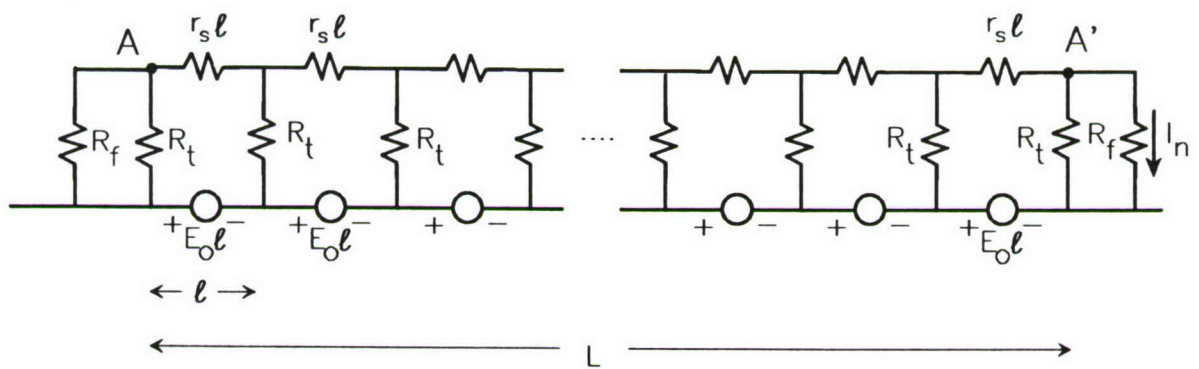
An MHD-EMP electric field, however, can interact with the periodically grounded neutral conductor to produce a net current in the neutral conductor. This current is denoted by I_n in Figure 22a. If the neutral conductor is connected to the ground far from the facility at the end of the line, there will be no adverse effect on the operation of internal power equipment. However, if the neutral conductor penetrates into the facility, there will be an injection of the MHD-EMP current into the facility. The effect of this current on the equipment within the facility will depend on the electrical connectivity of the ground conductor and the other internal equipment. Consequently, the effect cannot be predicted without detailed system information.

It is useful to predict the possible levels of the MHD-EMP current which could be injected into a facility by the grounded neutral conductor. Figure 22b shows an equivalent circuit useful for describing the current. This circuit is similar to that in Figure 12b except it has the phase conductors removed and two additional resistances added at each end of the periodically grounded line. These resistances are denoted by R_f and represent the footing resistance of the neutral conductors to the earth. The other circuit parameters are the same as in Figure 12b.

The determination of the current flowing in the neutral line to ground, I_n , may be evaluated either by using dc circuit analysis or by using the analytical model discussed in the previous section. As in the previous examples, the circuit analysis is feasible only for a small number of tower sections, with the analytical solution being better suited for the case of many towers.



a. Physical Line Configuration



b. Electrical Circuit Model

Figure 22. Three-Phase Line with Un-Grounded Δ Transformer and Periodically Grounded Neutral Conductor.

Using the expressions for the voltage and current on the overhead neutral wire given in Eqs. (12a) and (12b), along with the loading of the line by R_f at each end, the following analytical expression for the neutral current, I_n , can be developed:

$$I_n = \frac{E_o L (1 - e^{-\alpha L})^2}{r_s L (1 - e^{-\alpha L})^2 + \alpha L R_f (1 - e^{-2\alpha L})} \quad (27)$$

where the parameter αL is given by Eq. (25).

There are 6 independent parameters for evaluating this expression: E_o , L , R_f , R_t , r_s , and N . To generalize this result slightly, we can plot the current in the normalized form I_n/E_o as contours in the L - N plane, as was done in Figures 20 and 21. Doing this requires that the remaining 3 parameters be defined. The tower footing resistance is taken to be the same as in the previous study, i.e. $R_t = 25 \Omega$. Similarly, the grounding resistance at each end of the line is assumed to be that of a good substation ground, i.e. $R_f = 0.75 \Omega$. The neutral conductor is assumed to be a #2 stranded aluminum wire with a per-unit-length resistance (r_s) of $0.876 \Omega/\text{km}$.

Figure 23 presents the behavior of the normalized neutral current, as calculated using Eq. (27). As a check of the calculation, the same case was run using the dc circuit analysis, giving virtually identical results. Assuming that this neutral line is similar to that of a 12-kV line having a nominal tower separation distance of 60 m, the straight line on the figure represents the locus of points having this tower separation.

The data in Figure 23 can be viewed in several different ways to give insight into the behavior of the induced current. By taking vertical cuts along the lines of constant line length, a family of curves of the normalized current vs. the number of tower sections may be generated. These are shown in Figure 24.

Figure 25 presents the normalized MHD-EMP current vs. the line length for a different number of tower sections. It is clear that the MHD-EMP current at the end of the line is reduced when the number of tower sections is increased, because of the shunting effect of having a large number of towers.

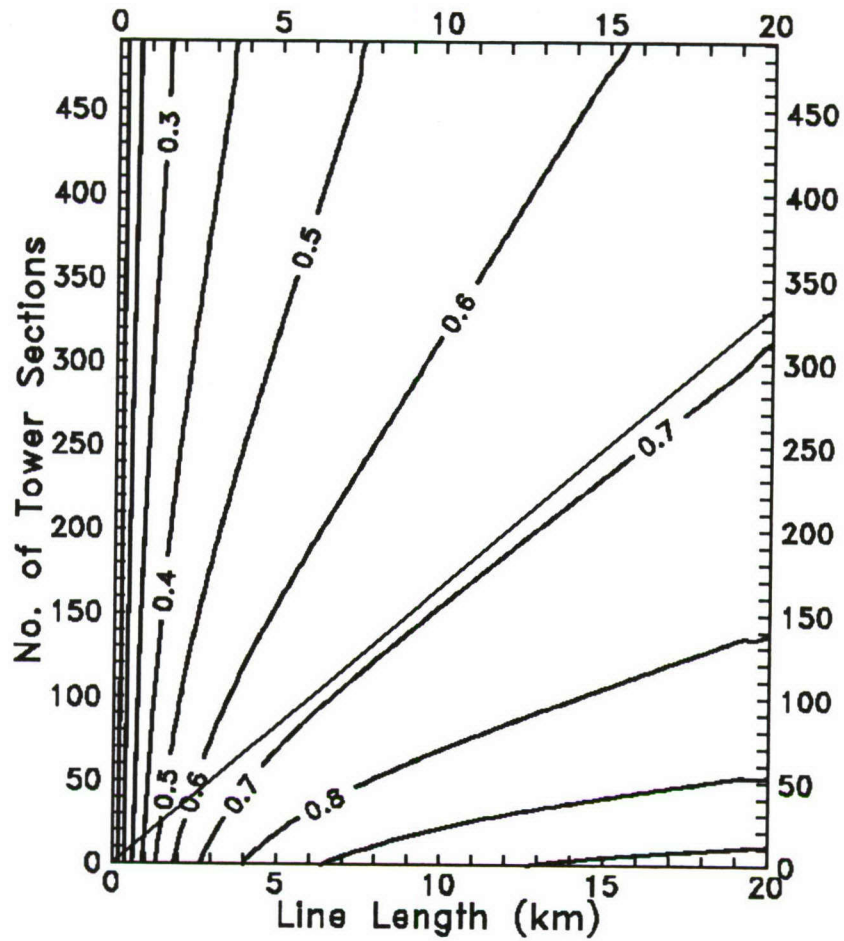


Figure 23. Contours of Normalized MHD-EMP-Induced Current I_n/E_0 ($A \cdot km/V$) at the End of the Periodically Grounded Neutral Conductor.

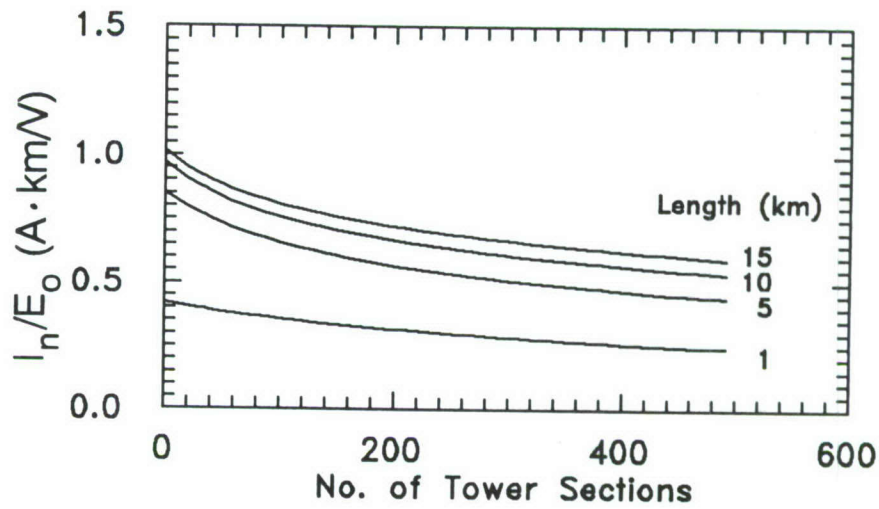


Figure 24. Normalized MHD-EMP-Induced Current vs. Number of Tower Sections for Different Line Lengths.

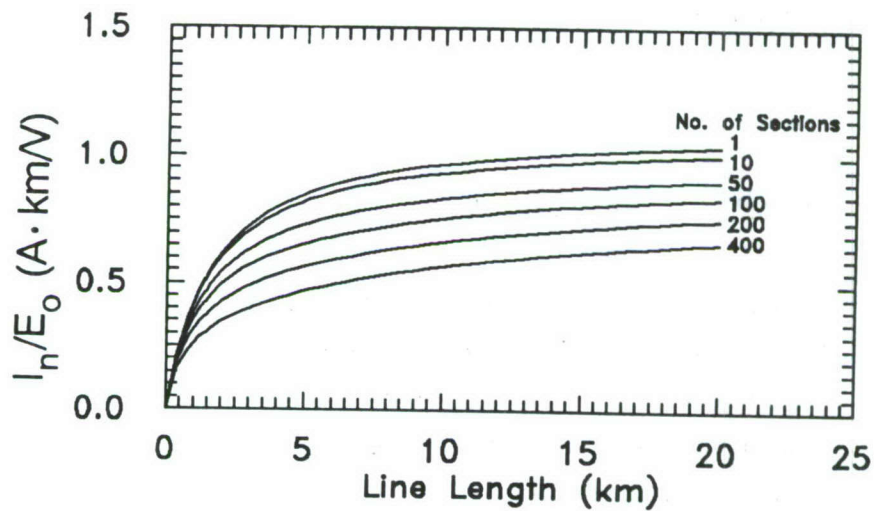


Figure 25. Normalized MHD-EMP-Induced Current vs. Line Length for Different Numbers of Tower Sections.

It is not realistic to increase the tower density on the line too much, however, since there is usually a minimum tower spacing distance permissible for each line class. Figure 26 shows the normalized MHD-EMP current vs. the line length for several different section spacings. The curve marked "60" represents the result for the nominal tower spacing distance of 60 m, while that marked "L" represents the case of only two support towers at each end of the line. There is a reduction of about 30% in the MHD-EMP current induced in the neutral conductor in this case.

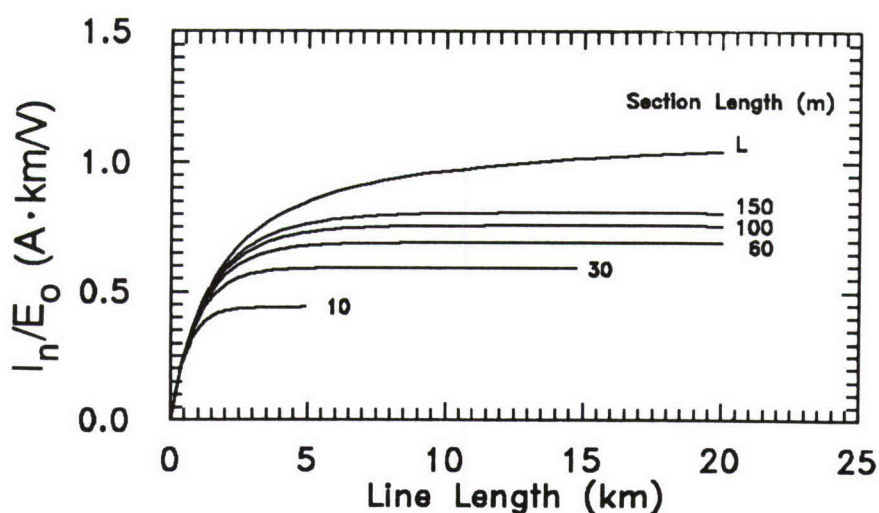


Figure 26. Normalized MHD-EMP-Induced Current vs. Line Length for Different Section Spacings.

3.4 Cumulative Probability Distribution for Line Responses

The induced current responses discussed above are all based on the assumption that the line is oriented in the direction of the maximum E-field, that is to say, in the west-east direction. In any real case, the line could have any direction, and consequently, the induced transformer neutral current would be reduced by a factor $\cos(\phi)$ where ϕ is the angle between the field and the line.

A useful way of describing this effect is to use a cumulative probability distribution [11] which presents the probability that a particular response will exceed a specified value. Figure 27 illustrates this function for the induced peak current, normalized to a maximum value of unity, for the $\cos(\phi)$ field variation.

This figure may be used to provide a rough indication of the probabilities of occurrence of an MHD-EMP response for lines either under or outside the x-ray patch. As previously mentioned, this model neglects the changes in strength of the MHD-EMP E-field outside the shield, as well as the changes in direction of the field. A similar cumulative probability distribution curve could be developed using data from a more detailed MHD-EMP environment calculational model if the E-field environments could be provided at a sufficiently large number of observation locations on the earth.

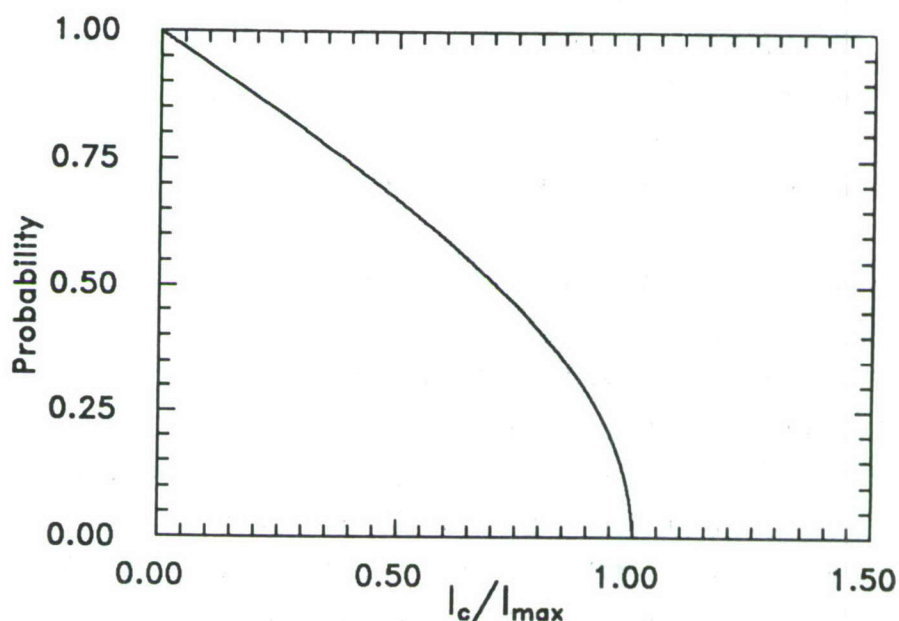


Figure 27. Universal Cumulative Probability Curve for Induced MHD-EMP Current Responses.

4.0 PARAMETRIC STUDY OF MHD-EMP EFFECTS ON A POWER TRANSMISSION SYSTEM

4.1 Introduction

To better illustrate the effects of the MHD-EMP environment on electrical power systems, a parametric analysis [12] was performed on a specific 500-kV power transmission line, using the estimated E_3 environments and the coupling models described in the previous sections. The behavior of the unloaded transformer magnetizing current was analyzed; the results are presented parametrically with respect to the MHD-EMP waveform type and amplitude and the transmission line total length and span length. The system configuration, the analysis overview, and the results of the parametric analysis are all described in more detail in this section.

4.2 Description of the 500-kV Transmission System

The transmission system was based on the Minnesota Power Company 500-kV line between Minneapolis and Dorsey, Minnesota. Specifically, the system consists of a 500-kV transmission line, terminated by three-phase transformer banks at both ends. Figure 28a illustrates a single line diagram of the test system. Pertinent data for this transmission line are listed in Table 5. During normal operation, the sky wires are not electrically connected to the transmission line towers. Tower configuration data specifies the location of the center of each phase bundle and each sky wire with respect to a Cartesian coordinate system with its origin located at the center of the tower base.

Each of the three-phase transformer banks consists of three single-phase transformers connected Δ /grounded Y. The grounded Y side is connected on the 500-kV transmission line (see Figure 28). The characteristics of each single-phase transformer are as follows:

Voltage Rating	115/288 kV
Power Rating	350 MVA
Leakage Reactance	0.10 pu
Magnetizing Current	0.002 pu
Winding Resistance	1.5 Ω

Table 5
Data for 500 kV Transmission Line

General Data

Configuration	3 conductor bundles per phase
Bundle Spacing	18 inches
Earth Resistivity	100 $\Omega \cdot m$

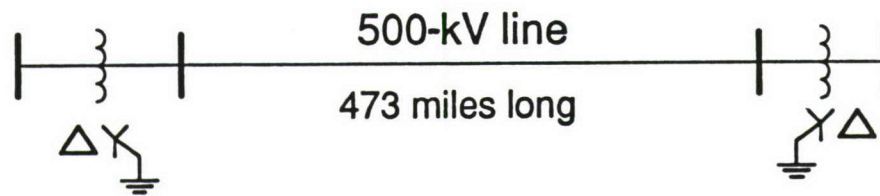
Conductor Data

Conductor	Type	O.D. (inches)	Resistance (Ω/km)
Ground Conductors	7/16 steel	0.4375	2.76
Phase Conductors	1192 ACSR	1.3020	0.05

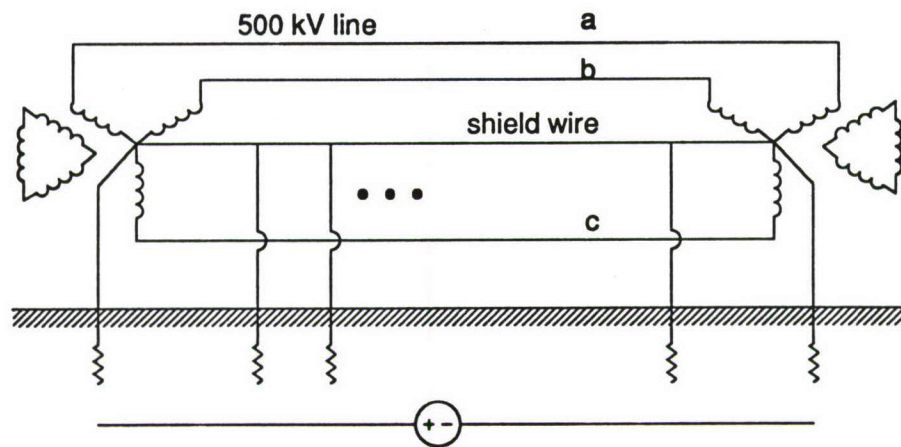
Tower Configuration Data

Conductor	x-Coordinate (feet)	y-Coordinate (feet)
Phase A	-32.0	97.5
Phase B	0.0	97.5
Phase C	32.0	97.5
Sky Wire 1	-35.0	129.5
Sky Wire 2	35.0	129.5

(Sky wire = transmission-line shield wire)



a. Single-Line Diagram



b. Three-Phase Diagram

Figure 28. Configuration of 500-kV Transmission-Line for Parametric Study.

The transformer core magnetization characteristics are described by specifying the flux linkage as a function of the magnetization current. This function is illustrated in Figure 29. The numerical values of this curve have been provided by GE.

The electric load of the system was neglected in the parametric analysis. Experimental evidence obtained from transformer testing in Minnesota [15] indicates a substantial effect on transformer saturation constants due to the electric load. This effect, however, is not included in this parametric study, but is discussed in Section 5.0.

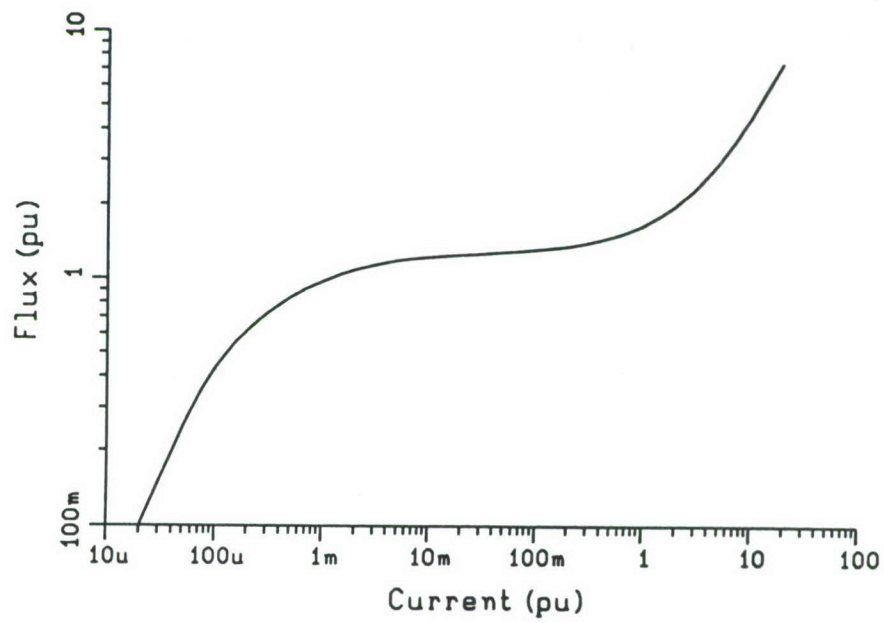


Figure 29. Transformer Core Magnetization Characteristics.

4.3 Description of the Parametric Analysis

The behavior of the 500-kV transmission system was analyzed in the presence of the E_3 excitation. A parametric analysis was performed with respect to the excitation E-field waveform type and amplitude, the transmission line total length, and the span length.

The two E_3 waveforms, defined as early time and late time waveforms and shown in Figures 2 and 3, were used in this analysis. Both of these waveforms are shown normalized, so that their peak values are 1 V/km. The transmission line system was analyzed for several different assumed peak amplitude values for each type of waveform. Specifically, the waveform amplitudes shown in Table 6 were used.

Table 6

Peak MHD-EMP E-Fields Used in Parametric Study

Early-Time Waveform Amplitude (V/km)	Late-Time Waveform Amplitude (V/km)
10	10
20	20
60	40
120	80
300	180
500	300

For each of these above E_3 waveforms, a parametric analysis was performed with the values of earth resistivity, tower footing resistance, transmission line total length, and span length shown in Table 7.

Table 7

Line and Ground Constants Used in Parametric Study

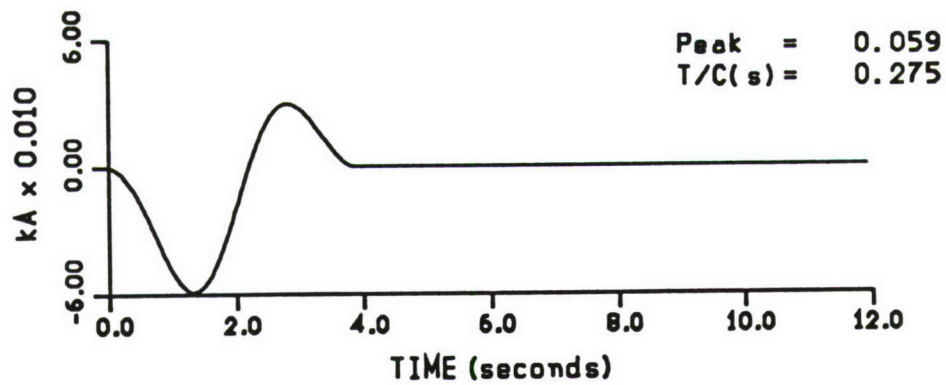
Soil Resistivity	100 $\Omega \cdot m$
Tower Footing Resistance	25 Ω and ∞
Line Length	30, 50, 100, 200, 400, and 1000 km
Span Length	0.16 and 0.40 km

The effects of MHD-EMP on the test system are assessed by computing the system transient response. The results of this study are described in the next section.

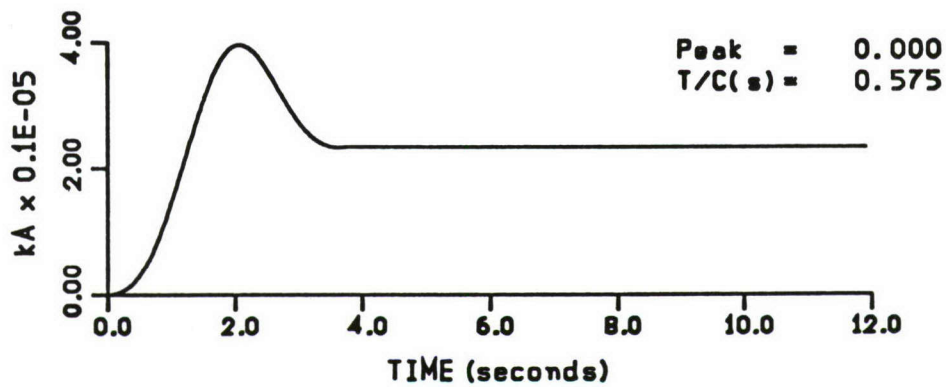
4.4 Parametric Study Results

The power system transient response was computed for each combination of the selected parameters given in Tables 6 and 7. The resulting transformer magnetization current and flux linkage, as well as the transmission-line zero-sequence current, were computed as a function of time for each case. Examples of these results are plotted in Figures 30 and 31.

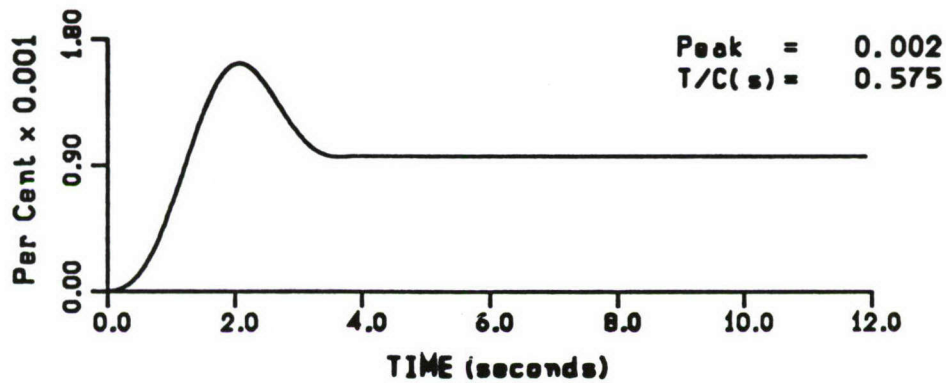
Since the parametric analysis results consist of a large number of plots, only selected characteristics of the obtained plots were tabulated so that the results could be presented in a compact form. Specifically, the maximum transformer dc offset of the magnetization current (for each set of selected parameters) and the time delay to reach magnetic core saturation were tabulated as a function of MHD-EMP waveform type and amplitude, soil resistivity, transmission line total length, and span length. The dc offset of the magnetization current is a very important quantity, since it determines the magnitude of the harmonics generated by the transformer.



a. Transmission-Line Zero-Sequence Current

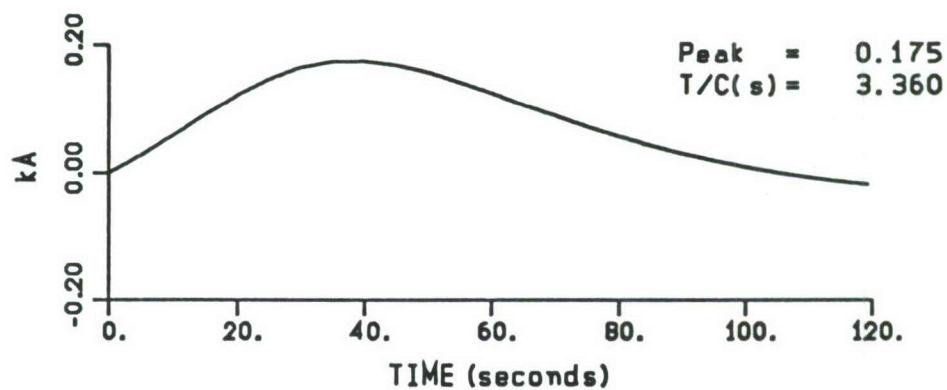


b. Transformer Magnetization Current

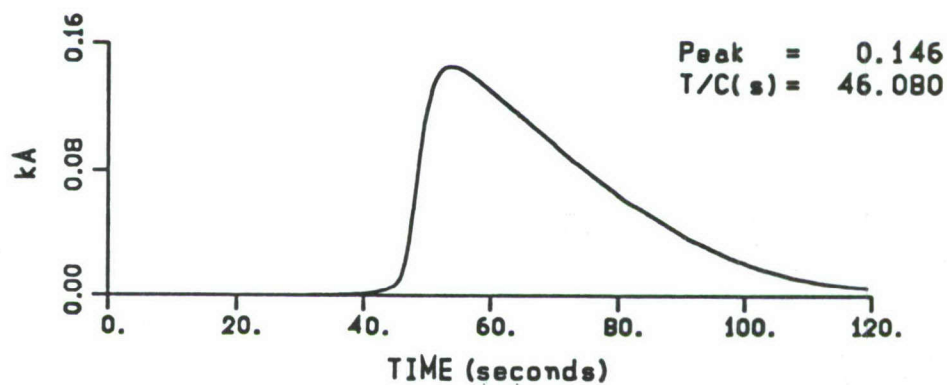


c. Transformer Magnetic Flux

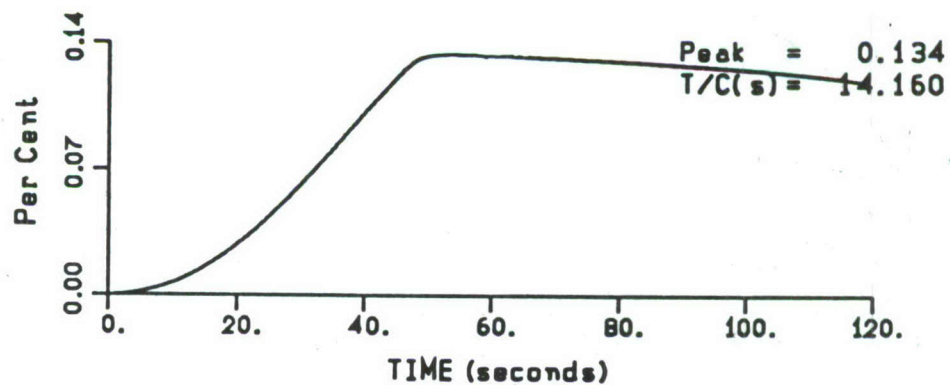
Figure 30. Transmission Line Response for the Early-Time E_3 Waveform (E_3 Amplitude = 10 V/km, $\rho = 100 \Omega \cdot \text{m}$, Shield Is Grounded, Line Length = 30 km, and Span Length = 0.16 km).



a. Transmission-Line Zero-Sequence Current



b. Transformer Magnetization Current

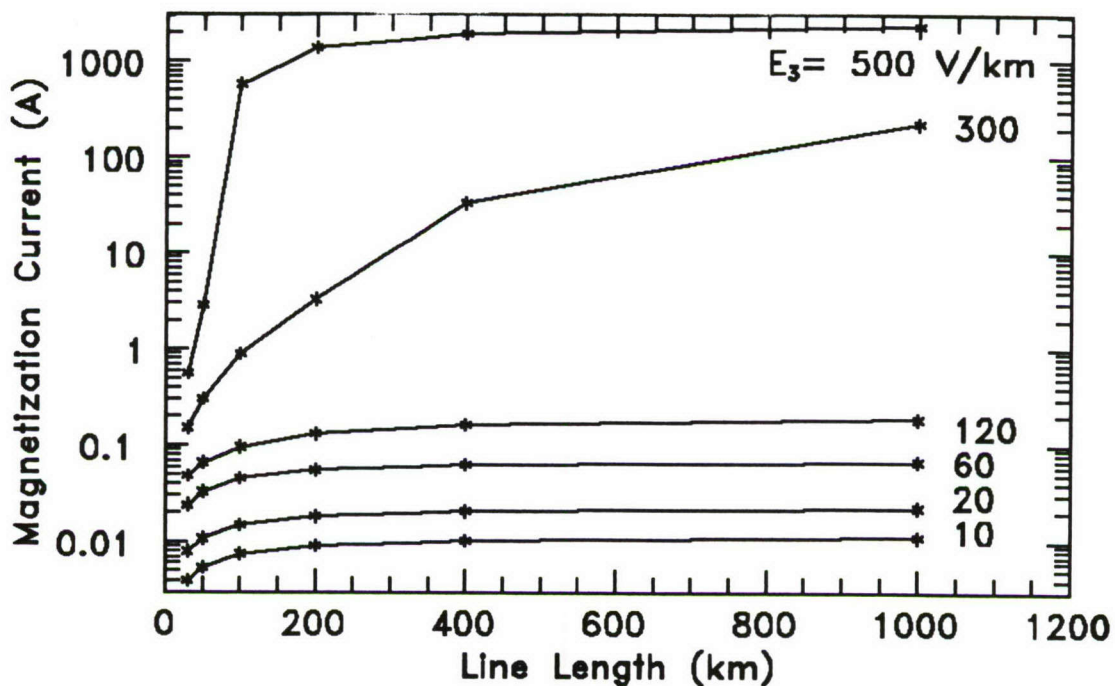


c. Transformer Magnetic Flux

Figure 31. Test System Response for the Late Time E_3 Waveform (E_3 Amplitude = 10 V/km, $\rho = 100 \Omega \cdot \text{m}$, Shield Is Grounded, Line Length = 1000 km, and Span Length = 0.16 km).

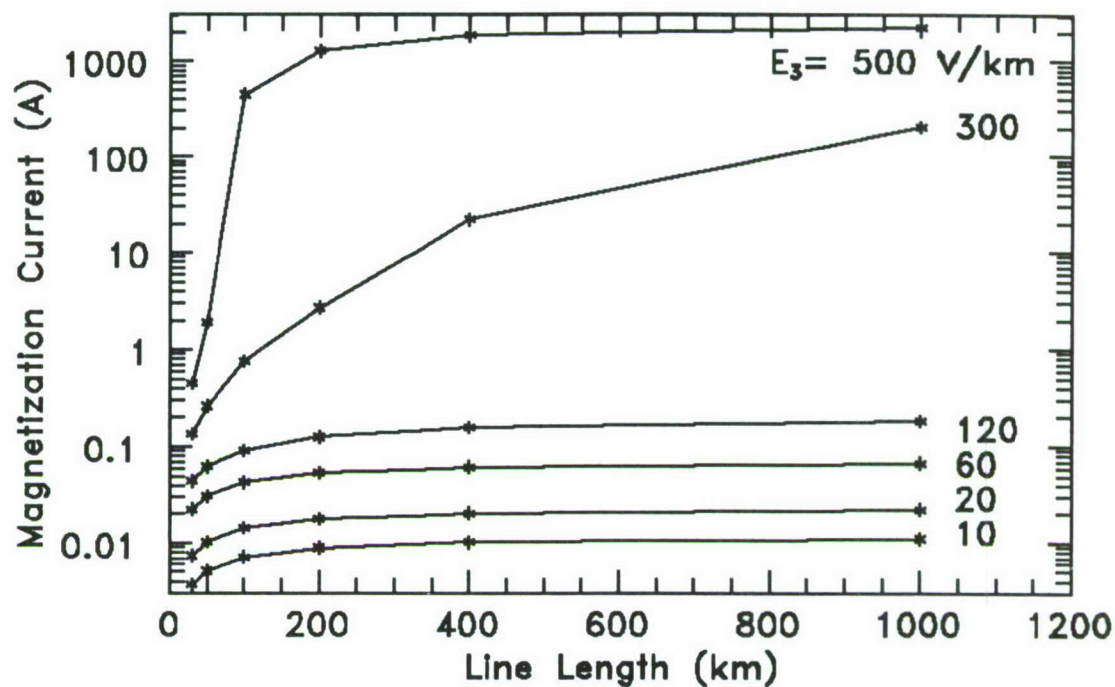
Figure 32 illustrates the maximum dc offset of the magnetization current in amperes for MHD-EMP excitation using the early-time waveform type as a function of the transmission line length and E-field amplitude. Parts "a" and "b" of the figure show the results obtained assuming that the shield wires are grounded at all towers, which were located with span lengths of 0.16 km and 0.40 km, for parts "a" and "b," respectively. Figure 32 shows the results obtained assuming the shield wires are insulated from the supporting towers.

For most parameter combinations and with early-time waveform excitation, the transformer did not reach saturation. Therefore, the time delay to saturation was not tabulated for the early-time waveform cases.

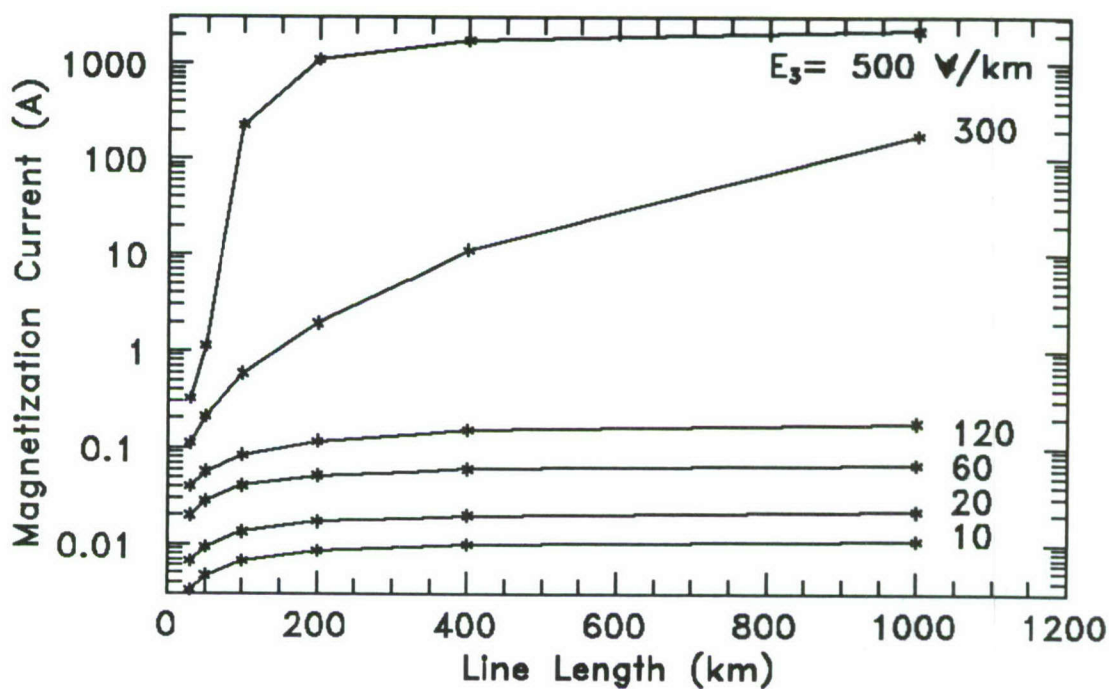


a. Shield Wire Connected to Tower with Span of 0.16 km

Figure 32. The Maximum Magnetization Current for the Early-Time MHD-EMP Waveform when $\rho = 100 \Omega \cdot \text{m}$.



b. Shield Wire Connected to Tower with Span of 0.40 km

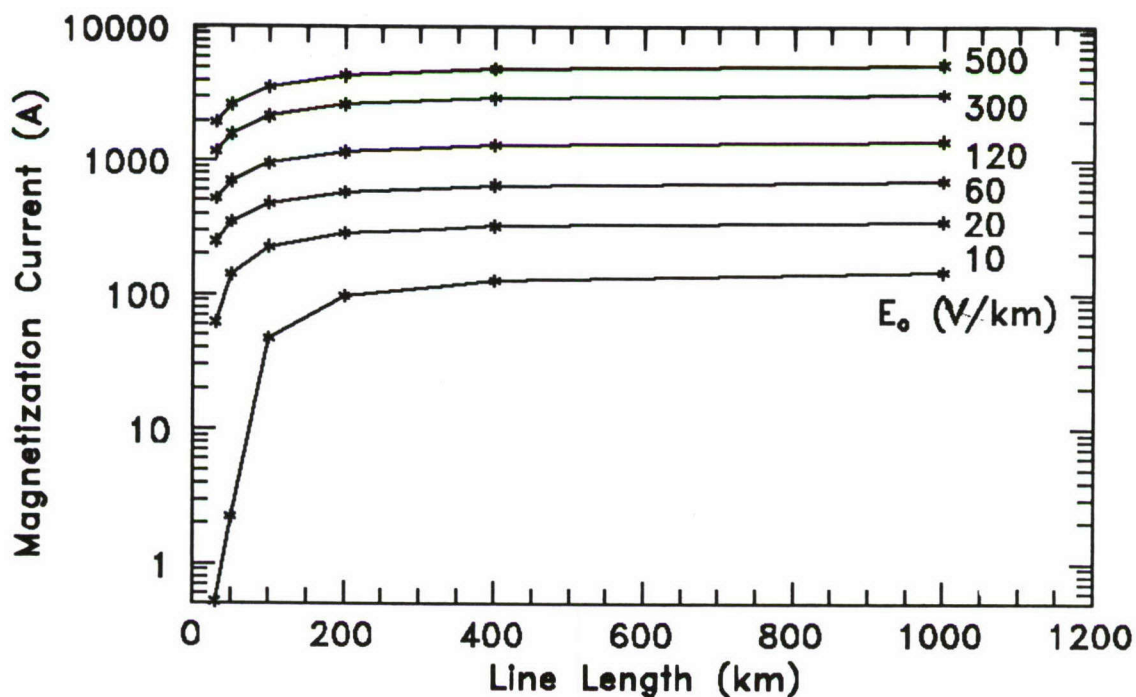


c. Shield Wire Insulated from Tower

Figure 32. The Maximum Magnetization Current for the Early-Time MHD-EMP Waveform when $\rho = 100 \Omega \cdot \text{m}$.

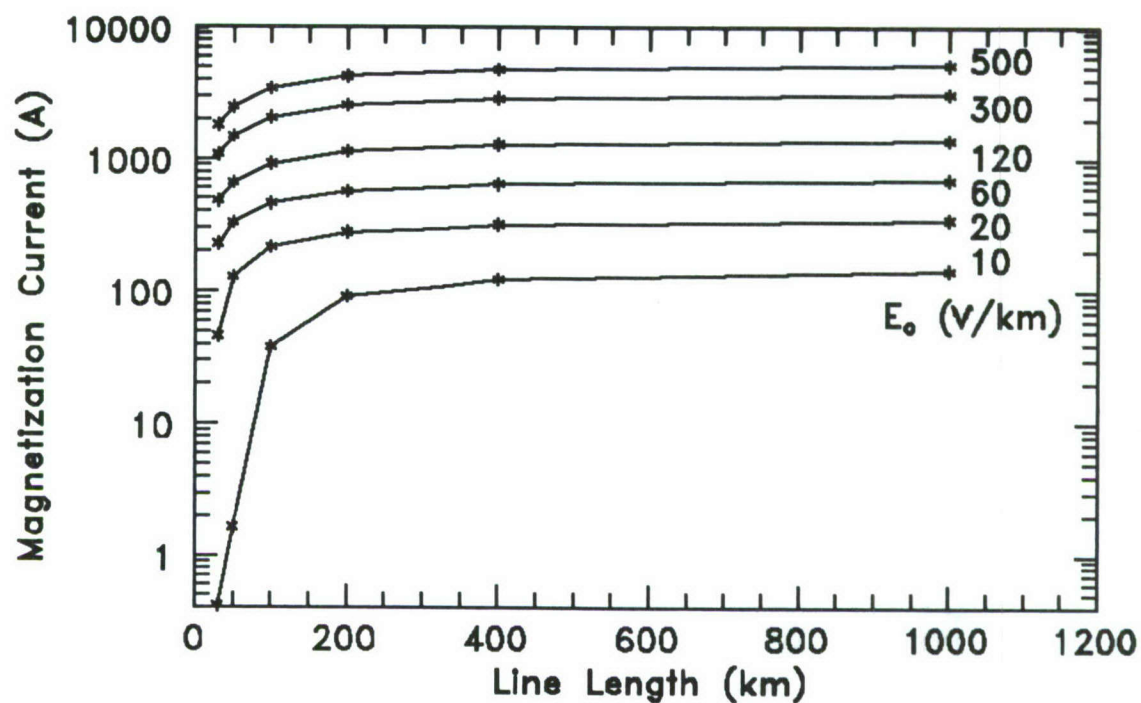
Figure 33 illustrates the maximum magnetization current (in amperes) flowing into the transformer for the late-time MHD-EMP waveform for various transmission line lengths and waveform amplitudes. Parts "a" and "b" of the figure present results obtained for the two tower spacings with the shield wire connected to the tower, and part "c" shows the results for the shield wires insulated from the supporting towers.

The time delay from the initiation of the late-time MHD-EMP waveform to saturation was also calculated and plotted for each combination of selected parameters. Specifically, the time delay to saturation is defined as the time interval from the initiation of the excitation waveform to the time instant that the transformer magnetization current reaches one tenth of its maximum value. The time delay to saturation as a function of transmission line length and the assumed E-field waveform amplitude are shown in Figure 34. The indicated time delay is in seconds. For some cases involving the smaller MHD-EMP amplitudes, transformer saturation was not obtained and the plots are truncated. Parts "a" and "b" of Figure 34 are for the shield wires grounded at every tower, and part "c" is for the insulated shield wires.

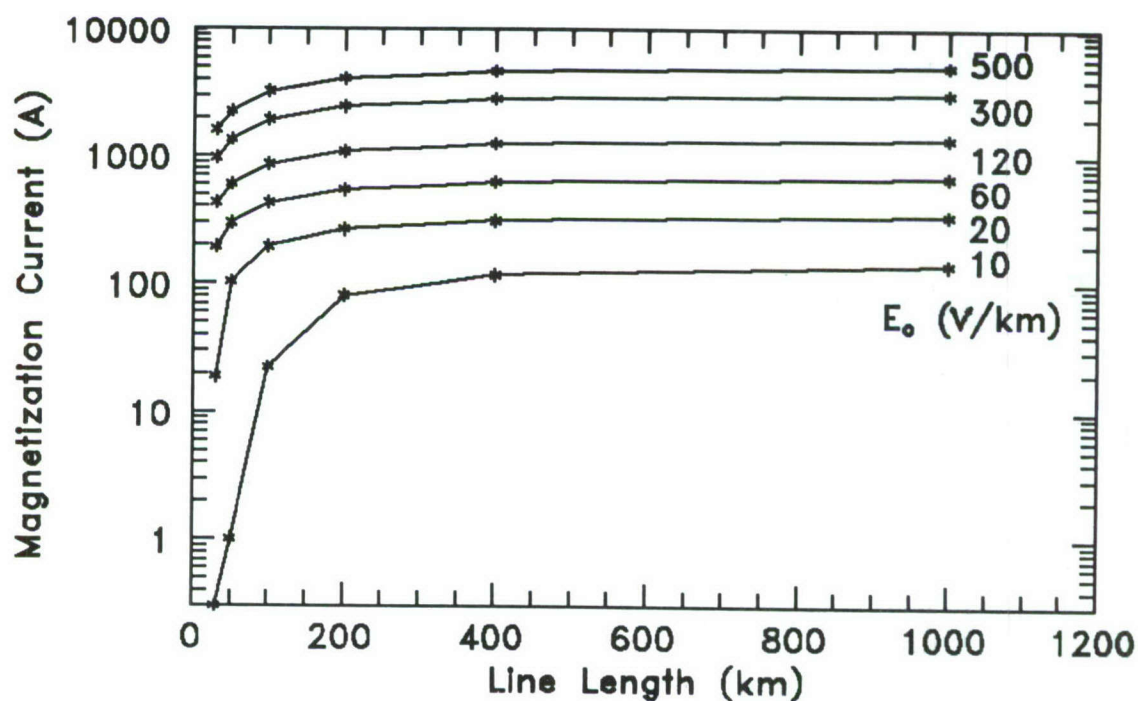


a. Shield Wire Connected to Tower with Span of 0.16 km

Figure 33. The Maximum Magnetization Current for the Late-Time MHD-EMP Waveform when $\rho = 100 \Omega \cdot \text{m}$.

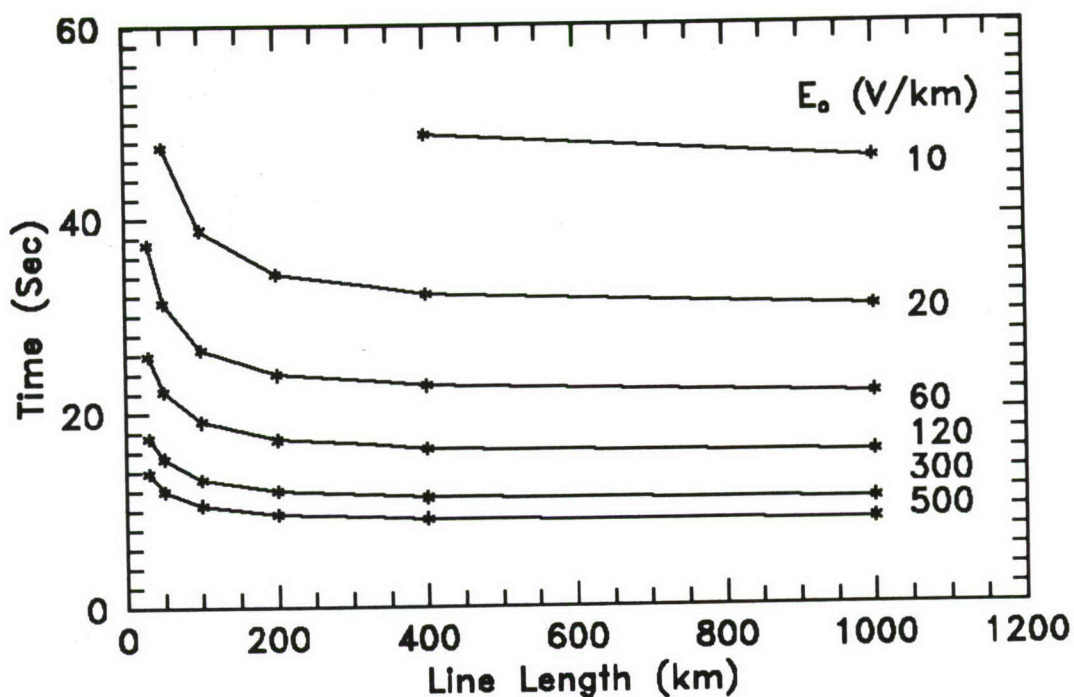


b. Shield Wire Connected to Tower with Span of 0.40 km

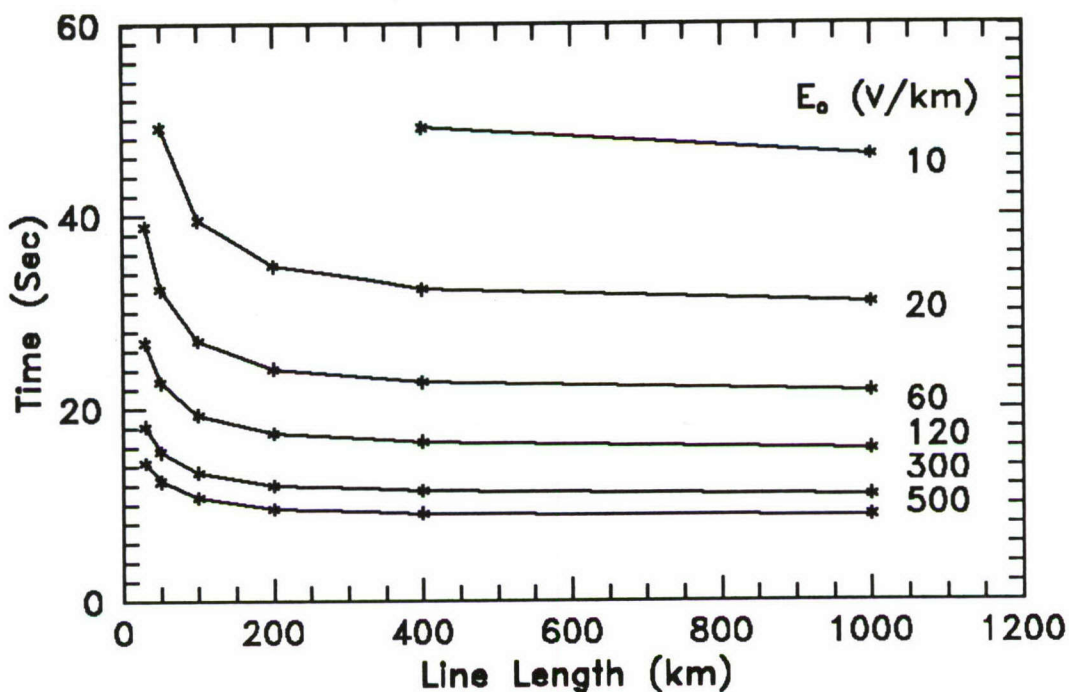


b. Shield Wire Not Connected to Tower

Figure 33. The Maximum Magnetization Current for the Late Time MHD-EMP Waveform when $\rho = 100 \Omega \cdot m$.

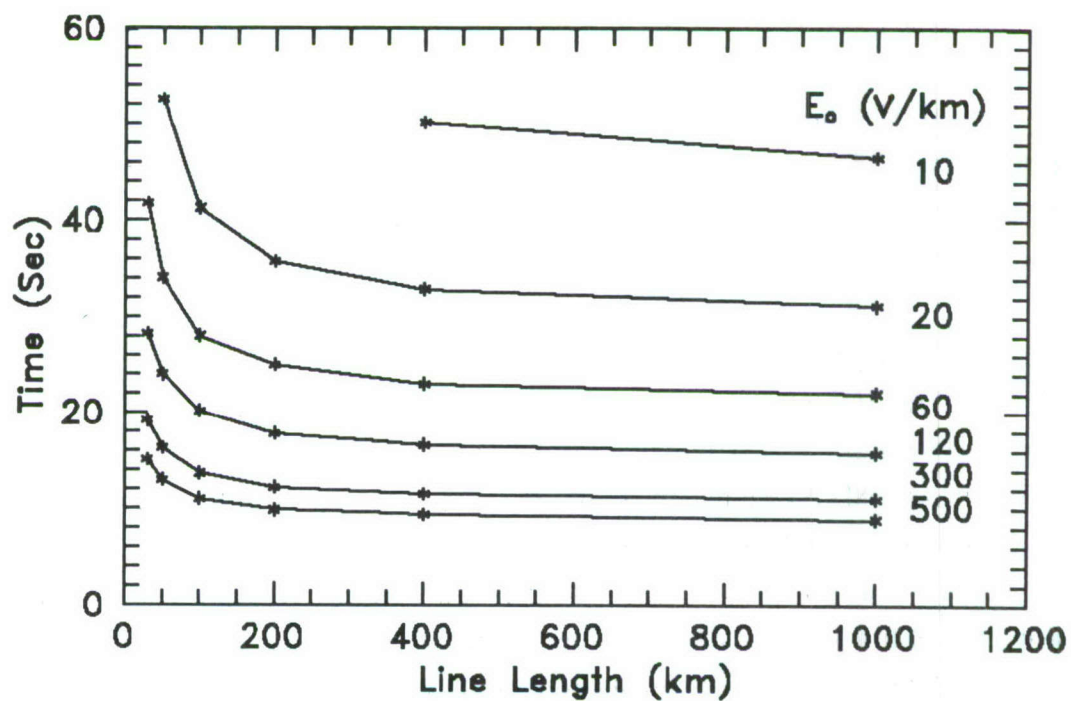


a. Shield Wire Connected to Tower with Span of 0.16 km



b. Shield Wire Connected to Tower with Span of 0.40 km

Figure 34. Time Delay to Transformer Saturation for the Late-Time MHD-EMP Waveform when $\rho = 100 \Omega \cdot \text{m}$.



c. Shield Wire Not Connected to Tower

Figure 34. Time Delay to Transformer Saturation for the Late-Time MHD-EMP Waveform when and $\rho = 100 \Omega \cdot m$.

5.0 MHD-EMP EFFECTS ON THE POWER SYSTEM

The MHD-EMP-induced currents on long lines can have an effect on the power system components connected to the lines [1]. The previous section has illustrated that these quasi-dc currents can cause transformer magnetization currents to increase. At the same time, the harmonic distortion of the 60-Hz power on the system increases, additional reactive power is required of the generator, and the power system relaxation time constant changes. Each of these phenomena can have an effect on the power system stability.

5.1 Harmonic Generation

Reference [13] describes a series of measurements made on a transmission-class system in which the harmonic content of the magnetization currents was measured with various levels of dc current injected into the transformer neutral. The transformers used in these tests were autotransformers.

The first configuration tested consisted of a bank of single-phase 500/230-kV autotransformers having a 34.5 tertiary winding. These transformers were rated at 120/230 MVA per phase, or 360/600 MVA for the complete three-phase unit. Figure 35 presents the measured harmonic content on the primary winding of one of the transformers, which was unloaded on the secondary. These data are shown for various levels of dc injection into the transformer neutral. Because the transformer was unloaded, the fundamental component of the current at 60 Hz, is relatively small, and it is shown along with the higher harmonics. To be consistent with ref.[13], the component of the current at 60 Hz in this report is referred to as the first harmonic. The waveform component at 120 Hz is the second harmonic, and so forth.

A second transformer which involved a smaller 230/115-kV autotransformer with a 13.8 tertiary winding was also considered in ref. [13]. This transformer was rated at 200/333 MVA, and had a three-legged core design. The phase conductor of the transformer which was measured had an electrical load attached. Figure 36 illustrates the harmonic content in the line current on the 230-kV side of this transformer for various levels of dc excitation. Because the resulting line current at the fundamental 60-Hz frequency was very high and off the scale, it is not shown on this plot. Only the second and higher harmonics are presented.

Measurements of E_3 responses were also made on a mock-up of a three-phase 480-V/12.47-kV/208-V power distribution system [14]. A 480-V/12.47-kV 300-kVA Y-Y step-up transformer was connected to a 12.47-kV/208-V 75-kVA Y-Y step-down transformer, and dc current was injected into the neutrals of the transformers. With the system energized by commercial 480-V power, measurements of the harmonic distortion were made. These results are presented in Figure 37, shown in the same format as the previous harmonic data. As in Figure 36, the 60-Hz component of the line power current was high (well over 2.0 A); consequently, it is not plotted in this figure.

In these plots, it is clear that small dc currents on the order of 2-5 A can have a significant effect on the harmonic content of power distribution systems. Similarly, currents on the order of 50-100 A can affect the power transmission system. Figure 10 indicates that for a 12-kV distribution system having a line length of only about 5 km, the normalized dc current I_c/E_0 induced by the MHD-EMP environment would be about 0.4 A·km/V. For an assumed peak MHD-EMP E-field strength of just 20 V/km, this results in a current of 8 A, which is above the levels of current observed to cause harmonic distortion in ref.[14]. Similarly, for a 500-kV power transmission line which is 100 km long, Figure 9 indicates that $I_c/E_0 \approx 40$ A·km/V. Again for a peak MHD-EMP E-field strength of 20 V/km, this results in a current of 800 A, which is well above the current levels observed to produce harmonic distortion. Of course, a larger MHD-EMP field strength or a longer line will make these effects even more pronounced. Thus, it is evident that the MHD-EMP environment will cause serious harmonic distortion in both power transmission and distribution systems.

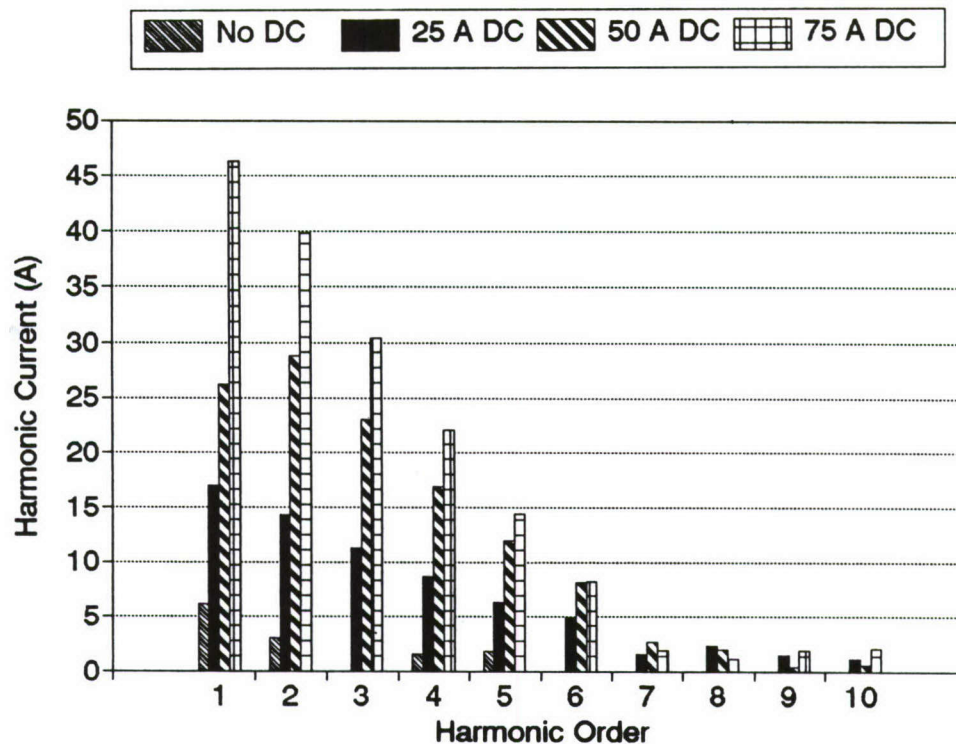


Figure 35. Measured Harmonic Content for Dc Injection in the Primary of an Unloaded 500/230-kV Autotransformer, from Ref.[13].

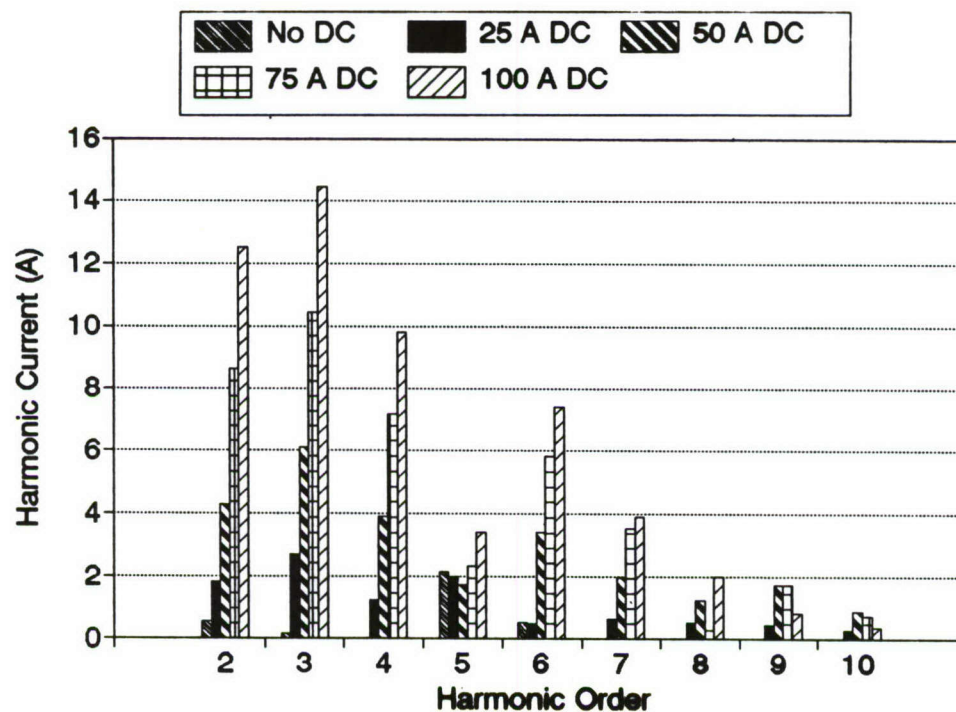


Figure 36. Measured Harmonic Content for Dc Injection in the Primary of a Loaded 230/115-kV Autotransformer, from Ref. [13].

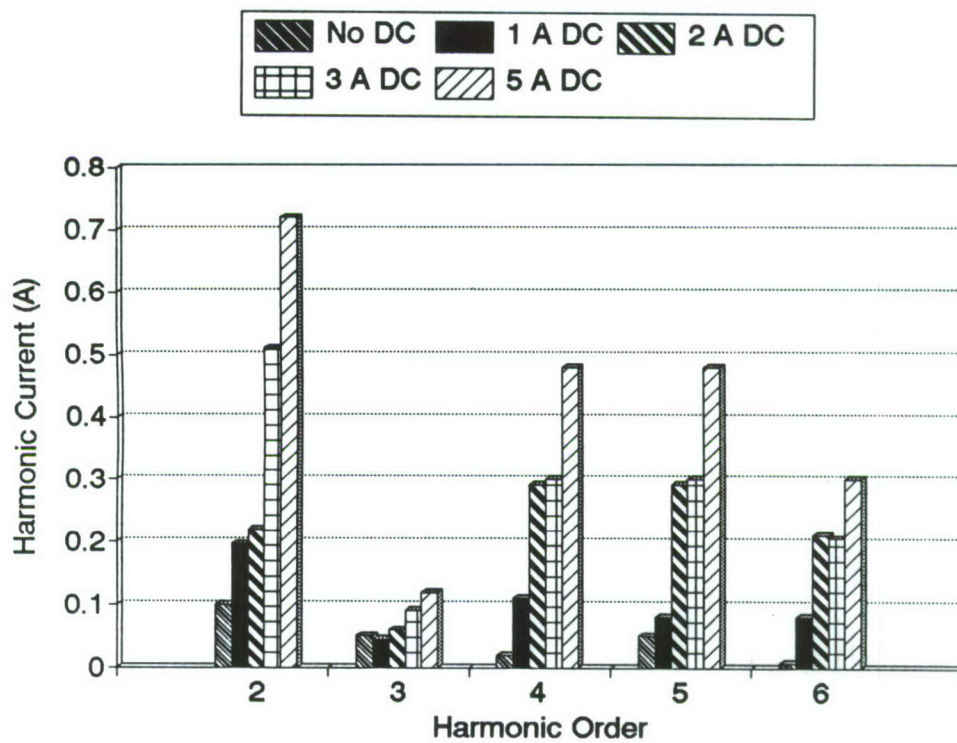


Figure 37. Measured Harmonic Content for Dc Injection in the Neutral of a Three-Phase 480-V/12.47-kV/208-V Power Distribution System, from Ref.[14].

5.2 Reactive Power Demand Caused by MHD-EMP

Reference [13] also reports the change in the reactive power flowing into the 500/230-kV autotransformer under dc excitation conditions. Figure 38 shows this power in Mvar per phase, as a function of the dc level. Similarly, measurements of the reactive power on the distribution system in ref.[14] were also made, and these results are summarized in Figure 39. Note that the vertical scale in figure 39 is in Kvar/phase.

Both of these increases in reactive power are significantly lower than the rated power levels of the transformers. Consequently, this increase in power will not be detrimental to the transformers. However, the power generation units will be required to produce this additional reactive power, and if the demand is too great, the generation facilities will not be able to provide sufficient power to maintain the proper operating voltage in the system. The voltage on the power system will consequently drop, and a power outage may ensue.

5.3 Changes in System Time Constant

The testing on the power distribution system in ref.[14] found that the characteristic relaxation time of the power system depends on the level of dc excitation. For a very small dc excitation, the time required for a transient perturbation in the 60-Hz current to decay (the time constant) can be on the order of several seconds. However, as the level of dc excitation increases, this time constant becomes less than one second. Figure 40 (from ref.[14]) illustrates the measured system time constant as a function of the dc injection.

The results of Figure 40 indicate that the effect of the E_3 waveform on a power distribution system will occur within 1 second of the application of the field. The early-time part of the E_3 waveform shown in Figure 4a has typical rise and fall times that are longer than the typical system relaxation time of 0.5 second. The late-time E_3 in the figure is much slower than this relaxation time. Thus, for all practical purposes, the MHD-EMP response can be treated as a purely dc effect, neglecting the R/L time constants inherent in the transformers.

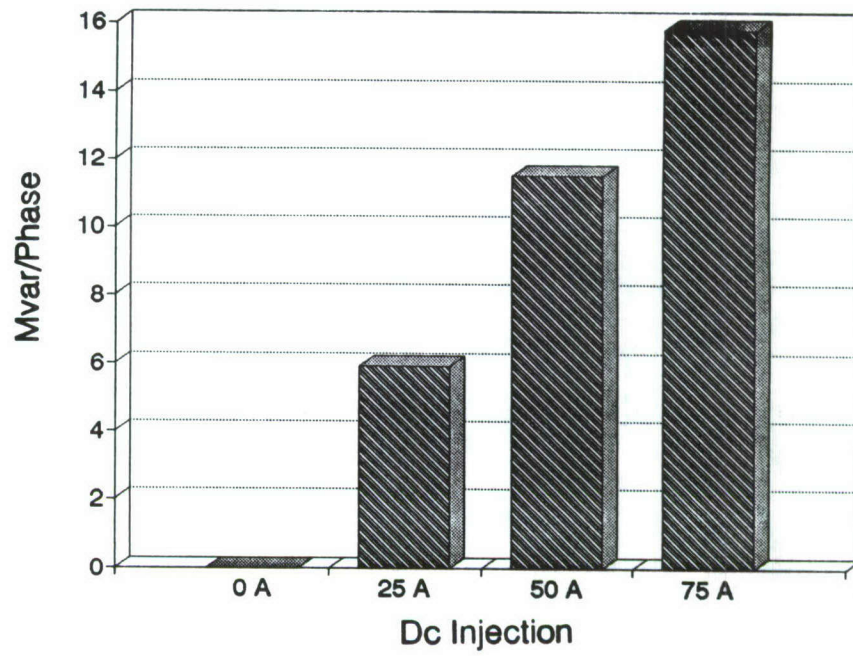


Figure 38. Reactive Power Demand for the 500/230-kV Transformer, from Ref. [13].

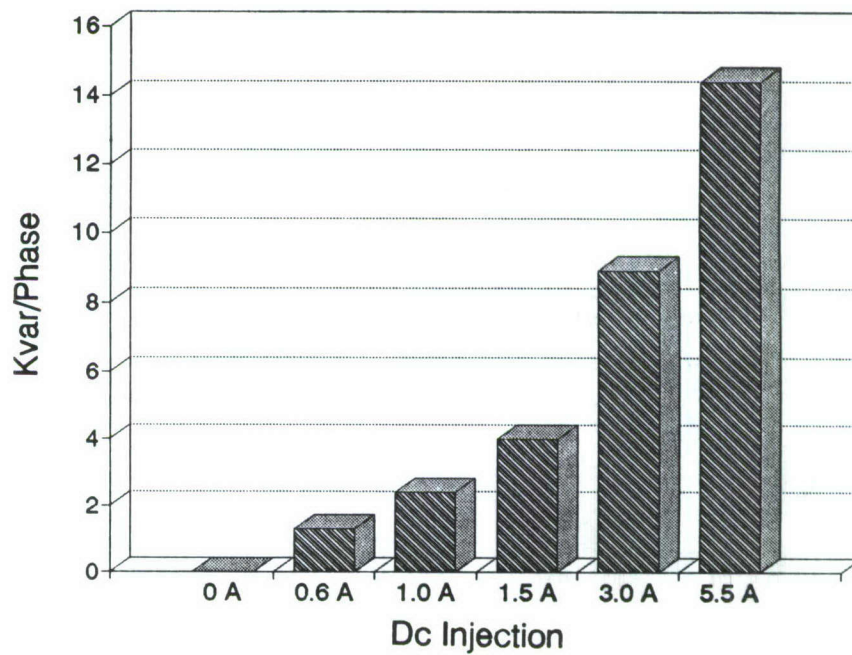


Figure 39. Reactive Power Demand for the 480-V/12.47-kV/208-V Power Distribution System, from Ref.[14].

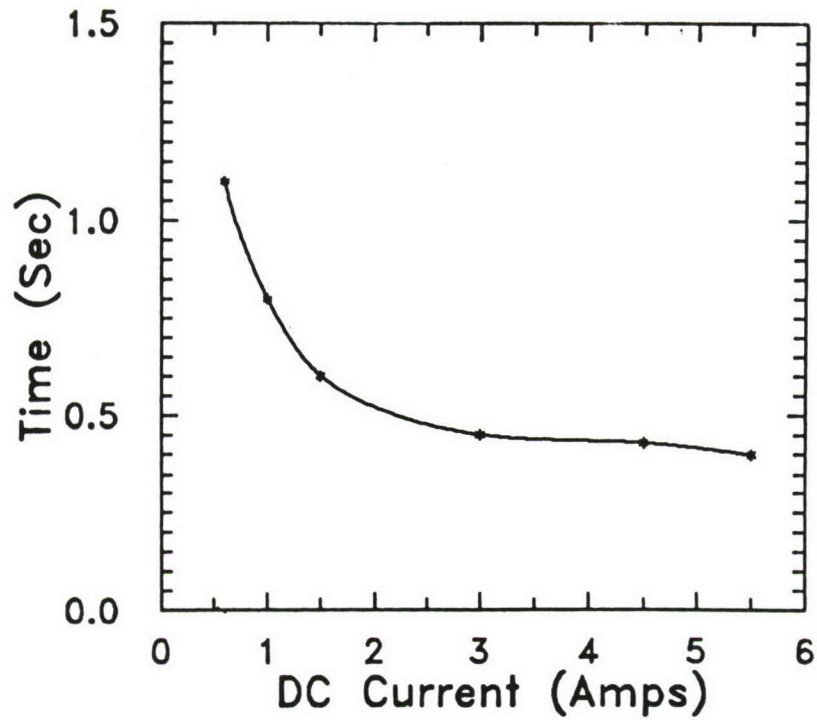


Figure 40. System Relaxation Time vs. DC Current Injection for the Three-Phase 480-V/12.47-kV/208-V Power Distribution System, from Ref.[14].

The system relaxation time discussed above was for the distribution system with a nominal 60-Hz power load. Recent tests in Minnesota suggest that the electric load has a substantial effect on transformer saturation time constants [15]. This fact also has been verified with the calculational model described in this report. Specifically, Figures 41-44 illustrate the effects of the electric load on the saturation time constants. The model selected is a system with the following parameters:

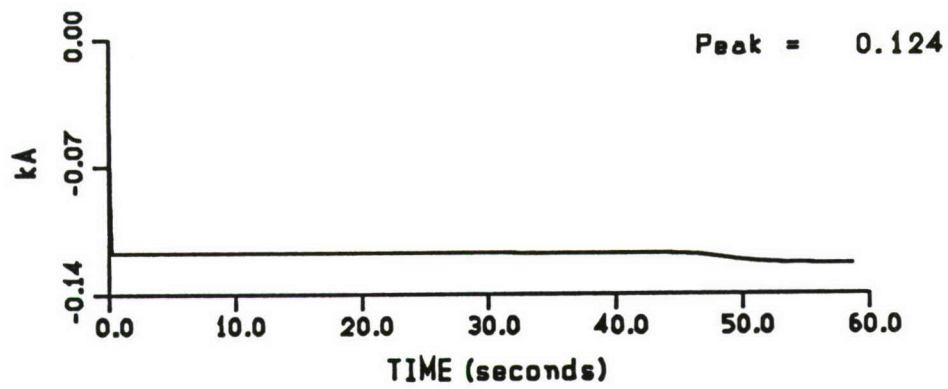
MHD-EMP Environment	20 V/km
Soil Resistivity	100 $\Omega \cdot m$
Line Length	30 km
Span Length	0.16 km
Tower Footing Resistance	25 Ω

The MHD-EMP waveform was assumed to be a step voltage to easily demonstrate the saturation time constant. Figure 41 illustrates the system response when the transformer is unloaded. Figures 42, 43, and 44 illustrate the system response when the transformer is loaded with 20%, 40%, and 100% load, respectively. The load connection is assumed to be wye-grounded. The saturation time constants are shown in Table 8.

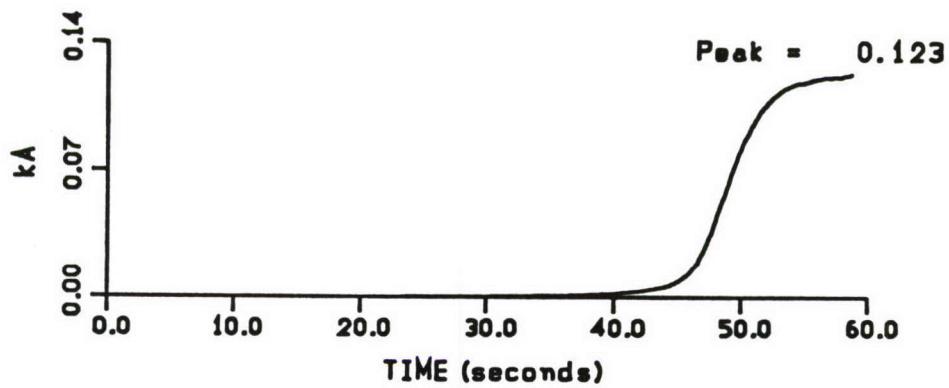
Table 8
Saturation Time Constants for Loaded Transformer

Waveform Type: 20 V/km Step Function
Shield Connected to Towers
Span Length: 0.16 km
Ground Resistivity: 100 $\Omega \cdot m$

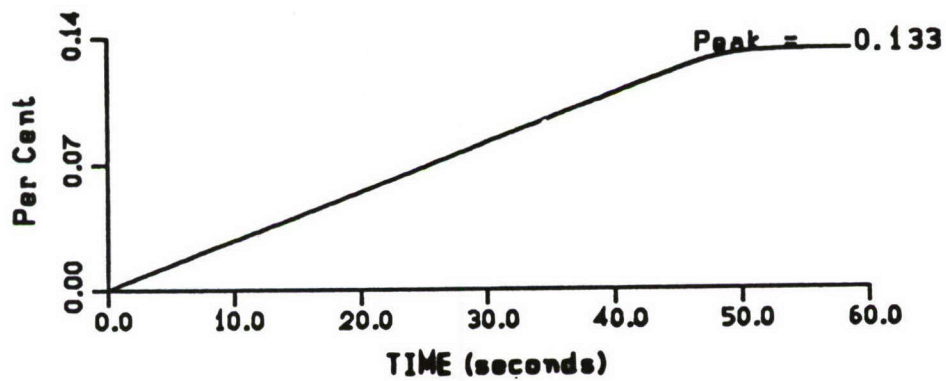
Transformer Load (in %)	Saturation Time Constant (Sec)
0 %	48
20 %	17
40 %	11
100 %	6



a. Line Zero-Sequence Current

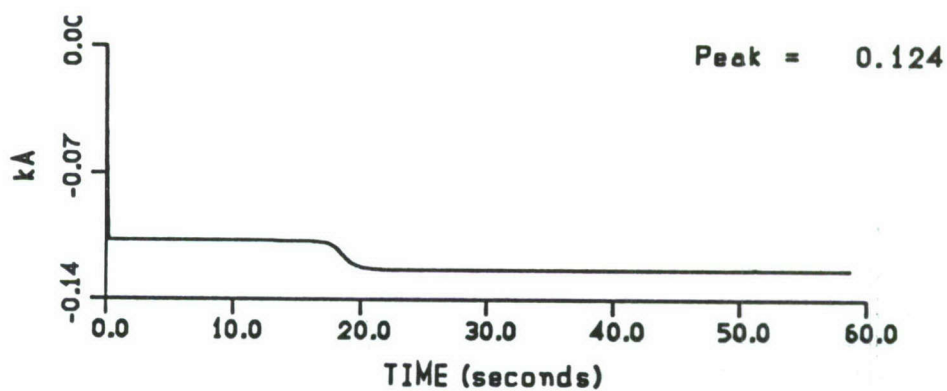


b. Transformer Magnetization Current

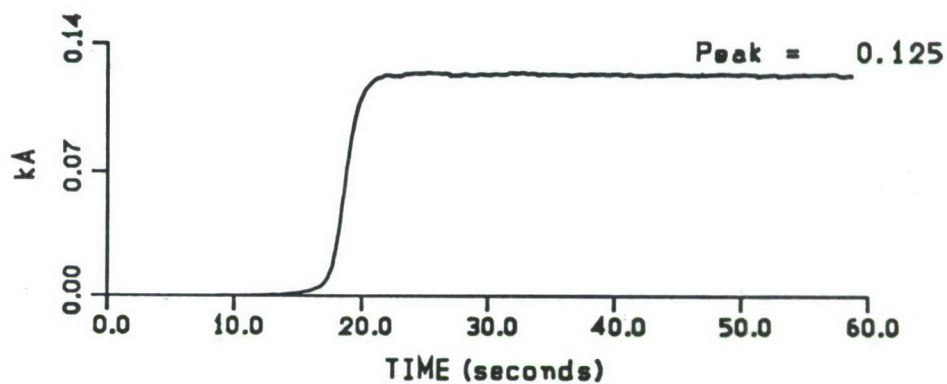


c. Transformer Magnetic Flux

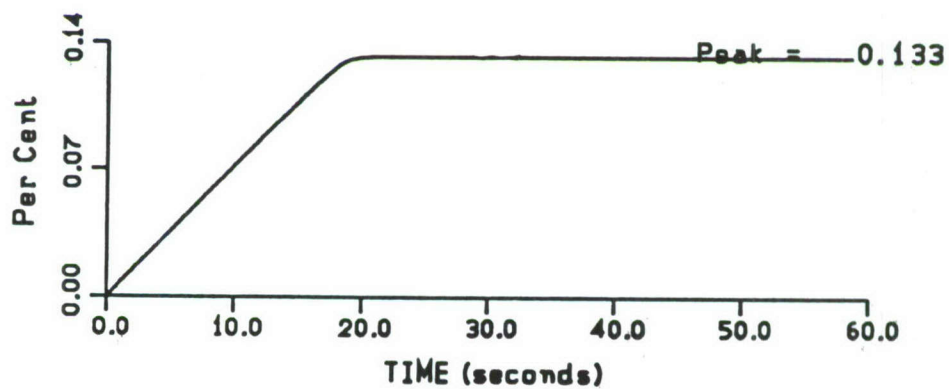
Figure 41. System Response to MHD-EMP with Transformer Unloaded.



a. Line Zero-Sequence Current

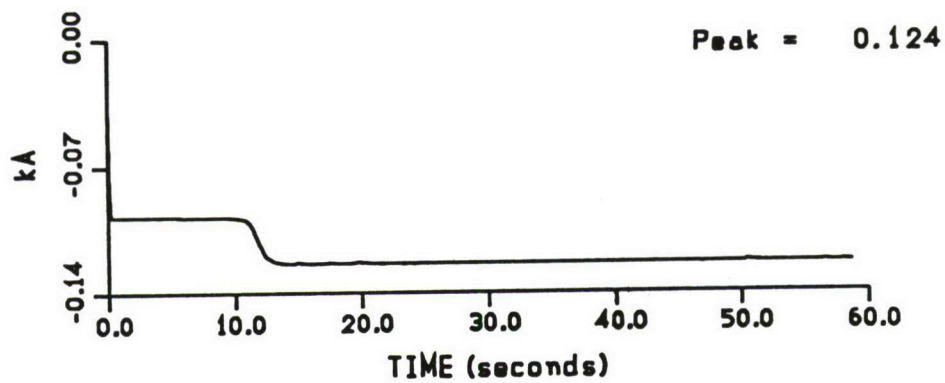


b. Transformer Magnetization Current

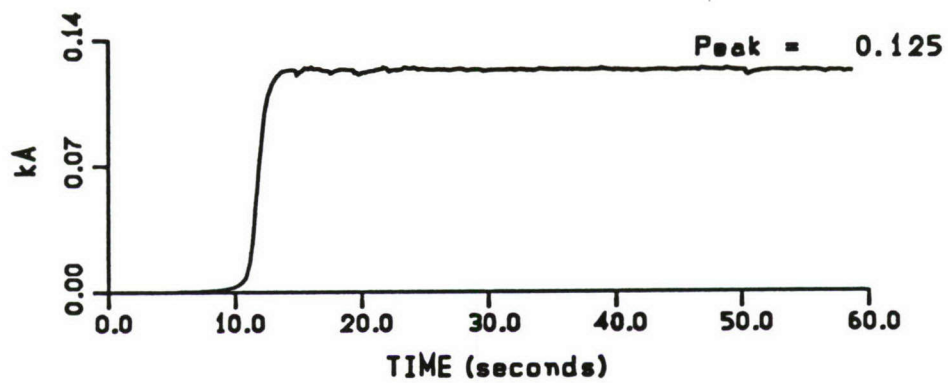


c. Transformer Magnetic Flux

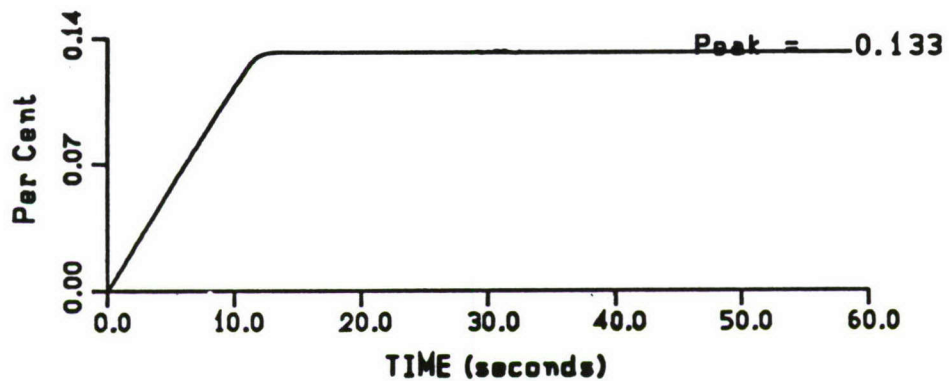
Figure 42. System Response to MHD-EMP with 20% Transformer Load.



a. Line Zero-Sequence Current

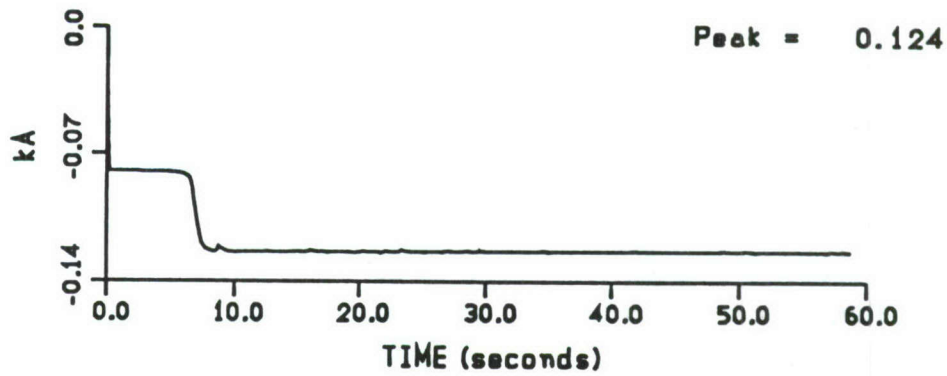


b. Transformer Magnetization Current

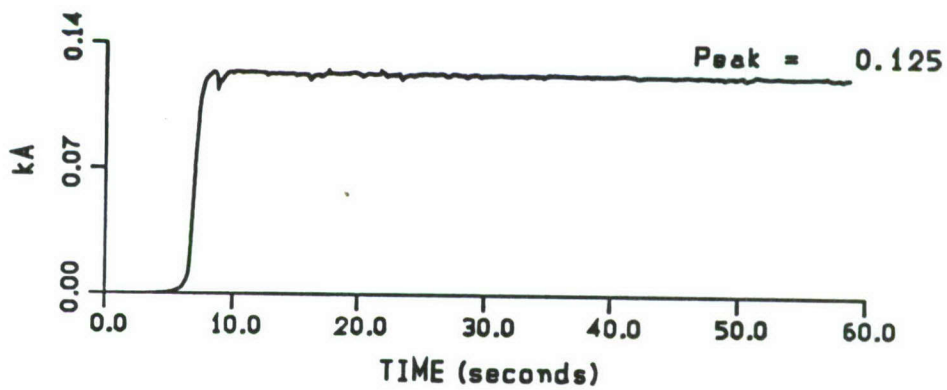


c. Transformer Magnetic Flux

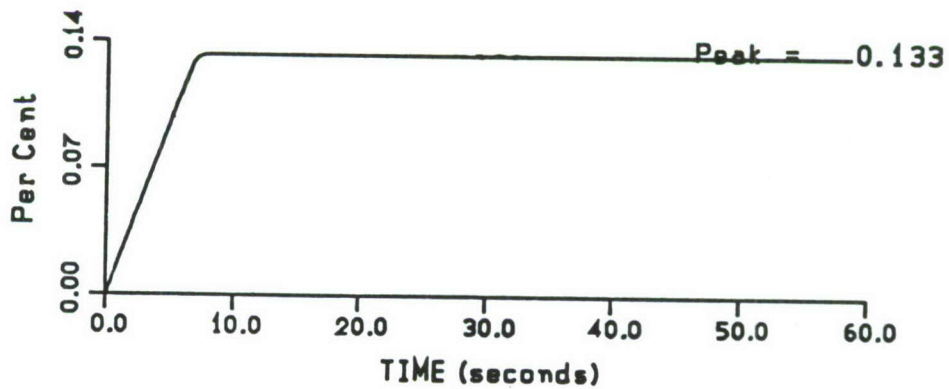
Figure 43. System Response to MHD-EMP with 40 % Transformer Load.



a. Line Zero-Sequence Current



b. Transformer Magnetization Current



c. Transformer Magnetic Flux

Figure 44. System Response to MHD-EMP with 100% Transformer Load.

When the electric load was assumed to be delta-connected, no effect was observed on the saturation time constants.

The observed results can be explained with a simplified model of the zero-sequence network. Specifically, one can think of the saturation time constant as determined by an equivalent R-L circuit model. In the equivalent model, the inductance is dominated by the transformer inductances, and the resistance is dominated by the transformer winding resistance and affected partly by the load resistance. The transformer magnetizing inductance can be thought of as being connected in parallel. For an autotransformer with tertiary winding, the influence of the electric load on the equivalent resistance of the zero-sequence model has been determined to be

$$Z_{eq} = (Z_H - Z_L) + (2Z_D + Z_L) (2Z_T + Z_L) / (Z_L + Z_T + Z_D) \quad (28)$$

and for the wye-wye connected transformer with a tertiary winding, the resistance is

$$Z_{eq} = Z_H + (Z_D + Z_L) Z_T / (Z_L + Z_T + Z_D) \quad (29)$$

In Eqs.(28) and (29) the following definitions are used:

- Z_H = Primary leakage impedance,
- Z_L = Secondary leakage impedance,
- Z_T = Tertiary leakage impedance,
- Z_D = Electric load impedance.

The above formulae should be viewed only as approximations. They can provide the approximate increase of the equivalent resistance due to the electric load. As an example, assuming a 20% electric load for a transformer with leakage impedance of $0.001 + j 0.10$ pu, the effect of the electric load is to double the equivalent resistance. Doubling the equivalent resistance will substantially decrease the saturation time constant due to the nonlinear characteristic of the magnetization inductance.

As in the case of the change in reactive power, these changes in the transformer time constants will not have a direct adverse effect on the power system components. System-wide, however, the overall effect of such changes in the operating parameters of the power system is not at all clear, and performing an assessment of these effects at this level is beyond the scope of this report.

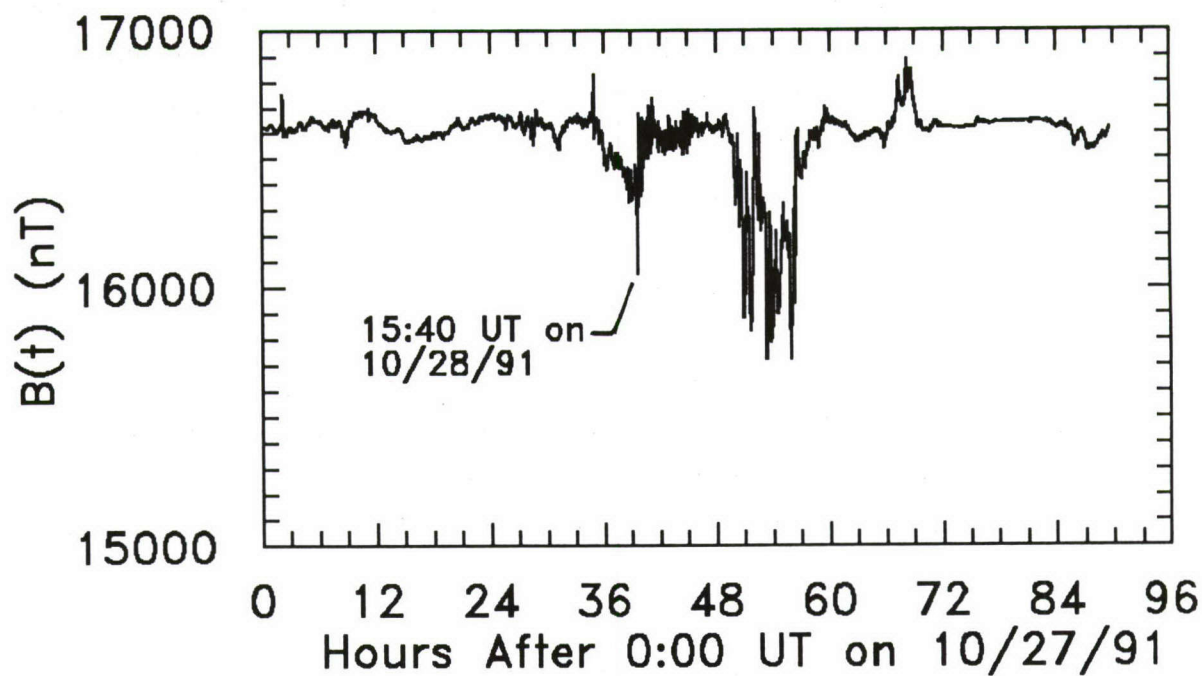
5.4 Observed Geomagnetic Storm Effects

As mentioned earlier in this report, the MHD-EMP environment is similar to that of a geomagnetic storm. Consequently, it is useful to look to the several reported power system malfunctions which have been ascribed to these naturally-occurring storms. Doing this can provide an indication of possible MHD-EMP effects on the commercial power system.

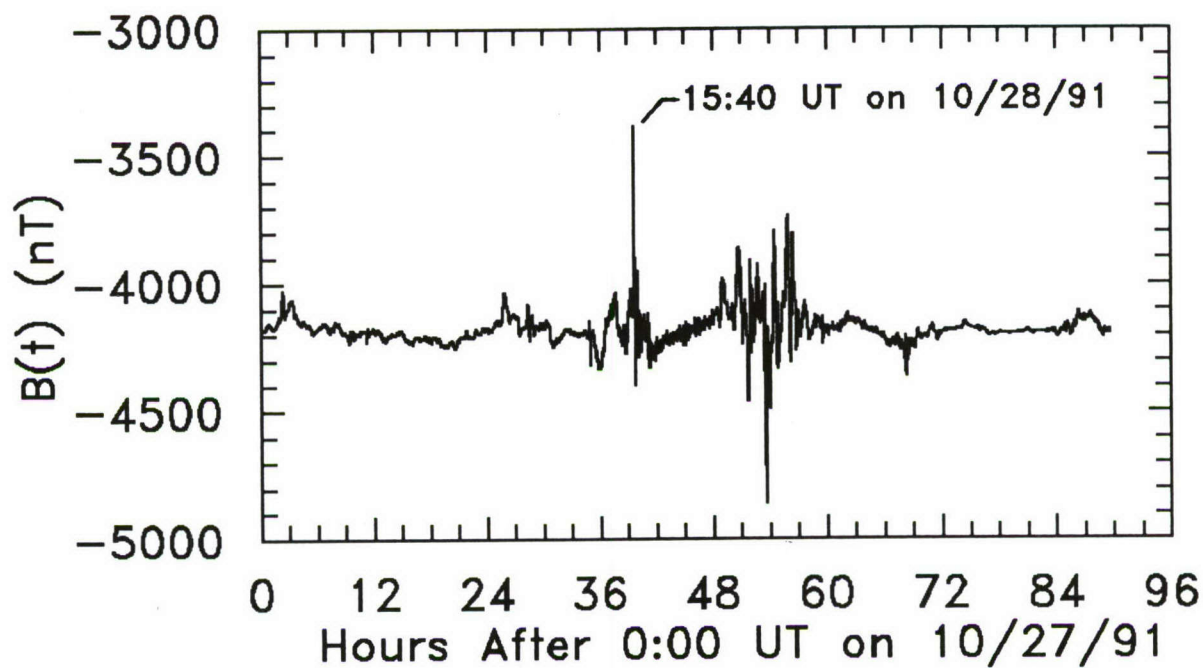
On October 28 and 29, 1991, a major geomagnetic storm occurred. This was given a K-Index of 9 from readings made in Boulder, Colorado, and in Loring, Maine. The storm began at 1540 universal time (1040 EST, 0940 CST, 0840 MST, 0740 PST) on October 28. A number of geomagnetic observatories across the US and Canada recorded the fluctuations of the geomagnetic field during this event and can provide data. Of particular interest are the data from the Canadian Geological survey of Canada [16], as the data are available at 10 second measuring intervals. Other data, such as those available from the U.S. Geological Survey, are typically available only with a one minute time resolution [17].

Figure 45 presents the measured North-South and East-West geomagnetic field at the Ottawa Magnetic Observatory, as provided by ref.[16]. These data are plotted as a continuous record for a three day period, starting on 10/27/91. The vertical axis is the absolute magnetic field (i.e., the static geomagnetic field plus a small time-varying component) in units of nano-teslas. The onset of the geomagnetic storm is defined to be at about 15:40 universal time on October 28, and this time is indicated on the plots. Note that the North-South B-field is the dominant component.

The electric field on the earth's surface corresponding to these magnetic fields may be calculated by numerically evaluating a convolution integral, as described in Appendix A of ref.[1]. This assumes a simple, homogeneous conducting half-space as a model of the earth. Figure 46 presents the resulting calculated E-fields on the earth for an assumed



a. North-South Component



b. East-West Component

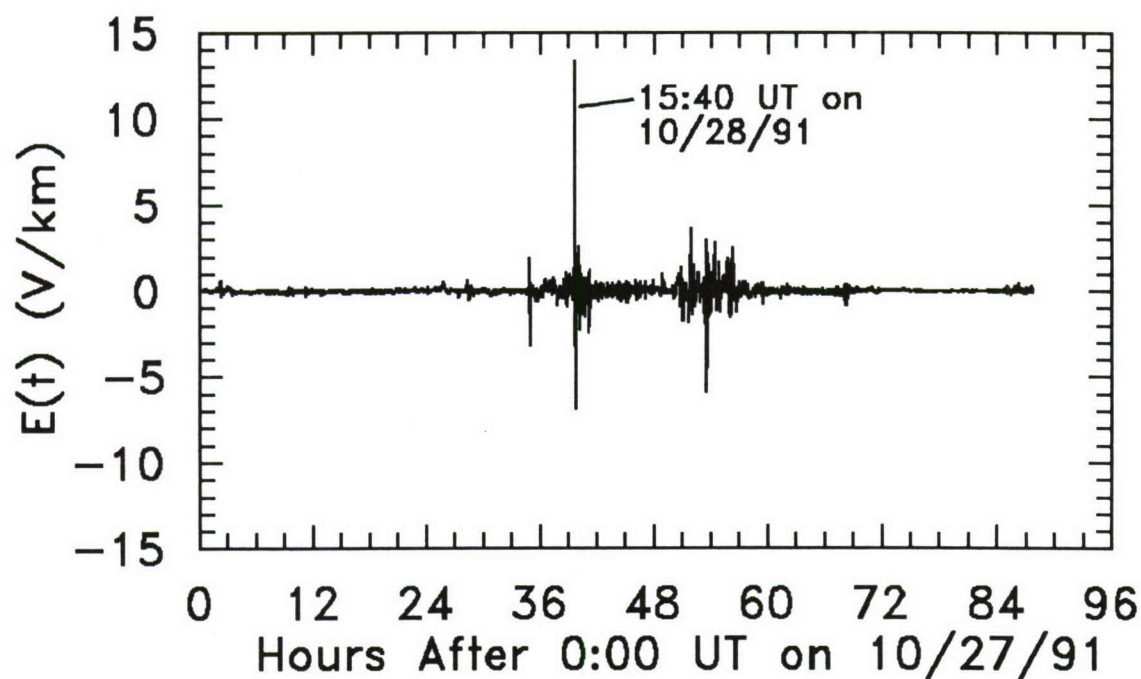
Figure 45. Measured Geomagnetic Field at Ottawa, Canada, from Ref.[16].

electrical conductivity of $\sigma_g = 0.0001$ mhos/m. Part a of the figure shows the North-South E-field, which is derived from the East-West B-field. Part b illustrates the East-West E-field. It is interesting to note that although the North-South B-field is the larger of the magnetic field components, the East-West E-field is not the dominant electric field. There is a 14 V/km spike in the North-South E-field which caused several problems in power systems across the U.S.

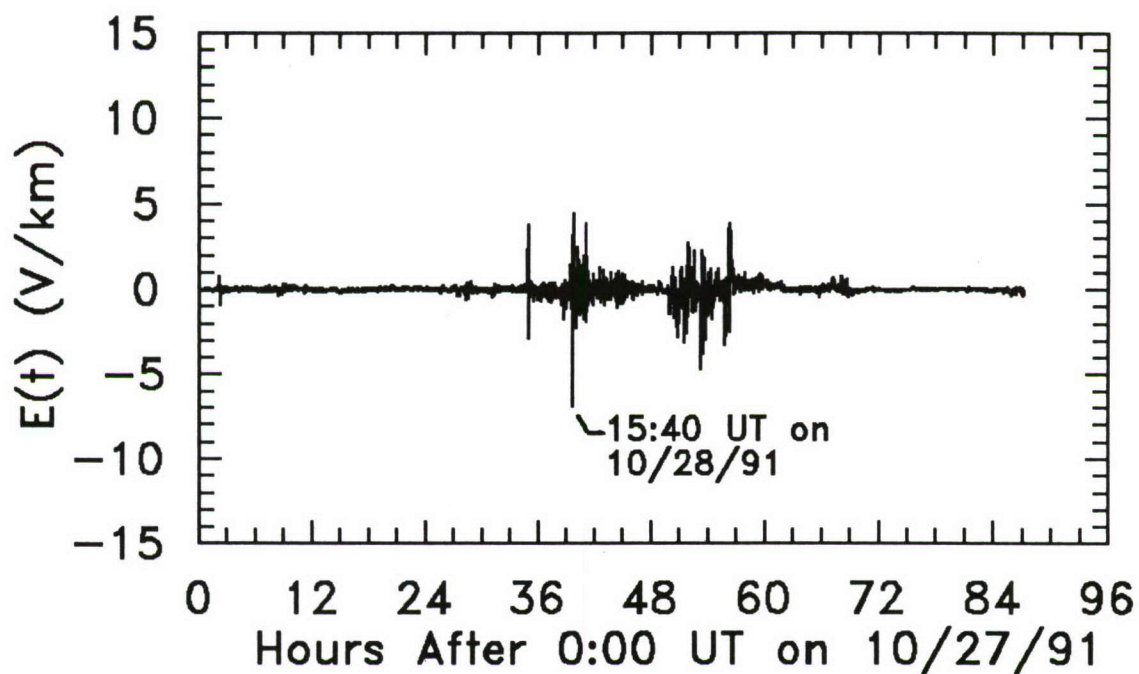
To observe in better detail the behavior of the earth-induced E-fields at the onset of the storm, Figure 47 presents the fields on an expanded time scale, in minutes after 15:30 universal time on October 28. From this plot, it is clear that the 10 second time resolution is not sufficiently small to adequately sample the fast-rising peaks in the E-field components. These electric fields actually could have been larger in amplitude than what is indicated in this figure.

This geomagnetic storm caused a number of power system problems which have been reported in [18]. These are reproduced below:

- NPCC (Northeast Power Coordinating Council) — The Radisson-Sandy Pond HVDC line tripped Monday morning (October 28) because filters on the line failed. Very early Tuesday morning, the Madawaska HVDC tie between Quebec and New Brunswick tripped. Transformer problems were reported, but not confirmed as solar storm related.
- MAAC (Mid-Atlantic Area Council) — PJM detected geomagnetic induced currents (GIC) due to the solar storms on several occasions. Late Monday night until early Tuesday morning (October 28-29), the GIC reached the Region's operating procedure "trigger level" and west-to-east electricity transfer limits were reduced. Public Service Electric & Gas Company also reduced the output of its Salem nuclear generating plants.
- MAIN (Mid-America Interconnected Network) — Transformers at the Point Beach nuclear units were "noisy" for a while, but the noise stopped when the system operators backed down on the var output of the generating units. Had this not worked, opening of a major 345 kV line from North appleton to Rocky Run would have been the next step to protect the transformers. MAIN also is checking to determine whether significant tie line flow changes on Monday (October 28) and the tripping of two generating units were solar storm related.
- MAPP (Mid-Continent Area Power Pool) — One utility in MAPP reported voltage fluctuations.



a. North-South Component



b. East-West Component

Figure 46. Computed Earth-Induced Electric Field for $\sigma_g = 0.0001$ Mhos/m.

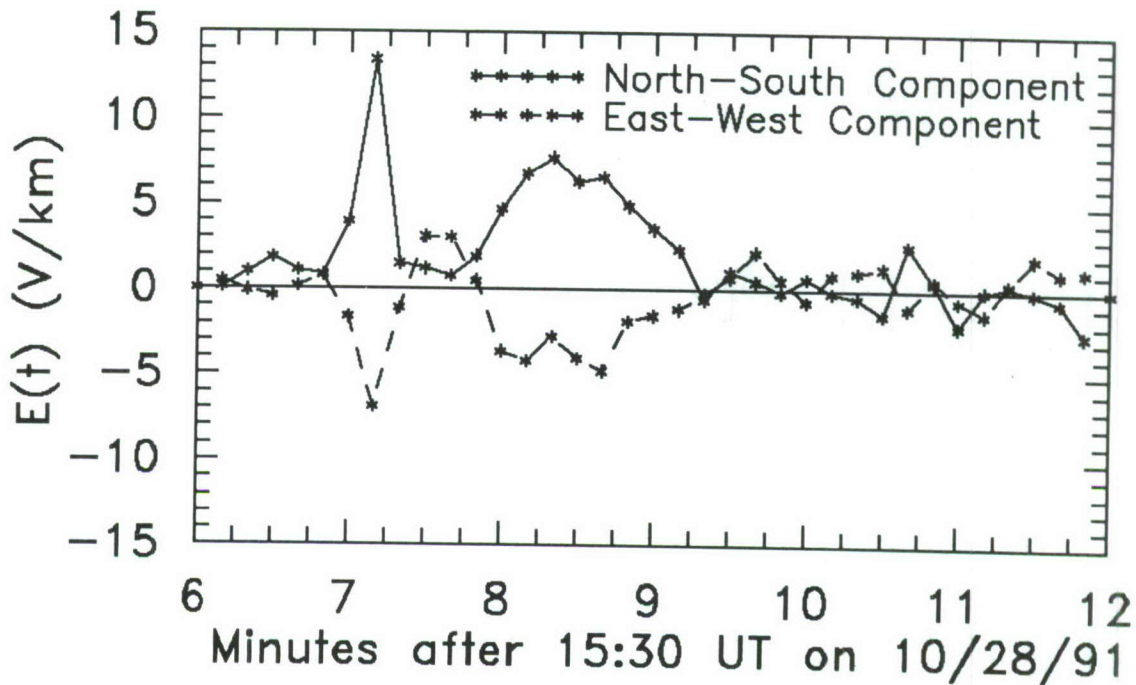


Figure 47. Computed E-Field Components for October 28, 1991.

- WSCC (Western Systems Coordinating Council) – BPA (Bonneville Power Administration) reported that on Monday (October 28) about 15 capacitor banks at seven substations (115 and 230 kV) tripped. The Blackwater HVDC tie between WSCC and SPP also tripped. Both British Columbia Hydro and Southern California Edison reported voltage excursions lasting several minutes that day.

Furthermore, ref.[19] documents the following anomalies for the same geomagnetic storm:

- BPA (Bonneville Power Administration) – At 0737 PST October 28, 1991, shunt capacitors started tripping and continued to trip until 0739 PST at Chemwa, Keeler, Tillamook, Bandon, McMinnville, Alvey, Cosmopolis, and Ling View substations. Operators reported "strange" transformer noises at Keeler and Peal Substations. Also, there was a report of transformer noise at Portland General Electric's Boardman Generation Plant.
- SCE (Southern California Edison) – At 0737 PST October 28, 1991, the 550 kV transmission system voltage dropped from 530–535 kV to 518–524 kV. It recovered within three minutes.

At 0801 PST October 28, 1991, the 550 kV transmission system voltage again dropped from 530–535 kV to 522–526 kV. It recovered within three minutes.

Also a fault recorder triggered on abnormal neutral current at the Serrano 230/500 kV substation which is located southeast of Los Angeles. Off-line analysis indicated the neutral current magnitude was between 150 and 200 amperes and principally third harmonic current with 32% 6th harmonic current. Phase A current evaluation revealed strong 2nd and 4th harmonic currents, 1.7% and 1.0% respectively, of the bank's rating.

- NMPS (New Mexico Public Service) — At 0838 MST October 28, 1991, the ac-dc-ac back-to-back tie at Blackwater went off line. Preliminary indications are that it was tripped by an overvoltage relay set to trip at 115% voltage for one second.
- NEPSCO (New England Public Service Co.) — At 1037 EST October 28, 1991, the New England Hydro Phase II dc tie with Hydro Quebec tripped. The problem caused by harmonics in the dc system appears to have occurred at the Radisson Terminal. NEPSCO was importing 930 MW at Sandy Pond at the time of the trip. The system was back in service within an hour.
- PSE&G (Public Service Electric & Gas Company) — At 2257 EST October 28, 1991, the Salem Unit was backed off to 80%.
- APS (Allegheny Power System) — At 1050 EST October 28, 1991, Allegheny Power System SCADA armed the capacitor bank trip restrain and enabled the Meadowbrook transformer gas detector trip. No capacitor banks tripped in the minutes before the restrain was initiated.

At 2259 EST October 28, 1991, the T4 transformers at Meadowbrook tripped on gas detection.

At 2316 October 28, 1991, APS removed T2 at Meadowbrook per operating procedures.

- WEPCO (Wisconsin Electric Power Co.) — Reported transformer growling at approximately 0930 CST October 28, 1991, at its Point Beach Power Plant. They backed off VAR generation during this period.
- VEPCo (Virginia Electric and Power Co.) — At 1041 EST October 28, 1991, 230kV — 100MVAR capacitor bank at Chuckatuck tripped due to neutral unbalance.

At 1041 EST October 28, 1991, 230kV — 150MVAR capacitor bank at Dooms tripped due to neutral unbalance.

At 1102 EST October 28, 1991, 115kV — 25MVAR capacitor bank at Staunton tripped due to neutral unbalance.

From these observations of geomagnetic storm effects on the power system, it is reasonable to conclude that the power system would respond to a MHD-EMP event. Figure 48 presents an overlay of the earth-induced E-field for the geomagnetic storm on October 28, and a normalized composite MHD-EMP E-field, similar to that shown in Figure 4a. The MHD-EMP waveform has been normalized here to have the same peak amplitude of about 14 V/km. Note that there is a remarkable similarity in these two waveforms: an early-time spike, followed by a later-time component.

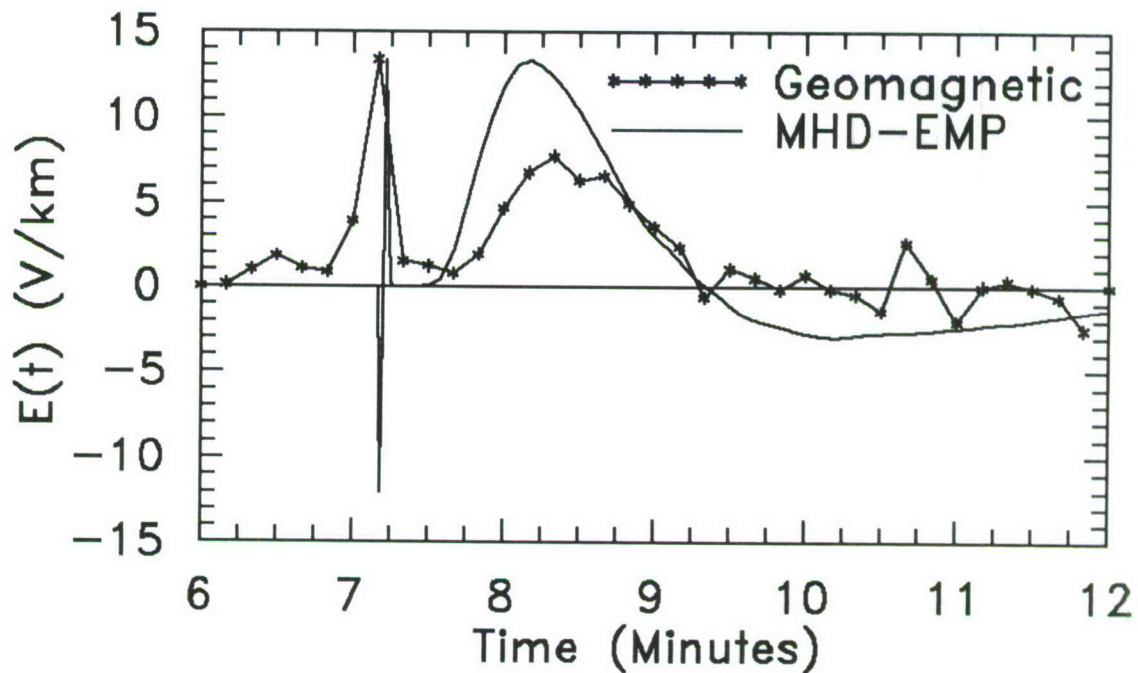


Figure 48. Comparison of MHD-EMP with Geomagnetic Storm E-field Waveforms.

6.0 SUMMARY AND CONCLUSIONS

This report has discussed the interaction of electrical transmission and distribution systems with the MHD-EMP, or E_3 , environment. A simplified form of the earth-induced electric field has been postulated, and a number of different calculations of coupling to various line configurations have been performed.

The time variations of the MHD-EMP electric field are sufficiently slow that an analysis of quasi-dc coupling to the lines is feasible. This analysis reduces the electromagnetic field coupling problem to that of a relatively simple electrical circuit. The power system reacts to the external MHD-EMP excitation with its own R/L time constant, which depends on the electrical configuration and parameters of the system being considered. For the MHD-EMP environment to be able to induce currents in the power system, a dc path to ground at both ends of a long length of electrical conductor is required. One way of obtaining this configuration is to use grounded-wye transformers at each end of the line. For an E_3 electric field strength of 20 V/km and the assumed line and transformer parameters, typical peak quasi-dc currents for a 500-km, 500-kV transmission line was found to be on the order of 1600 A. For a 50-km, 69-kV subtransmission line and for a 30-km, 12-kV distribution line, these MHD-EMP-induced currents are between 70 and 190 A, and between 40 and 110 A, respectively, depending on how well the transformers are grounded. Removing the ground connection of the grounded-wye transformer or using an ungrounded delta transformer in its place are two ways of eliminating this MHD-EMP current.

For high-voltage transmission systems, we found in a sample calculation that times required to saturate loaded power transformers range from 6 to 11 seconds. For lower-voltage distribution-class systems, the saturation time can be on the order of a second. Response times for both of these systems are seen to decrease nonlinearly with an increase in the MHD-EMP field strength.

The MHD-EMP environment has been shown to cause saturation in transformers in both transmission and distribution systems. Using measured transformer response data for a dc current injection into the neutrals, we have observed that quasi-dc current levels corresponding to E-field strengths as low as 20 V/km for typical line lengths can generate 60-Hz harmonics. Thus, it is evident that the MHD-EMP environment will cause serious harmonic distortion in both power transmission and distribution systems.

We also note that there is an increase in the reactive power flow within the system when it is excited by the MHD-EMP environment. Specific data for the increase in reactive power demand for both transmission- and distribution-class transformers have been presented. This increase in reactive power arises due to the saturation of the transformers and can cause instabilities in power system operation. The severity and duration of these system instabilities is presently unknown.

From this work, it is clear that MHD-EMP field strengths on the order of 20 V/km can have measurable effects on transformer operation in the form of core saturation, harmonic generation, and an increase in reactive power demand. Geomagnetic storms with E-field peaks on the order of just 10 to 15 V/km have been known to cause problems in the power system. Larger MHD-EMP E-field strengths will only increase the severity of these effects. The system-wide impact of MHD-EMP on a large power network in which several different transformers experience these effects simultaneously remains to be determined.

REFERENCES

1. Legro, J.R., et al., *Study to Assess the Effects of Magnetohydrodynamic Electromagnetic Pulse on Electric Power Systems*, ORNL/Sub/83-43374/1/V3, Oak Ridge National Laboratory, May 1985.
2. Albertson, V.D. and J.A. Van Baelen, "Electric and Magnetic Fields at the Earth's Surface Due to Auroral Currents," *IEEE Trans. PAS*, Vol. PAS-89, No. 2, April 1970.
3. Legro, J.R., et al., *Study to Assess the Effects of Electromagnetic Pulse on Electric Power Systems*, ORNL/Sub/83-43374/1/V1, Oak Ridge National Laboratory, Sept. 1985.
4. Chavin, S., et al., *MHD-EMP Code Simulation of Starfish*, MRC-R-516, Mission Research Corporation, Santa Barbara, CA, August, 1979.
5. Austin Research Associates, private communication with F.M. Tesche, Austin, TX, March 1991.
6. **TableCurve** Curve Fitting Software, Jandel Scientific Co., Corte Madera, CA, July 1990.
7. Sunde, E.D., *Earth Conduction Effects in Transmission Systems*, Van Norstrad, New York, 1949.
9. Guillemin, E.A., *The Mathematics of Circuit Analysis*, MIT Press, Massachusetts Institute of Technology, 1949.
9. Morse, P.M., and H. Feshbach, *Methods of Theoretical Physics*, McGraw-Hill, New York, 1953.
10. Balabanian, N., *Fundamentals of Circuit Theory*, Allyn and Bacon, Boston, 1961.
11. Kruse, V., et al., "Flashover Vulnerability of Transmission and Distribution Lines to High Altitude Electromagnetic Pulse," *IEEE Trans. PD*, Vol. PD-5, No. 2, April 1990.
12. Millard, D.P., A.P. Sakis Meliopoulos, and G.J. Cokkinides, "Parametric Analysis of EMP Induced Overvoltages on Power Lines," *IEEE Trans. PD.*, Vol. PD-3, No. 3, pp. 1224-1231, July 1988.

13. Kappenman, J.G., *Transformer DC Excitation Field Test and Results*, Special Panel Session Report 90TH0291-PWR, IEEE PES Summer Meeting, July, 12, 1989.
14. McConnell, B.W., *Impact of Quasi-DC Currents on Three-Phase Distribution Transformer Installations*, ORNL/Sub/89-SE912/1, Oak Ridge National Laboratory, to be published.
15. Kappenman, J.G., private communication with P.R. Barnes, Oak Ridge National Laboratory, July, 1991.
16. Van Beek, G. Jansen, private communication with F.M. Tesche, Geological Survey of Canada, November 20, 1991.
17. Green, A.W., private communication with F.M. Tesche, U.S. Geological Survey, November 25, 1991.
18. *NERC 1991 October Review*, North American Electric Reliability Council, 101 College Road East, Princeton, NJ, 08540-6601.
19. *Preliminary Report of Geomagnetically Induced Currents for the Week of October 27, 1991*, memo dated November 1, 1991, Electric Research and Management, Inc., P.O. Box 165, State College, PA, 16804.

INTERNAL DISTRIBUTION

- | | |
|---------------------|--------------------------------|
| 1-10. P. R. Barnes | 19. R. B. Shelton |
| 11. V. D. Baxter | 20. J. N. Stone |
| 12. G. E. Courville | 21. T. A. Stone |
| 13. P. S. Gillis | 22. J. P. Stovall |
| 14. N.J. Jett | 23. ORNL Patent Office |
| 15. M. A. Kuliasha | 24. Central Research Library |
| 16. V. C. Mei | 25. Document Reference Section |
| 17. B. W. McConnell | 26-27. Laboratory Records |
| 18. D. T. Rizy | 28. Laboratory Records-RC |

EXTERNAL DISTRIBUTION

ORNL LIST

29. V. D. Albertson, Dept. of Electrical Engineering, University Of Minnesota, 123 Church Street, S.W., Minneapolis, MN 55455.
30. J. C. Allen, Southwestern Electric Power Co., P. O. Box 21106, Shreveport, LA 71156.
31. R. W. Allen, New England Power Service Co., 25 Research Drive, Westboro, MA 01582.
32. G. Applegren, Main Coordination Center, 1n301 Swift Road, P.O. Box 278, Lombard, Illinois 60148.
33. M. R. Apprill, Engineering & System Operations, Missouri Public Service, 10700 East 350 Highway, Kansas City, MO 64138.
34. G. H. Baker, HQ DNA/RAEE, 6801 Telegraph Road, Alexandria, VA 22310-3398.
35. P. Balma, Public Service Electric, 80 Park Plaza, Newark, NH 07101.
36. D. L. Bartel, Wisconsin Power & Light Co., 222 West Washington Ave., P. O. Box 192, Madison, WI 53701-0192.
37. J. E. Benning, Power System Engineering/Operations, PSI Energy, 1000 East Main Street, Plainfield, IN 46168.
38. Robert E. Benson, Chief Electrical Engineer, New York State Electric & Gas Corp., 4500 Vestal Parkway East, Binghamton, NY 13903.

39. G. D. Birney, Western Area Power Administration, P. O. Box 3402, Golden, CO 80401.
40. P. D. Blair, Energy and Materials Program, Congress of the United States, Office of Technology Assessment, Washington, DC 20510.
41. W. T. Boston, Tennessee Valley Authority, 6N 31B Signal Place, 1101 Market Street, Chattanooga, TN 37402-2801.
42. Larry Bressler, Western Area Power Administration, P. O. Box 3402, Golden, CO 80401.
43. B. G. Buchanan, Computer Science Department, University of Pittsburgh, 206 Mineral Industries Building, Pittsburgh, Pennsylvania 15260.
44. W. J. Budney, Distribution Systems, Public Service Electric & Gas Co., 80 Park Plaza, Newark, NJ 07101.
45. C. K. Bush, Atlanta Electric, P.O. Box 1264, Pleasantville, NJ 08232.
46. R. F. Campbell, Transmission & Electrical Projects, Tennessee Valley Authority, 3N 53A Missionary Ridge Place, Chattanooga, TN 37402-2801.
47. H. S. Cabayan, Lawrence Livermore National Laboratory, P.O. Box 5504, L-81, Livermore, CA 94550.
48. J. Chadwick, 902 Glamis Circle, Signal Mountain, TN 37377.
49. D. J. Christofersen, Manager, Electrical Engineering Division, United Power Association, P. O. Box 800, Elk River, MN 55330-0800.
50. P. Chrzanowski, Evaluation & Planning Program, Lawrence Livermore National Lab, P.O. Box 808, L-81, Livermore, CA 94550.
51. R. F. Chu, Research Engineer, Philadelphia Electric Co., Research Division (S10-1), 2301 Market Street, Philadelphia, PA 19101.
52. Lynn Coles, Principal Policy Advisor, SERI, 1617 Cole Boulevard, Golden, CO 80401.
53. O. R. Compton, Richmond Plaza, P. O. Box 26666, Richmond, Virginia 23261.
54. T. B. Cook, 80 Castlewood Dr., Pleasanton, CA 94566.
55. G. H. Coplon, U.S. Department Of Energy, Rm. 8F089, 1000 Independence Avenue, S.W., Washington, DC 20585.

56. J. J. Cuttica, Research and Development, Gas Research Institute, 8600 W. Bryn Mawr Avenue, Chicago, Illinois 60631.
57. G. Dahlen, Royal Institute of Technology, Tds, P.O. Box 70043, S-10044, Stockholm, Sweden.
58. S. J. Dale, Manager Transmission Technology Institute, ABB Power T&D Company Inc., Centennial Campus, 1021 Main Campus Drive, Raleigh, NC.
59. L. W. DeJong, Iowa Public Service Co., P. O. Box 778, Sioux City, IA 51102.
60. A. R. Donnell, Northwestern Public Service Co., 3rd St. & Dakota Ave., S.E., Huron, SD 57350.
61. Raymond Dunlop, Director of Research, New England Power Service Co., 25 Research Drive, Westborough, MA 01582.
62. H. Elbadaly, Underground T&D Research Manager, Consolidated Edison Company, 4 Irving Place, New York, NY 10003.
63. D. Fagnan, Philadelphia Electric Co., 2301 Market Street, Philadelphia, PA 19101.
64. W. E. Ferro, Electric Research and Management, Inc., P.O. Box 165, State College, PA 16804.
65. R. Gates, EMP Program Manager, FEMA, RM 606, 500 C Street, S.W., Washington, DC 20472.
66. P. R. Gattens, Allegheny Power, 800 Cabin Hill Dr., Greensburg, PA 15601.
67. M. R. Gent, President, North American Electric Reliability Council, 101 College Road East, Princeton, New Jersey 08540-8060.
68. J. D. Gregory, Southern Company Services, Inc., P. O. Box 2625, Birmingham, AL 35202-2625.
69. V. Guten, National Security Agency (M-352), Fort Mead, MD 20755.
70. I. Gyuk, Program Manager, U.S. Department of Energy, 1000 Independence Ave., S.W., Washington, DC 20585.
71. Wayne Hilson, Manager, Transmission and Electrical Systems Department, Missionary Ridge, 3 North 41, 1101 Market Street, Chattanooga, TN 37402-2801, .
72. E. R. Holcomb, Texas Utilities Electric Co., 1506 Commerce Street, Dallas, TX 75201.

73. M. B. Hunter, Puget Sound Power & Light Co., 13635 N.E. 80th Street, Redmond, WA 98052-4098.
74. Joe Iannucci, Pacific Gas & Electric, 3400 Crow Canyon, San Ramon, CA 94583.
75. J. Kappenman, Minnesota Power, 30 W. Superior St., Duluth, Minnesota 55802.
76. S. Kashyap, Defense Research Establishment — Ottawa, Electronics Division, 3701 Carling Ave., Ottawa, Ontario K1A0Z4, Canada.
77. J. L. King, System Executive Operations, Entergy Corporation, P. O. Box 61005, 225 Baronne St., New Orleans, LA 70161.
78. J. L. Koepfinger, Director, Systems Studies and Research, Duquesne Light Company, One Oxford Center, 301 Grant Street (19-5), Pittsburgh, PA 15279.
79. R. A. Kramer, Northern Indiana Public Service Co., 5265 Hohman Avenue, Hammond, IN 46320.
80. E. Larsen, General Electric, ESDS Bldg. 2, Rm 642, One River Road, Schenectady, NY 12345.
81. Major Robert Launstein, Defense Nuclear Agency, DNA/RAEE, 6801 Telegraph Rd., Alexandria, VA 22310.
82. J. L. Layton, Systems Operation, Carroll Electric Membership Corp., 155 Temple Road, Carrollton, GA 30117.
83. G. R. Leidich, System Planning Engineering Dept., Centerior Energy, 6200 Oak Tree Boulevard, Independence, OH 44131.
84. R. C. Liebentritt, Omaha Public Power District, 444 South 16th Street Mall, Omaha, NE 68102-2247.
85. R. C. Liimatainen, Committee on Science, Space and Technology, 374 Rayburn House Office Bldg., Rm. B., Washington, DC 20515.
86. J. Lloyd, CEHND-ED-SY, U.S. Army, Engineering Division Huntsville, P.O. Box 1600, Huntsville, AL 35807.
87. C. L. Longmire, Mission Research Corporation, P.O. Drawer 719, Santa Barbara, CA 93102.
88. D. J. Lorden, New England Power Service, 25 Research Drive, Westborough, MA 01582.

89. A. P. Meliopoulos, Georgia Tech, School of Electrical Engineering, Atlanta, GA 30332.
90. S. R. Mendoza, Salt River Project, P.O. Box 52025, Phoenix, AZ 85072-2025.
91. N. V. Mesland, Tot Keuring Van Elektrotechnische, Materialen, 6800 ET Arnhem, P.O. Box 9035, The Netherlands.
92. Walter E. Myers, R&D Manager, Bonneville Power Administration, P. O. Box 3621, Portland, OR 97208.
93. D. L. Nickel, Manager, ABB Power Systems, Inc., 777 Penn Center Blvd., Pittsburgh, PA 15235-5927.
94. S. Nilsson, Program Manager, Electric Power Research Institute, Electrical Systems Division, 3412 Hillview Avenue, P.O. Box 10412, Palo Alto, CA 94303.
95. B. M. Pasternack, American Electric Power Service Corp., 1 Riverside Plaza, P.O. Box 16631, Columbus, OH 43216-6631.
96. J. Z. Ponder, PJM Interconnection, 955 Jefferson Ave., Norristown, PA 19426.
97. J. W. Porter, Electric Power Research Institute, Suite 100, 1019 Nineteenth St. N.W., Washington, DC 20036.
98. M. Rabinowitz, Electric Power Research Institute, 3412 Hillview Avenue, P.O. Box 10412, Palo Alto, CA 94303.
99. J. J. Ray, Division of Syst. Planning, BPA, P.O. Box 3621, Portland, OR 97208.
100. T. W. Reddock, Electrotek Concepts, Inc., 10305 Dutchtown Rd., Suite 103, Knoxville, TN 37932.
101. J. R. Rempel, Physicist, Defense Intelligence Agency, Washington, DC 20340-6761.
102. H. L. Robidoux, Metropolitan Edison Company, 2800 Pottsville Pike, P. O. Box 16001, Reading, PA 19640-0001.
103. Dietrich J. Roesler, U.S. Department of Energy, CE-141, 1000 Independence Avenue SW, Washington, DC 20585.
104. F. Rosa, Division of System Intg., Nuclear Regulatory Commission, MS P1030, Washington, DC 20555.
105. V. G. Rose, Pacific Gas & Electric Co., 123 Mission Street, San Francisco, CA 94106.

106. C. H. Rush, Construction Department, Philadelphia Electric Co., 2301 Market St. (S25-1), Philadelphia, PA 19101.
107. J. E. Scalf, Florida Power & Light Company, P. O. Box 14000, 700 Universe Blvd., Juno Beach, FL 33408.
108. Virgil Schafer, Engineering Division Manager, Tri-State Generation and Trans. Assoc., 12076 Grant Street, Denver, CO 80233.
109. W. G. Schiffmacher, Long Island Lighting Company, Office of Engineering & Constr., 1660 Walt Whitman Road, Melville, NY 11747.
110. W. J. Scott, Hq DNA/RAEE, 6801 Telegraph Road, Alexandria, VA 22310-3398.
111. Joe Sefcik, Nuclear Design, Lawrence Livermore National Lab, P.O. Box 808, L-22, Livermore, CA 94550.
112. C. H. Shih, Manager, Electrical Research, American Electric Power Service Corp., 1 Riverside Plaza, Columbus, OH 43215.
113. M. L. Sloan, Austin Research Associate, 1101 Capital of Texas Highway S., Building B, Suite 210, Austin, TX 78746.
114. R. B. Spence, Bonneville Power Administration, P.O. Box #3621 - MOEA, Portland, OR 97208.
115. G. I. Stillman, Research & Development, New York Power Authority, 1633 Broadway, New York, NY 10019.
116. P. Sullivan, Philadelphia Electric Co., 2301 Market Street (S10-1), Philadelphia, PA 19101.
117. R. L. Taylor, Director - Power Supply, Florida Power & Light Co., 9250 W. Flagler, Miami, FL 33102.
118. L. L. Taylor, Northern States Power Company, 414 Nicollet Mall, Minneapolis, MN 55401.
119. E. R. Taylor, ABB Power Systems, Inc. , 777 Penn Center Blvd., Pittsburgh, PA 15235-5927.
120. A. N. Terreri, Electrical Operations, Green Mountain Power Corp., P. O. Box 850, South Burlington, VT 05402.
121. F. M. Tesche, Consulting Scientist, 6921 Spanky Branch Dr., Dallas, TX 75248.

122. M. V. Thaden, Potomac Electric Power Co., 1900 Pennsylvania Ave., NW, Rm. 311, Washington, DC 20068.
123. G. F. Thompson, Northeast Utilities Service Co., P. O. Box 270, Hartford, CT 06141-0270.
124. J. Towle, 3906 Bagley Ave. N., Suite 100, Seattle, WA 98103.
125. E. F. Vance, 6885 HWY 1187, Fort Worth, TX 76140.
126. D. R. Volzka, Senior Project Engineer, Wisconsin Electric Power Company, 333 West Everett Street, Milwaukee, WI 53201.
127. Jan Wagers, Power Systems Planning, City of Colorado Springs, Department of Utilities, 30 South Nevada, Colorado Springs, CO 80903.
128. C. L. Wagner, 4933 Simmons Dr., Export, PA 15632.
129. R. Walling, General Electric Company, Building 2, Rm 507, One River Road, Schenectady, NY 12345.
130. R. C. Webb, Defense Nuclear Agency, RAEE, 6801 Telegraph Road, Alexandria, VA 22310.
131. L. B. Wideman, Houston Lighting & Power Co., P. O. Box 1700, Houston, TX 77001.
132. E. P. Wigner, Consultant, 8 Ober Road, Princeton, NJ 08540.
133. M. W. Wik, Forsvarets Materielverk, Stockholm, S-11588, Sweden.
134. D. Woodford, Suite 400, 1619 Pembina Ave., Winnipeg, Manitoba, R-3T-2G5, Canada.
135. S. E. Wright, Electric Power Research Institute, 3412 Hillview Ave., P.O. Box 10412, Palo Alto, CA 94303.
136. F. S. Young, Director, Electrical Systems Division, Electric Power Research Institute, P.O. Box 10412, Palo Alto, CA 94303 .
137. R. M. Youngs, Seattle City Light, 1015 Third Avenue, Seattle, WA 98104.
138. R. W. Zwickl, Space Environment Laboratory, Mail Stop R/E/SE, Boulder, CO 80303.
139. J. A. Zychinski, Union Electric Company, P. O. Box 149, M/C 661, St. Louis, MO 63166.
140. Office of Assistant Manager for Energy, Research and Development, DOE-ORO, P.O. Box 2001.

141-150. OSTI, U.S. Department of Energy, P.O. Box 62, Oak Ridge, TN 37831.

DNA LIST

- 151. Air Force Space Command, Headquarters, DEES/D C DE MIO, Peterson AFB, CO 80914-5001.
- 152. Atomic Energy, The Pentagon, Assistant to the Secretary of Defense, Executive Assistant, Washington, DC 20301-3050.
- 153. BDM International Inc., Library, P.O. Box 9274, Albuquerque International, Albuquerque, NM 87119.
- 154. BDM International Inc., E. Dorchak, 7915 Jones Branch Drive, McLean, VA 22102-3396.
- 155. Booz-Allen & Hamilton, Inc., Technical Library, 4330 East West Highway, Bethesda, MD 20814-4455.
- 156. Central Intelligence Agency, OSWR/STD/MTB, Washington, DC 20505.
- 157. Central Intelligence Agency, OSWR/NED, Washington, DC 20505.
- 158. Defense Communications Engineer Center, Code R410, 1860 Wiehle Avenue, Reston, VA 22090-5285.
- 159. Defense Intelligence Agency, Director, RTS-2B, Washington, DC 20340.
- 160. Defense Intelligence Agency, Director, VP-TPO, Washington, DC 20340.
- 161. Defense Nuclear Agency, RAEV, 6801 Telegraph Road, Alexandria, VA 22310.
- 162-171. Defense Nuclear Agency, RAEE, 6801 Telegraph Road, Alexandria, VA 22310.
- 172-173. Defense Nuclear Agency, TITL, 6801 Telegraph Road, Alexandria, VA 22310.
- 174. Defense Nuclear Agency, RAAE, 6801 Telegraph Road, Alexandria, VA 22310.
- 175. Defense Research Establishment Ottawa, S. Kashyap, Ottawa, Ontario, Canada K1A0Z4.
- 176. Defense Technical Information Center, DTIC/FDAB, Cameron Station, Alexandria, VA 22304-6145.

177. Department of the Navy, Command & Control Programs, OP 941, Washington, DC 20350.
178. Department of Commerce, NOAA/MASC Security Office, MC43, G. Reeve, 325 Broadway, Boulder, CO 80303.
179. Department of Commerce, NOAA/MASC Security Office, MC43, W. Utlaut, 325 Broadway, Boulder, CO 80303.
180. Department of Commerce, NOAA/MASC Security Office, MC43, D. Peach, 325 Broadway, Boulder, CO 80303.
181. Department of the Air Force, Air Force CTR For Studies & Analysis, AFCSA/SAMI (R. Griffin), Washington, DC 20330-5420.
182. E-Systems, Inc., ECI Division, Mail Stop 3, Tech Info CTR, P.O. Box 12248, St. Petersburg, FL 33733.
183. EG&G Special Projects Inc., J. Giles, Albuquerque Operations, 2450 Alamo Avenue, SE, Albuquerque, NM 87106.
184. Electro-Magnetic Applications, Inc., D. Merewether, P.O. Box 8482, Albuquerque, NM 87198-8482.
185. General Research Corp., W. Naumann, P.O. Box 6770, Santa Barbara, CA 93160-6770.
186. Harry Diamond Laboratories, Director, SLCHD-NW-TN (G MERKEL), 2800 Powder Mill Road, Adelphi, MD 20783-1197.
187. Harry Diamond Laboratories, Director, SLCHD-NW-EP (21100), 2800 Powder Mill Road, Adelphi, MD 20783-1197.
188. Harry Diamond Laboratories, Director, W. Patterson, 2800 Powder Mill Road, Adelphi, MD 20783-1197.
189. Harry Diamond Laboratories, Director, SLCIS-IM-TL (81100), 2800 Powder Mill Road, Adelphi, MD 20783-1197.
190. IIT Research Institute, I. Mindel, 10 W. 35th Street, Chicago, IL 60616-3703.
191. Institute for Defense Analyses, Tech Info Services, 1801 N. Beauregard Street, Alexandria, VA 22311-1772.
192. Jaycor, R. Poll, P.O. Box 1577, Santa Monica, CA 90406-1577.
193. Jaycor, E. Wenaas, P.O. Box 85154, San Diego, CA 92186-5154.

194. Jaycor, M. Schultz, Jr., 1608 Spring Hill Road, Vienna, VA 22182-2270.
195. Joint Strategic Target Planning Staff, The Joint Staff, JLWT (Threat Analysis), Offutt AFB, NE 68113-50001.
196. Joint Strategic Target Planning Staff, The Joint Staff, JKC (DNA REP), Offutt AFB, NE 68113-50001.
197. Kaman Sciences Corporation, DASAC, Santa Barbara Operations, P.O. Box 1479, Santa Barbara, CA 93102-1479.
198. Kaman Sciences Corp., Library/B. Kinslow, P.O. Box 7463, Colorado Springs, CO 80933-7463.
199. Kaman Sciences Corp., Washington Operations Division, DASAC, 2560 Huntington Ave., Suite 200, Alexandria, VA 22303.
200. Kamana Sciences Corporation, Technical Library, Dikewood Division, 6400 Uptown Blvd., N.E. Suite 300E, Albuquerque, NM 87110.
201. Metatech Corporation, W. Radasky, P.O. Box 1450, Goleta, CA 93116-1450.
202. Mission Research Corp., J. Lubell, 4935 North 30th Street, Colorado Springs, CO 80919-4199.
203. Mission Research Corp., A. Chodorow, 1720 Randolph Rd., SE, Albuquerque, NM 87106-4245.
204. Mission Research Corp., Tech Info Center, P.O. Drawer 719, Santa Barbara, CA 93102-0719.
205. National Security Agency, Director, R-54, Fort George G Meade, MD 20755-6000.
206. Naval Research Laboratory, Commanding Officer, Code 2627 (TECH LIB), Washington, DC 20375-5000.
207. Office of the Sec of Defense, Director, Document Control, Net Assessment, Room 3A930, The Pentagon, Washington, DC 20301.
208. Office Secretary Defense, U S Nuclear Command & Central Sys Support Staff, SAB H Sequine, Pentagon, Room 3E 172, Washington, DC 20301-3040.
209. Pacific-Sierra Research Corp., H. Brode, 12340 Santa Monica Blvd, Los Angeles, CA 90025-2587.
210. R & D Associates, Document Control, P.O. Box 92500, Los Angeles, CA 90009.

211. R & D Associates, J P Castillo, P.O. Box 9377, Albuquerque, NM 87119-9377.
212. Rockwell International Corp., G. Smith, P.O. Box 3105, Anaheim, CA 92803-3105.
213. S-Cubed, J. Knighten, A Division of Maxwell Laabs, Inc., P.O. Box 1620, La Jolla, CA 92038-1620.
214. Science & Engrg Associates, Inc., Robert L. Charters, P.O. Box 3348, Seattle, WA 98009-3348.
215. Science Applications Intl. Corp., P.J. Dowling, 2860 S Circle Dr., St. 2400, Colorado Springs, CO 80906.
216. Science Applications Intl. Corp., W. Chadsey, P.O. Box 1303, McLean, VA 22102-1303.
217. Space & Naval Warfare Systems CMD, Commander, Technical Library, Department of the Navy, Washington, DC 20363-0001.
218. SRI International, J. Prewitt, 333 Ravenswood Ave., Menlo Park, CA 94025-3434.
219. Strategic Air Command/XRFS, Headquarter, XRFS, Department of the Air Force, Offutt AFB, NE 68113-5001.
220. The Joint Staff, J-3/Nuc. Operations Br., Strat. Operations Br., Washington, DC 20318 .
221. The Joint Staff, C3S (ER) Analysis Div, Washington, DC 20318.
222. The Joint Staff, J-6F D Butts, Washington, DC 20318.
223. TRW Inc., DH4/2461, G.E. Morgan, TRW Space & Defense, One Space Park, Redondo Beach, CA 90278-1071.
224. U S Army Engineer Div Huntsville, Division Engineer, CEHND-SY J LOYD, P.O. Box 1600, West Station, Huntsville, AL 35807-4301.
225. U S Army Strategic Defense Command, CSSD-SL, P.O. Box 1500, Huntsville, AL 35807.
226. U S Army Nuclear & Chemical Agency, Commander, MONA-NU (D. Bash), 7500 Backlick Rd., Bldg. 2073, Springfield, VA 22150-3198.
227. Under Secretary of Defense, Director, Strat & Theater NUC Forces, The Pentagon, RM 3E 129, Strat & Theater NUC Forces (O&SS), Washington, DC 20301-3090.

- 228. USA Survivability Management Office, Director, SLCSM-SE J BRAND, 2800 Powder Mill Road, Adelphi, MD 20783-1145.
- 229. USAF/LEEEU, HQ, LEEE, Washington, DC 20330.
- 230. Weapons Laboratory, NTN, Kirtland AFB, NM 87117-6008.
- 231. Weapons Laboratory, NTAA, Kirtland AFB, NM 87117-6008.
- 232. Weapons Laboratory, WL/SUL, Kirtland AFB, NM 87117-6008.